A Theoretical Study of Quantum Molecular Reaction Dynamics
and of the Effects of Intense Laser Radiation on a Diatomic Molecule

Peter Sabatino Dardi
(Ph.D. Thesis)

Department of Chemistry, and Materials and Molecular Research Division

of the Lawrence Berkeley Laboratory, University of California

Berkeley, California 94720

DISCLAIMER

MASTER

A Theoretical Study of Quantum Molecular Reaction Dynamics and
of the Effects of Intense Laser Radiation on a Diatomic Molecule

Peter Sabatino Dardi

Abstract

Within the very broad field of molecular dynamics, we have
concentrated on two simple yet important systems. The systems are
simple enough so that they are adequately described with a single Born -
Oppenheimer potential energy surface and that the dynamics can be
calculated accurately. They are important because they give insight
into solving more complicated systems.

First we discuss $H + H_2$ reactive scattering. We present an exact
formalism for atom - diatom reactive scattering which avoids the problem
of finding a coordinate system appropriate for both reactants and
products. This is done by using an over complete basis where expansion
functions are included which are localized in each arrangement
channel. The interaction between different arrangements is described
using an energy independent nonlocal exchange kernel. We present
computational results for collinear $H + H_2$ reactive scattering which
agree very well with previous calculations. We also present a coupled
channel distorted wave Born approximation for atom - diatom reactive
scattering which we show is a first order approximation to our exact
formalism. We present coupled channel DWBA results for three
dimensional $H + H_2$ reactive scattering. Reaction probabilities and

cross sections agree very well with previous exact calculations for energies near the threshold to reaction.

The second system which we study is an isolated HF molecule in an intense laser field. Using classical trajectories and quantum dynamics, we look at energy absorbed and transition probabilities as a function of the laser pulse time and also averaged over the pulse time. Calculations are performed for both rotating and nonrotating HF. We examine one and two photon absorption about the fundamental frequency, multiphoton absorption, and overtone absorption. We find that, in general, classical mechanics does not predict the correct time behavior or rotational state distributions. For the time averaged properties classical mechanics describes very well the multiphoton absorption but less well the other cases. We construct Poincaré surfaces of section to help understand the classical dynamics for nonrotating HF.

William H. Miller

To my Parents and Bridgette

Table of Contents

Acknowledgements

It is a pleasure to acknowledge the support and guidance of Professor William H. Miller which has made this work possible. Professor George C. Schatz is gratefully acknowledged for sharing his expertise in three dimensional atom – diatom scattering.

During my stay at Berkeley, I have benefitted greatly from the stimulating interaction with past and present members of the Miller group including, Tucker Carrington, Boyd Waite, Ralph Jaquet, Koichi Yamashita, Domenic Ali, Yitzhak Weissman, Charles Cerjan, Steven Schwartz, Kim White, John Tromp, and Beverly Ruff. Special thanks are due for my collaborators in the group for their friendship and insights, specifically Stephen Gray, who shared his skills during our exciting investigation of HF in a laser field; Shenghua Shi, who taught me much while we worked on exact collinear $H + H_2$ scattering; and Lynn Hubbard, who I worked with on DWBA for three dimensional $H + H_2$ scattering. Our journal club provided a chance to share our knowledge and broaden our backgrounds, and I am grateful to the participants, Tucker Carrington, Shenghua Shi, Robert Tico, Jeff Cina, Mitchio Okumura, and Stephen Bohan.

I have had the pleasure of several insightful discussions with Professor Robert E. Wyatt on various aspects of HF in a laser field.

I would like to thank my friends who help to keep life in perspective and especially Bridgette, who has and will continue to share the joy and the sorrow.

I acknowledge the support of the Director, Office of Energy

"However, the man of science has slipped so much that he accepts the slavery inflicted on him by national states as his inevitable fate. He even degrades himself to such an extent that he helps obediently in the perfection of the means for the general destruction of mankind....
My answer is: while it true that an inherently free and scrupulous person may be destroyed, such an individual can never be enslaved or used as a blind tool.

If the man of science of our day could find the time and courage to think honestly and critically over his situation and the tasks before him and if he would act accordingly, the possibilities for a sensible and satisfactory solution of the present dangerous international situation would be considerably improved."

Albert Einstein, October 1952

"To me the killing of any human being is murder; it is also murder when it takes place on a large scale as an instrument of state policy."

Albert Einstein, 1929

I. Introduction

The field of theoretical molecular dynamics includes a fairly broad range of topics. In general, though, it can be roughly divided into two main catagories, molecular scattering[1] and unimolecular dynamics.[2,3] Molecular scattering theory is the study of the collision of an atom and a molecule or two molecules in order to learn reaction (nuclear rearrangement) rates and magnitudes of internal energy transfer. Unimolecular dynamics theory is the study of molecules with large amounts of internal energy (which were energetically excited through collisions or the absorption of light) to understand how the molecule distributes the energy; and if it reacts, either dissociating or rearranging, to find the rate of reaction and distribution of energy in the products.

Molecular dynamics both theoretical and experimental is the study of elementary processes involving isolated molecular systems. These processes are the microscopic view (scattering cross sections and unimolecular reaction rates) of the macroscopic world (thermal rate constants) of chemistry. The goal is to understand the microscopic world better in the hope that this will lead to a better understanding of macroscopic phenomena. For gas phase or atmospheric chemistry, where everything is basically a series of isolated elementary processes, molecular dynamics can yield directly measurable rate constants by accounting for the statistical distibution of the relative energy of collision partners in a gas (by taking a Boltzmann average).[4,5] Even for condensed phases, liquids and solids, where events are not isolated,

molecular dynamics provides a framework through which to understand the more complicated phenomena.

The methods of studying molecular dynamics are far from straightforward. The backbone of molecular dynamics is the Born-Oppenheimer approximation[6] which allows for the independent solution of the electronic and nuclear motions because of the different timescales of their motion. In the Born-Oppenheimer approximation, the nuclei are described as moving under forces of the other nuclei and the forces created by the electrons averaged over their very rapid motion. Therefore, to begin solving any molecular dynamics problem, first the potential energy corresponding to this force field must be found. This alone is extremely difficult and has only been done completely for the simplest systems.[7] A great deal of effort has gone into finding good approximations based on a small section of the entire potential energy surface.[8,9] This is still an open area of research and poses a great challenge.

Another complication is due to the breakdown of the Born-Oppenheimer approximation.[10] Because of the coupling between different electronic states, the nuclei cannot be assumed to be moving under the potential of just one electronic state. They have a probability of undergoing a transition from one electronic state to another, i.e., an electronically nonadiabatic transition. For most realistic systems these effects are important.[11] The phenomena resulting from this breakdown are given the names intersystem crossing or radiationless transitions.[12] Solving the problem exactly including the electronic and nuclear motion is far too hard. Several approximate methods have been

developed for dealing with this problem,[13,14,15] which have met with some success. The systems that we consider below have fairly accurate, known potentials and have well separated electronic states implying that the Born-Oppenheimer approximation should be valid.

The actual problem of solving the dynamics of the nuclear motion begins after obtaining an adequate potential energy surface or an approximation to it. Solving the dynamics rapidly becomes impossibly difficult for all but the simplest of systems without making approximations. For molecular scattering the only exact converged calculation to date was on $H + H_2$ [16] (not counting model systems such as collinear $H + H_2$). Looking at unimolecular dynamics, the understanding of something as simple as the photodissociation of formaldehyde[17,18] can evade complete understanding.

The numerous approximations that can be made to the nuclear motion will not be discussed here since most of them will not be discussed further. Two approximations should be mentioned since they will be discussed below. The first approximation, which is perhaps the most important in molecular dynamics, is to use classical mechanics[2,19] in lieu of quantum mechanics. It is hoped that since nuclei are relatively massive that this is a good approximation. This is not strictly true, of course, and the correspondence principle indicates when classical mechanics is truely valid. It is not appropriate to give a complete account here of the validity of classical mechanics for use in molecular dynamics. Below its validity for one particular application will be discussed in detail. The second approximation is the distorted wave Born approximation (DWBA).[20] DWBA is a first order perturbation theory

applied to scattering. The DWBA results approach the exact results as the magnitude of the perturbation goes to zero. One can see clearly the importance of approximations to the nuclear dynamics since exact calculations are essentially impossible for complicated systems. It is critical then to have some exact calculations so that approximate methods can be tested against them.

Here we consider two problems which represent perhaps respectively the simplest problem of molecular scattering and of unimolecular dynamics. In both cases reasonably accurate potentials are well known. The first results that will be presented in chapter II will be for the standard test problem, $H + H_2$ scattering. The goal of these calculations has been to develop techniques for performing essentially exact calculations which are easily generalizable to different systems. We have performed DWBA calculations[21] which at low energies have been the first quantitative confirmation of the 3-dimensional results on $H + H_2$.[16] Also, we have performed closely related exact scattering calculations[22] on the model collinear $H + H_2$ scattering. The methods that we have applied should be straightforward to extend to any collinear or 3-dimensional atom-diatom system where the potential is known. It appears very promising that these methods will allow exact quantum calculations in 3-dimensions for reacting systems besides $H + H_2$ for the first time.

In chapter III results are presented for absorption of very intense infrared radiation by a diatomic molecule.[23] Exact quantum and classical calculations are performed. An isolated diatomic molecule has essentially trivial dynamics since there is only one vibrational degree

of freedom. The interesting aspect of this problem is that we examine the coherent absorption[24] process itself in detail. In order to understand how molecules are prepared in highly excited states by the absorption of very intense light, the actual absorption process must be studied since time dependent perturbation theory is not valid for very high intensities. Even a simple problem of a diatom in a laser field proved interesting. A diatomic molecule is a convenient system to study simple multiphoton and overtone processes which are important even in the initial excitation of larger systems to high energies. Also, we were able to gain some insight into the validity of using classical mechanics to study the infrared absorption of small molecules.

II. Reactive scattering

A. Introduction

Until about 20 years ago Transition State Theory[4],[5],[25] was the only way to obtain numerical estimates of bimolecular reactive rate constants. Due to developments in scattering theory[26] and numerical methods[27], it is now becoming possible to test the statistical assumptions of transition state theory and directly calculate state to state transition probabilities and rate constants. Even with all of the progress in computational technology and a large amount of effort from many groups[28],[29], it is still very difficult to do molecular reactive scattering calculations. Essentially all reactive scattering calculations have been for atom – diatom systems. Even within this narrow category, a vast majority of the calculations[30] have been limited to collinear models and then mostly for $H + H_2$ scattering. All of the reactions considered in this chapter will be assumed to have an isolated, electronically adiabatic Born – Oppenheimer[6] potential energy surface.

One of the serious complications in reactive scattering is that the natural coordinate system for the reactants in the entrance channel is different from that for the products in the exit channel[31]. It is difficult to define a consistent, well behaved set of coordinates for the entire reaction. If a different set of coordinates is used for different parts of the reaction, they must eventually be matched[32]. The purpose of our work has been to develop methods which avoid many of

these complications. This is done by using an over complete basis which includes basis functions localized in each arrangement channel. The interaction between the different arrangement channels is accounted for using an exchange kernel. These exchange interactions are analogous to the treatment of interactions between electrons in Hartree – Fock theory[33]. The original idea was first developed by Miller[22a] based on a variational method. This method can yield essentially exact results. Here, we also make use of a distorted wave Born approximation (DWBA), a first order perturbation theory, version of this formalism which was first developed by Hubbard, Shi, and Miller[34].

Here we apply this exact scattering method to collinear $H + H_2$ reactive scattering and the DWBA method to three dimensional $H + H_2$[21]. At low energies, i.e., in the threshold region to reaction, one would expect DWBA results to be very accurate since reaction should only be a small perturbation on the dynamics. Previous DWBA calculations in molecular scattering[35-64], many were for three dimensional $H + H_2$, yielded results which were in error by as much as several orders of magnitude. They often yield surprisingly accurate relative cross sections, though, which has found use[65] in determining vibrational and rotational final state distributions for many reactions through Franck – Condon methods[66-68]. In all of these previous molecular applications, the nonreactive distorted wavefunctions are determined from a single channel elastic scattering calculation with the only difference being how well the vibrations and rotations are accounted for adiabatically and therefore what elastic potential is used. For example, in much of the work of S. H. Suck and coworkers[51-57], the asymptotic molecular

wavefunctions are assumed frozen throughout the collision, and the elastic potentials are obtained by averaging the full potential over the frozen wavefunctions (DWBA – FM for frozen molecule). Two somewhat more accurate treatments have been developed by Tang, Poe, Sun, Choi, and coworkers[42-50] and also by Clary and Connor[59-64]. In the first, vibrational wavefunctions are allowed to distort adiabatically to the presence of the incident atom[42-45,59-63] (DWBA – VA for vibrationally adiabatic), and in the second the molecular wavefunction is taken as a product of separately determined vibrationally and rotationally adiabatic wavefunctions[46-49,64] (DWBA – RA for rotationally adiabatic). Very recently, Sun et. al.[50] have improved on previous DWBA results substantially by allowing the molecular wavefunction to be fully adiabatic (ATM, adiabatic T matrix theory). Many, though not all, of the above applications are actually approximate forms of DWBA since the wavefunctions in the reactant and product arrangement channels are calculated at different levels of approximation.

The major difficulty with the previous DWBA methods is that they failed to calculate the nonreactive wavefunction accurately enough. The nonreactive wavefunction in the interaction region cannot be described accurately enough using only one diatomic molecular wavefunction even if there is only one diatomic state energetically allowed asymptotically. Here we solve for the nonreactive wavefunction using coupled channel methods which yield essentially exact nonreactive wavefunctions. This idea of using coupled channel distorted wavefunctions was developed independently by Emmons and Suck[58], who presents the formalism for three dimensional reactive collisions, and by Hubbard, Shi, and Miller[34], who

present a formalism for collinear atom − diatom collisions with an application to collinear $H + H_2$ with excellent results.

For collinear $H + H_2$ there have been many quantum mechanical studies done before[69-79]. Our method based on Miller's[22a] variational method offers the advantage of being straightforward to extend to other more complicated systems. There have been three previous applications[22b-d] based on Miller's variational formalism[22a]. The first by Wolken and Karplus[22d] for three dimensional $H + H_2$ included only the ground vibrational state in the couple channel expansion for H_2, so they did not obtain converged results. The other applications by Garrett and Miller[22b] and Adams and Miller[22c], both for collinear $H + H_2$, differed from our approach in two respects. First they used in their expansion for the nonreactive wave function the ground vibrational state of H_2 and square integrable functions to account for the energetically forbidden, i.e., closed, asymptotic vibrational channels. In our approach, we expand the wavefunction in both open and closed vibrational states of H_2. Our approach has the advantage of not requiring modification for calculations at higher energies with more than one open channel and of not being dependent on the choice of square integrable functions. The second difference is that both Garrett and Miller[22b], and Adams and Miller[22c] expand the exchange kernel operator, $\hat{V}_{ex}(R,R')$ over a basis set. We instead show how $\hat{V}_{ex}(R,R')$ can be written in terms of the energy independent exchange kernel $W_{ex}(R,R')$ which was first defined by Hubbard, Shi, and Miller[34] in their DWBA calculation. This has the advantage that $W_{ex}(R,R')$ does not have to be recalculated at different energies. Also, we evaluate $W_{ex}(R,R')$ on a grid without contracting it

onto a basis, so that our results are independent of any basis
functions.

Here, we extend the coupled channel distorted wave, DWBA − CC
approach of Hubbard, Shi, and Miller[34] to the three dimensional H + H_2
reaction, making detailed comparisons with accurate quantum results.
Since we account exactly for the nonreactive wavefunction, we should and
do obtain excellent aggreement with the exact quantum results for
energies in the threshold region where reaction probabilities are not
too large. At energies where the reaction probabilities are less than
about 0.1, the results converged with respect to the addition of more
molecular basis functions. At higher energies we found, as Hubbard,
Shi, and Miller[34] found in the collinear case, that the probabilities
became unstable with respect to the addition of more basis functions.
We also introduce a very accurate approximation to DWBA − CC through the
use of the coupled states approximation, DWBA − CS. This work
represents the first quantitative comparision with the exact quantum
results of Schatz and Kuppermann[16] for three dimensional H + H_2 on the
Porter − Karplus[80] potential energy surface.

We also present results for "exact" calculations for collinear H +
H_2 scattering on the Porter − Karplus[80] potential surface with
comparisons to other quantum mechanical calculations. We perform our
calculations over a very large range of energies from the deepest
tunnelling region to energies with three open asymptotic vibrational
channels. Over this whole range cf energies we obtained excellent
agreement with previous calculations. These results are very
encouraging for a method which is apparently straightforward to extend

to other systems.

B. Theory

1. Atom — diatom scattering formalism

Here we develop a scattering formalism based on the variational method of Miller[22a] specific to atom — diatom scattering at energies below the energy required for three separate atoms. In this section the discussion will remain very general with no reference to the specific coordinate system or dimensionality. Below we will describe the specifics for both collinear and 3 — dimensional $H + H_2$.

a. Expansion of the wavefunction and definition of the exchange operator

For $A + BC$ scattering, assuming that the total energy is insufficient for three separated atoms, there are, in general, three asymptotic arrangements possible, $A + BC$, $B + AC$, and $C + AB$, although some of these may not be energetically allowed at low scattering energies. For collinear atom — diatom scattering there are only two possible arrangements, but most of the rest of our development follows with this in mind with other exceptions noted where necessary. Within each of these arrangements the diatom asymptotically can be in different internal states, n, again with the constraint that there be enough energy. In keeping with the common terminology we will refer to energetically allowed asymptotic states (including arrangements, diatom internal states, and orbital angular momentum, if appropriate) as open channels and energetically forbidden asymptotic states as closed

channels.

Wa first expand the wavefunction,

$$|\Psi_{n_i}^a> = \sum_n |\phi_n^1>|f_{n+n_i^a}^1> + \sum_{n'} |\phi_{n'}^2>|f_{n'+n_i^a}^2> + \sum_{n''} |\phi_{n''}^3>|f_{n''+n_i^a}^3>, \quad \text{(II.1)}$$

where $|\phi_n^b>$ is the direct product of the (vibrational and rotational) molecular wavefunction for the isolated diatom for arrangement b and of the orbital angular momentum state with n representing the combined index which describes the product uniquely and $|f_{n+n_i^a}^b>$ is the corresponding radial wavefunction assuming initial state n_i in arrangement channel a. The exact form of $|\phi_n^b>$ will depend on the dimensionality and on the particular coordinate system. Note that in the collinear atom – diatom case there are only two arrangements possible. This expansion is over complete, but this should cause no problems for reasonable expansions since asymptotically the basis functions are well separated. We will need to account for the nonorthogonality of the $|\phi_n>$ in different arrangement channels.

The scattering wavefunction satisfies the equation,

$$(\hat{H} - E) |\Psi_{n_i}^a> = 0, \quad \text{(II.2)}$$

where $\hat{H}$ is the Hamiltonian operator. Taking eqn. (II.2) we multiply from the left by $<R^b|<\phi_{n_f}^b|$ to give,

$$<R^b|<\phi_{n_f}^b| \hat{H} - E |\Psi_{n_i}^a> = 0, \quad \text{(II.3)}$$

where $<\phi_{n_f}^b|$ is defined below eqn. (II.1) and $<R^b|$ is the translational coordinate corresponding to the internal state $<\phi_{n_f}^b|$ which is included so that the function with which we project covers the entire space. By

doing this we are projecting out the final state and thus examining the coupling into this state. Now combining eqn. (II.1) with (II.3) gives,

$$\sum_n <R^b| <\phi^b_{n_f}|\hat{H} - E|\phi^1_n> |f^1_{n+n^a_i}> + \sum_{n'} <R^b| <\phi^b_{n_f}|\hat{H} - E|\phi^2_{n'}> |f^2_{n'+n^a_i}>$$

$$\sum_{n''} <R^b| <\phi^b_{n_f}|\hat{H} - E|\phi^3_{n''}> |f^3_{n''+n^a_i}> = 0$$

(II.4)

The b th term of eqn. (II.4) accounts for coupling within the same arrangement channel, i.e., the elastic and inelastic effects. The other two terms account for the rearrangement or reactive part of the interaction. We define the exchange operator,

$$\hat{v}^{bc}_{n_f n'} = <\phi^b_{n_f}| \hat{H} - E |\phi^c_{n'}>,$$

(II.5)

with b ≠ c.

We will first solve a zero order equation to account for all the elastic and inelastic nonreactive effects exactly,

$$\sum_n <R^a| <\phi^a_{n_f}| \hat{H} - E |\phi^a_n> |^o f^a_{n+n^a_i}> = 0,$$

(II.6)

where $|^o f^a_{n+n^a_i}>$ is the "exact" nonreactive wavefunction. We solve this equation by direct numerical integration. We use this zero order wavefunction as a distorted wavefunction and the exchange operator accounts for the interactions responsible for rearrangement.

The formal solution for the full wavefunction can be written down using the set of coupled Lippman – Schwinger type equations,

$$|f^b_{n+n^a_i}> = \delta_{ba}|^o f^b_{n+n^a_i}> + \sum_{n',n''} {}^o G^b_{nn'} \hat{v}^{bc}_{n''n'} |f^c_{n'+n^a_i}>$$

$$+ \sum_{n',n''} {}^o G^b_{nn'} \hat{v}^{bd}_{n''n'} |f^d_{n'+n^a_i}>,$$

(II.7)

with equivalent expressions for c and d where b ≠ c ≠ d, δ_{ba} is the

standard Kroneker delta function and $^oG_{nn'}^b$ is the zero order,

nonreactive Greens function which is described in detail in Appendix

II.A. This set of coupled equations can also be written in matrix form,

$$
\begin{pmatrix} |f^1_{n+n_i^a}> \\ |f^2_{n+n_i^a}> \\ |f^3_{n+n_i^a}> \end{pmatrix} = \begin{pmatrix} \delta_{a1}\ |^of^1_{n+n_i^a}> \\ \delta_{a2}\ |^of^2_{n+n_i^a}> \\ \delta_{a3}\ |^of^3_{n+n_i^a}> \end{pmatrix} + \sum_{n'n''} \begin{pmatrix} ^oG^1_{nn''} & 0 & 0 \\ 0 & ^oG^2_{nn''} & 0 \\ 0 & 0 & ^oG^3_{nn''} \end{pmatrix} \tag{II.8}
$$

$$
\begin{pmatrix} 0 & \hat{v}^{12}_{n''n'} & \hat{v}^{13}_{n''n'} \\ \hat{v}^{21}_{n''n'} & 0 & \hat{v}^{23}_{n''n'} \\ \hat{v}^{31}_{n''n'} & \hat{v}^{32}_{n''n'} & 0 \end{pmatrix} \begin{pmatrix} |f^1_{n+n_i^a}> \\ |f^2_{n+n_i^a}> \\ |f^3_{n+n_i^a}> \end{pmatrix} \quad ,
$$

or using vector notation for the arrangement indices,

$$
|\underset{\sim}{f}_{n+n_i^a}> = |^o\underset{\sim}{f}_{n+n_i}> + \sum_{n'n''} {}^o\underset{\sim}{G}_{nn''} \hat{\underset{\sim}{v}}_{n''n'} |\underset{\sim}{f}_{n+n_i^a}>. \tag{II.9}
$$

This equation can be solved iteratively for $|\underset{\sim}{f}_{n+n_i^a}>$ to give the
infinite sum,

$$
|\underset{\sim}{f}_{n+n_i^a}> = |^o\underset{\sim}{f}_{n+n_i}> + \sum_{n'n''} {}^o\underset{\sim}{G}_{nn''} \hat{\underset{\sim}{v}}_{n''n'} |^o\underset{\sim}{f}_{n+n_i}> \tag{II.10}
$$

$$
+ \sum_{n'n''n'''n^0} {}^o\underset{\sim}{G}_{nn''} \hat{\underset{\sim}{v}}_{n''n'''} {}^o\underset{\sim}{G}_{n'''n^0} \hat{\underset{\sim}{v}}_{n^0n'} |^o\underset{\sim}{f}_{n'+n_i}> + \cdots
$$

which can be formally summed to yield,

$$
|\underset{\sim}{f}_{n+n_i^a}> = |^o\underset{\sim}{f}_{n+n_i}> + \sum_{n'n''n'''} {}^o\underset{\sim}{G}_{nn''} (\underset{\sim}{\delta}_{mm'} - \sum_{m'} \hat{\underset{\sim}{v}}_{mm'} {}^o\underset{\sim}{G}_{m'm'})^{-1}_{n''n'''}
$$

$$
\widetilde{\underset{\sim}{v}}_{n'''n'} |^o\underset{\sim}{f}_{n'+n_i}>, \tag{II.11}
$$

where the matrix inverse is taken over the matrix of the combined index of internal state labels and arrangement index. From this equation we get the transition matrix,

$$T_{n''n'} = \sum_{n'''} (\delta_{mm'} - \sum_{m''} \hat{V}_{mm''} \, {}^o G_{m''m'})^{-1}_{n''n'''} \, \hat{V}_{n'''n'}.$$ (II.12)

b. Relationship between $\hat{V}_{nn'}$ and $W_{nn'}$ operators

First we take the Hamiltonian and write it as,

$$\hat{H} = \hat{K}_b + \hat{V}_b + \hat{h}_b,$$
$$\hat{h}_b = \hat{k}_b + \hat{v}_b,$$ (II.13)

where $\hat{K}_b$ is the translational kinetic energy operator relative to arrangement b, $\hat{k}_b$ is the isolated diatomic kinetic energy operator, $\hat{v}_b$ is the asymptotic diatomic vibrational potential, $\hat{V}_b$ is the potential energy operator with $\hat{v}_b$ subtracted off plus the orbital angular momentum kinetic energy operator. It follows that $\hat{h}_b$ is the asymptotic diatomic Hamiltonian operator so that,

$$\hat{h}_b \, |\phi_n^b\rangle = \epsilon_n^b \, |\phi_n^b\rangle,$$ (II.14)

where ϵ_n^b is the n th diatomic eigenvalue for arrangement b since h_b does not operate on the orbital angular momentum part of $|\phi_n^b\rangle$. Using the definition of the exchange operator, eqn. (II.5), along with eqns. (II.13) and (II.14), we get,

$$\sum_n \hat{v}_{n_f n}^{ba} \, |{}^o f_{n+n_i}^a\rangle = \sum_n \langle \phi_{n_f}^b | \, \hat{H} - E \, |\phi_n^a\rangle |{}^o f_{n+n_i}^a\rangle,$$

$$= \sum_n \langle \phi_{n_f}^b | \, \hat{K}_a + \hat{V}_a + \hat{h}_a - E \, |\phi_n^a\rangle |{}^o f_{n+n_i}^a\rangle,$$

$$= \sum_n \langle \phi_{n_f}^b | \; \hat{K}_a - \hat{V}_a - E_a \; | \phi_n^a \rangle |^o f_{n+n_i}^a \rangle, \quad (II.15)$$

with $E_a = E - \epsilon_n^a$. We know that the nonreactive wavefunction satisfies eqn. (II.6) which combines with eqns. (II.13) and (II.14) to give,

$$\sum_n \langle R^a | \langle \phi_{n_f}^a | \; \hat{K}_a + \hat{V}_a - E_a \; | \phi_n^a \rangle |^o f_{n+n_i}^a \rangle = 0,$$

$$\sum_n \langle R^a | \langle \phi_{n_f}^a | \phi_n^a \rangle (\hat{K}_a - E_a) |^o f_{n+n_i}^a \rangle + \sum_n \langle R^a | \langle \phi_{n_f}^a | \hat{V}_a | \phi_n^a \rangle |^o f_{n+n_i}^a \rangle = 0$$

which can be rearranged to give,

$$(\hat{K}_a - E_a) |^o f_{n_f+n_i}^a \rangle = - \sum_n V_{n_f n}^a \; |^o f_{n+n_i}^a \rangle, \quad (II.16)$$

since $\langle \phi_{n_f}^a | \phi_n^a \rangle = \delta_{n_f,n}$ and we define $V_{n'n}^a = \langle \phi_{n'}^a | \hat{V}_a | \phi_n^a \rangle$. Combining this with eqn. (II.15) gives,

$$\sum_n \hat{V}_{n_f n}^{ba} |^o f_{n+n_i}^a \rangle = \sum_n [\langle \phi_{n_f}^b | \phi_n^a \rangle (-\sum_{n'} V_{nn'}^a |^o f_{n'+n_i}^a \rangle) + \langle \phi_{n_f}^b | \hat{V}_a | \phi_n^a \rangle |^o f_{n+n_i}^a \rangle]$$

$$= \sum_n \langle \phi_{n_f}^b | \hat{V}_a | \phi_n^a \rangle |^o f_{n+n_i}^a \rangle - \sum_n \sum_{n'} \langle \phi_{n_f}^b | \phi_n^a \rangle V_{nn'}^a |^o f_{n'+n_i}^a \rangle$$

$$= \sum_n [\langle \phi_{n_f}^b | \hat{V}_a | \phi_n^a \rangle - \sum_{n'} \langle \phi_{n_f}^b | \phi_{n'}^a \rangle V_{n'n}^a] |^o f_{n+n_i}^a \rangle$$

$$\sum_n \hat{V}_{n_f n}^{ba} |^o f_{n+n_i}^a \rangle = \sum_n W_{n_f n}^{ba} |^o f_{n+n_i}^a \rangle, \quad (II.17)$$

where we have defined the energy independent exchange operator $W_{n_f n}^{ba}$,

$$W_{n_f n}^{ba} = \langle \phi_{n_f}^b | \; \hat{V}_a \; | \phi_n^a \rangle - \sum_{n'} \langle \phi_{n_f}^b | \phi_{n'}^a \rangle V_{n'n}^a . \quad (II.18)$$

This operator was first defined by Hubbard, Shi, and Miller[34] for use in a collinear multichannel distorted wave calculation. We see in eqn.

(II.18) the effect of an overcomplete basis. If the sum over n' covers a complete set of states we can remove this complete set and see that $W^{ba}_{n_f n}$ identically vanishes. The over completeness of the basis should not cause any problems for the finite bases that we will be considering.

Next, we consider the exchange operator acting on the zero order Greens function matrix,

$$\sum_{n'} \hat{V}^{ab}_{n_f n'} \, {}^{0}G^{b}_{n'n_i} = \sum_{n'} \langle \phi^a_{n_f} | \hat{H} - E | \phi^b_{n'} \rangle \, {}^{0}G^{b}_{n'n_i} ,$$

$$= \sum_{n'} \langle \phi^a_{n_f} | \hat{K}_b + \hat{V}_b - E_b | \phi^b_{n'} \rangle \, {}^{0}G^{b}_{n'n_i} ,$$

$$= \sum_{n'} \langle \phi^a_{n_f} | \hat{K}_b - E_b | \phi^b_{n'} \rangle \, {}^{0}G^{b}_{n'n_i}$$

$$+ \sum_{n'} \langle \phi^a_{n_f} | \hat{V}_b | \phi^b_{n'} \rangle \, {}^{0}G^{b}_{n'n_i} . \qquad (II.19)$$

Now, we make use of the definition of the Greens function,

$$\sum_{n'} \langle R^b | \langle \phi^b_{n} | \, \hat{K}_b + \hat{V}_b - E_b \, | \phi^b_{n'} \rangle \, {}^{0}G^{b}_{n'n_i} = - \delta_{nn_i} ,$$

$$\langle R^b | (\hat{K}_b - E_b) \, {}^{0}G^{b}_{nn_i} + \sum_{n'} V^b_{nn'} \langle R^b | {}^{0}G^{b}_{n'n_i} = - \delta_{nn_i} . \qquad (II.20)$$

Combining eqns. (II.19) and (II.20) we get,

$$\sum_{n'} \hat{V}^{ab}_{n_f n'} \, {}^{0}G^{b}_{n'n_i} = \sum_{n'} \langle \phi^a_{n_f} | \phi^b_{n'} \rangle [- \delta_{n'n_i} - \sum_{n} V^b_{n'n} \, {}^{0}G^{b}_{nn_i}]$$

$$+ \sum_{n'} \langle \phi^a_{n_f} | \hat{V}_b | \phi^b_{n'} \rangle \, {}^{0}G^{b}_{n'n_i}$$

$$= - \langle \phi^a_{n_f} | \phi^b_{n_i} \rangle + \sum_{n'} \langle \phi^a_{n_f} | \hat{V}_b | \phi^b_{n'} \rangle \, {}^{0}G^{b}_{n'n_i}$$

$$- \sum_{n'n} \langle \phi^a_{n_f} | \phi^b_{n'} \rangle \, v^b_{n'n} \, {}^o G^b_{nn_i}$$

$$\sum_{n'} \hat{v}^{ab}_{n_f n'} \, {}^o G^b_{n'n_i} = \sum_{n'} W_{n_f n'} \, {}^o G^b_{n'n_i} - S^{ab}_{n_f n_i} \, , \qquad (II.21)$$

where we have used eqn. (II.18) and defined the overlap matrix,

$$S^{ab}_{n_f n_i} = \langle \phi^a_{n_f} | \phi^b_{n_i} \rangle. \qquad (II.22)$$

Substituting eqns. (II.17) and (II.21) into eqn. (II.10) yields,

$$|\underset{n+n_i^a}{f}\rangle = |{}^o\underset{n+n_i^a}{f}\rangle + \sum_{n'n''n'''} \, {}^o G_{nn''} (\delta_{mm'} + S_{mm'}$$

$$- \sum_{m''} W_{mm''} \, {}^o G_{m''m'})^{-1}_{n''n'''} \, W_{n'''n'} \, |{}^o\underset{n'+n_i^a}{f}\rangle, \qquad (II.23)$$

where the notation implies that the inverse matrix is taken over the
combined arrangement and internal state indices then the n'', n'''
element is taken of the inverted matrix. In this form we have replaced
the energy dependent exchange operator $\hat{V}_{nn'}$ with an energy independent
operator $W_{nn'}$ while gaining an overlap term $S_{nn'}$. $W_{nn'}$ is just
dependent on the potential and the expansion basis functions $|\phi_n\rangle$. It
is this form on which we base our further development.

c. Determination of the reactance matrix, K, and the scattering
matrix, S

For the purpose of determining the wavefunction, we assume that the
wavefunction is real and, therefore, that asymptotically it fits real
boundary conditions. Below we show how to relate our solution with real
boundary conditions to the standard scattering boundary conditions and
thereby obtain the S matrix. The asymptotic form that we assume for the

wavefunction is,

$$\left| {}^{o}f_{n+n_i}^a \right> \sim \left| s_n^a \right> + \left| c_n^a \right> {}^{o}K_{nn_i}^a \ ,$$

$$\left| f_{n+n_i}^a{}_b \right> \sim \left| s_n^a \right> + \left| c_n^a \right> K_{nn_i}^a{}_b \ , \qquad\qquad (II.24)$$

where

$$s_n^a \equiv \left< R \middle| s_n^a \right> = \frac{\sin[k_n^a R_a - (J + j_a)\ \pi/2]}{|v|^{1/2}} \ ,$$

$$c_n^a \equiv \left< R \middle| c_n^a \right> = \frac{\cos[k_n^a R_a - (J + j_a)\ \pi/2]}{|v|^{1/2}} \ , \qquad\qquad (II.25)$$

with

$$|v| = \left| \frac{\hbar k_n^a}{\mu} \right| \ , \qquad \text{and} \qquad k_n^a = \left[\frac{2\mu(E - \epsilon_n^a)}{\hbar^2} \right]^{1/2} \ ,$$

for n being an energetically open channel where $K_{nn_i}^a b$ is the reactance matrix, ${}^{o}K_{nn_i}^a$ being the zero order, nonreactive, reactance matrix, v is the translational velocity, k_n is the asymptotic translational wave vector for internal state n and arrangement a, and μ is the reduced mass for translation in the appropriate arrangement channel. J is the total angular momentum quantum number and j_a is the rotational angular momentum quantum number in arrangement a. We have picked a representation of the angular momentum with J, and j_a and their projections. For collinear scattering both J and j_a are set to zero in this equation. The form for $\left| s_n \right>$ and $\left| c_n \right>$ in the asymptotic closed channels can be various linear combinations of exponentially growing and decaying terms depending on convenience. We will specify our choice below when we give more details of our specific calculations. The exact asymptotic form of the wavefunction affects the specific form of the

Greens function ,see appendix II.A.

In order to calculate the Greens function we also need the irregular solution for the nonreactive wavefunction, see appendix II.A. We are free to pick for the irregular wavefunction any solution which is linearly independent of the regular solution although its form will also affect the form of the Greens function. Here we will assume that the irregular nonreactive wavefunction asymptoticly goes as,

$$|{}^{o}g^{a}_{n+n_{1}}> ~ |c_{n}>,$$
(II.26)

where $|c_{n}>$ was defined in eqn. (II.25). As we show in appendix II.A, with these forms for the regular and irregular nonreactive wavefunctions, the asymptotic form for the Greens function becomes,

$$^{o}G^{a}_{nn'} ~ \frac{2}{\hbar} |c^{a}_{n}><^{o}f^{a}_{n+n'}|.$$
(II.27)

Given the asymptotic forms in eqns. (II.24) and (II.27), the asymptotic form of the total wavefunction, eqn. (II.23) becomes,

$$|f_{n+n_{1}}^{a}> ~ |s_{n}> + |c_{n}>^{o}g_{nn_{1}} + \frac{2}{\hbar} \sum_{n'n''n'''} |c_{n}><^{o}f_{nn''}|$$

$$(\delta_{mm'} + S_{mm'} - \sum_{m''} W_{mm''} {}^{o}G_{m''m'})^{-1}_{n''n'''} W_{n'''n'} |{}^{o}f_{n'+n_{1}}>,$$

$$|f_{n+n_{1}}^{a}> ~ |s_{n}> + |c_{n}>[{}^{o}g_{nn_{1}} + \frac{2}{\hbar} \sum_{n'n''n'''} <^{o}f_{nn''}|(\delta_{mm'}$$
(II.28)

$$+ S_{mm'} - \sum_{m''} W_{mm''} {}^{o}G_{m''m'})^{-1}_{n''n'''} W_{n'''n'} |{}^{o}f_{n'n_{1}}>,$$

and it follows that,

$$
\underset{\sim}{K}_{n'+n_i^a} = {}^o\underset{\sim}{K}_{nn_i^a} + \frac{2}{\not{K}} \sum_{n'n''n'''} <{}^o\underset{\sim}{f}_{nn'}| (\underset{\sim}{\delta}_{mm'} + \underset{\sim}{S}_{mm'}
$$

$$
- \sum_{m''} \underset{\sim}{W}_{mm''} \, {}^o\underset{\sim}{G}_{m''+m'})^{-1}_{n''n'''} \; \underset{\sim}{W}_{n'''n'} \; |{}^o\underset{\sim}{f}_{n'n_i}>. \qquad \text{(II.29)}
$$

Basically, most of the calculational effort goes towards calculating this reactance matrix.

Now, we will outline how the scattering matrix, S, is calculated from the reactance matrix, K. Asymptotically, the wavefunction only has finite density in·open channels therefore the S matrix is only defined for these transitions. If the wavefunction $|\underset{\sim}{f}_{n+n_i^b}>$ and the reactance matrix $\underset{\sim}{K}_{nn'}$ are considered matrices in the channel numbers, then we need to consider only the block of these matrices over the open channels. So, we begin with,

$$
|\underset{\sim}{f}^{oo}_{n+n_i^a}> \sim |\underset{\sim}{s}^o_n> + |\underset{\sim}{c}^o_n> \; \underset{\sim}{K}^{oo}_{nn_i} \; ,
$$

where the o or oo designate that only the open channels, n, are kept in the vectors or matrices. Now we take the position representation, eqn. (II.24), and replace the sines and cosines by the equivalent complex exponentials,

$$
\underset{\sim}{f}^{oo}_{n+n_i^a}(R) = <R|\underset{\sim}{f}^{oo}_{n+n_i^a}> \sim \frac{\sin[\underset{\sim}{k}_n R_a - (J+j_a)\frac{\pi}{2}]}{|v|^{1/2}} + \frac{\cos[\underset{\sim}{k}_n R_a - (J+j_a)\frac{\pi}{2}]}{|v|^{1/2}} \underset{\sim}{K}^{oo}_{nn_i},
$$

$$
\sim |v|^{-1/2} \; [\; \frac{e^{i[\underset{\sim}{k}_n R_a - (J+j_a)\frac{\pi}{2}]} - e^{-i[\underset{\sim}{k}_n R_a - (J+j_a)\frac{\pi}{2}]}}{2i}
$$

$$
+ \frac{e^{i[\underset{\sim}{k}_n R_a - (J+j_a)\frac{\pi}{2}]} + e^{-i[\underset{\sim}{k}_n R_a - (J+j_a)\frac{\pi}{2}]}}{2} \; \underset{\sim}{K}^{oo}_{nn_i} \;]
$$

$$
\sim |v|^{-1/2} \; [\; \frac{-e^{-i[\underset{\sim}{k}_n R_a - (J+j_a)\frac{\pi}{2}]}}{2i} \; (\delta_{nn_i} - i\underset{\sim}{K}^{oo}_{nn_i})
$$

$$- \quad + \frac{e^{i[k_n R_a - (J+j_a)\frac{\pi}{2}]}}{2i} (\delta_{nn_i} + i \underset{\sim}{K}_{nn_i}^{oo})]. \qquad (II.30)$$

Now rearranging eqn. (II.30) we obtain,

$$\sum_{n'} 2i f_{n+n'}^{oo}(R)(\delta_{nn'} - i \underset{\sim}{K}_{nn'}^{oo})_{n'n_i}^{-1} \sim \frac{-e^{-i[k_n R_a - (J+j_a)\frac{\pi}{2}]}}{|v|^{1/2}} + \frac{e^{i[k_n R_a - (J+j_a)\frac{\pi}{2}]}}{|v|^{1/2}}$$

$$\sum_{n'} (\delta_{nn'} + i \underset{\sim}{K}_{nn'}^{oo})(\delta_{nn'} - i \underset{\sim}{K}_{nn'}^{oo})_{n'n_i}^{-1} . \qquad (II.31)$$

We compare eqn. (II.31) with the equation for the scattering wavefunction in terms of the S matrix[81],

$$\underset{\sim}{f}_{n+n_i}^{+}(R) \sim \frac{-e^{-i[k_n R_a - (J+j_a)\frac{\pi}{2}]}}{|v|^{1/2}} + \frac{e^{i[k_n R_a - (J+j_a)\frac{\pi}{2}]}}{|v|^{1/2}} \underset{\sim}{S}_{nn_i} , \qquad (II.32)$$

to identify,

$$\underset{\sim}{f}_{n+n_i}^{+}(R) = 2i \sum_{n'} \underset{\sim}{f}_{n+n'}(R) (\delta_{mm'} - i \underset{\sim}{K}_{mm'}^{oo})_{n'n_i}^{-1} , \qquad (II.33a)$$

$$\underset{\sim}{S}_{nn_i} = \sum_{n'} (\delta_{nn'} + i \underset{\sim}{K}_{nn'}^{oo}) (\delta_{mm'} - i \underset{\sim}{K}_{mm'}^{oo})_{n'n_i}^{-1} . \qquad (II.33b)$$

We use eqn. (II.33b) to obtain the S matrix from the K matrix obtained from eqn. (II.29).

d. The DWBA limit

In this section we will discuss how to take the first order perturbation (DWBA) limit of the scattering formalism developed in sections a-c. We will show how this is equivalent to a multichannel version of DWBA developed by Hubbard, Shi, and Miller[34]. DWBA is basically first order order perturbation theory, so we need to keep the

perturbation, in this case reaction, only through first order. Starting with the T matrix defined in eqn. (II.12), we constuct,

$$\hat{T}^{DWBA}_{n''n'} = \hat{V}_{n''n'} \, , \tag{II.34}$$

which is just the first reactive contribution to the infinite sum in eqn. (II.10). Based on the DWBA form of the T matrix in eqn. (II.34), the reactance matrix, K, becomes,

$$K^{DWBA}_{nn_i} = {}^0K_{nn_i} + \frac{2}{\hbar} \sum_{n''n'} \langle {}^0f_{n+n''} | W_{n''n'} | {}^0f_{n'+n_i} \rangle \, , \tag{II.35}$$

where the first term is diagonal in arrangement indices, only a nonreactive contribution, and the second term is purely off diagonal in arrangement indices, only a reactive contribution.

When calculating the S matrix from this DWBA K matrix, we need to include the reactive part of the K matrix only through first order to be consistant with the approximation to the T matrix. First we write the open block of the K matrix separating the reactive and nonreactive contributions,

$$DWBA K^{oo}_{nn_i} = {}^0K^{oo}_{nn_i} + {}^RK^{oo}_{nn_i} \, ,$$

where

$$^RK^{oo}_{nn_i} = \frac{2}{\hbar} \sum_{n''n'} \langle {}^0f_{nn''} | W_{n''n'} | {}^0f_{n'n_i} \rangle \, .$$

It should be noted that while we only need the open block of ${}^RK$, the sum over n'' and n' covers both open and closed channels. Then we substitute this expression for K into the equation for the S matrix eqn. (II.33b),

$$S_{nn_i} = \sum_{n'} (\delta_{nn'} + i^o K^{oo}_{nn'} + i^R K^{oo}_{nn'})(\delta_{mm'} - i^o K^{oo}_{mm'} - i^R K^{oo}_{mm'})^{-1}_{n'n_i} . \tag{II.36}$$

Next, we expand this equation assuming $^R K^{oo}_{nn'}$ is small,

$$S_{nn_i} = \sum_{n'n''} (\delta_{nn'} + i^o K^{oo}_{nn'} + i^R K^{oo}_{nn'})(\delta_{mm'} - i^o K^{oo}_{mm'})^{-1}_{n'n''}$$

$$[\delta_{mm'} - i\sum_m {}^R K^{oo}_{mm'} (\delta_{kl} - i^o K^{oo}_{kl})^{-1}_{m'm''}]^{-1}_{n''n_i} ,$$

$$\approx \sum_{n'} (\delta_{nn'} + i^o K^{oo}_{nn'})(\delta_{mm'} - i^o K^{oo}_{mm'})^{-1}_{n'n_i} + \sum_{n'} i^R K_{nn'}(\delta_{mm'} - i^o K^{oo}_{mm'})^{-1}_{n'n_i}$$

$$+ \sum_{n'n''n^0} (\delta_{nn'} + i^o K^{oo}_{nn'})(\delta_{mm'} - i^o K^{oo}_{mm'})^{-1}_{n'n''}(i^R K^{oo}_{n''n^0})$$

$$(\delta_{kl} - i^o K^{oo}_{kl})^{-1}_{n^0 n_i} , \tag{II.37}$$

where in the last expression we keep terms only through first order in $^R K^{oo}_{nn'}$. Rearranging eqn. (II.37), we get,

$$S_{nn_i} \approx \sum_{n'} (\delta_{nn'} + i^o K^{oo}_{nn'})(\delta_{mm'} - i^o K^{oo}_{mm'})^{-1}_{n'n_i} + \sum_{n'n''n^0} [(\delta_{nn'} - i^o K^{oo}_{nn'})$$

$$+ (\delta_{nn'} + i^o K^{oo}_{nn'})](\delta_{mm'} - i^o K^{oo}_{mm'})^{-1}_{n'n''}$$

$$(i^R K^{oo}_{n''n^0})(\delta_{kl} - i^o K^{oo}_{kl})^{-1}_{n^0 n_i}$$

$$S_{nn_i} \approx \sum_{n'} (\delta_{nn'} + i^o K^{oo}_{nn'})(\delta_{mm'} - i^o K^{oo}_{mm'})^{-1}_{n'n_i} \tag{II.38}$$

$$+ \sum_{n''n^0} (\delta_{mm'} - i^o K^{oo}_{mm'})^{-1}_{nn''}(2i^R K^{oo}_{n''n^0})(\delta_{kl} - i^o K^{oo}_{kl})^{-1}_{n^0 n_i} .$$

The first term of the expression in eqn. (II.38) contributes only to the nonreactive part of the S matrix, i.e., the terms is purely diagonal in

arrangement index. In the second term, $^oK_{mm'}^{oo}$, is purely diagonal in arrangement index while $^RK_{n''n}^{oo}{}_0$ is purely off diagonal. As a result, the second term is purely off diagonal and therefore only contributes to the reactive part of S. The nonreactive part of S to first order is just the contribution from the purely nonreactive scattering calculation. Higher order contributions, though, effect both the reactive and the nonreactive part of S. We can now explicitly write a reactive block of the first order S matrix as,

$$^{DWBA}S_{nn_1}^{ba} = \sum_{n''n_0} 2i(\delta_{mm'} - i^oK_{mm'}^{bb})^{-1}_{n'n''} {}^R K_{n''n_0}^{ba}(\delta_{kl} - i^oK_{kl}^{aa})^{-1}_{n_0 n_1}, \quad (II.39)$$

where the DWBA reactive K matrix is given in, the second term of eqn. (II.35), and we only allow the channel numbers to vary over the open channels.

Now, we want to show how this derivation is exactly equivalent to a standard DWBA treatment with a multichannel nonreactive distorted wavefunction. This multichannel DWBA treatment was first developed by Hubbard, Shi, and Miller[34] for application to collinear H + H_2. We begin with the standard DWBA expression for the S matrix,

$$S_{n_f n_1}^{ba} = (\frac{-i}{\hbar}) <{}^o\psi_{n_f}^{b} {}^-| \hat{H} - E |{}^o\psi_{n_1}^{a} {}^+>, \quad (II.40)$$

where $\hat{H}$ is the total Hamiltonian operator, E is the total energy and $^o\psi$ is the distorted wavefunction with the correct incoming or outgoing boundary conditions. In this case we will pick for the distorted wavefunction the "exact" multichannel nonreactive wavefunction defined in eqn. (II.6). We now expand the distorted wavefunction in terms of the $|\phi_n^a>$ defined below eqn. (II.1),

$$S^{ba}_{n_f n_i} = (\frac{-1}{\hbar}) \sum_{nn'} <^o f^b_{n_f n} {}^-|<\phi^b_n| \hat{H} - E |\phi^a_{n'}>|^o f^a_{n'n_i} {}^+>, \tag{II.41}$$

where each expansion only includes one arrangement since there is no coupling between the arrangements in the distorted wavefunctions as seen in eqn. (II.6). Using eqn. (II.33a) and a similar expansion for f^-,

$$\left|f^-_{n_f n}\right> = 2i \sum_{n'} \left|f_{n'n}\right> (\delta_{mm'} + iK^{oo}_{mm'})^{-1}_{n_f n'}, \tag{II.42}$$

we obtain from eqn. (II.4),

$$S^{ba}_{n_f n_i} = (\frac{4i}{\hbar}) \sum_{nn'n''n'''} (\delta_{mm'} - i^o K^{bb}_{mm'})^{-1}_{n_f n''} <^o f^b_{n''n}|<\phi^b_n|\hat{H} - E|\phi^a_{n'}>$$

$$|^o f^a_{n'n'''}>(\delta_{mm'} - i^o K^{aa}_{mm'})^{-1}_{n'''n_i}, \tag{II.43}$$

where n'' and n''' only vary over the open channels, but n and n' vary over open and closed channels. Substituting from eqn. (II.5) this equation becomes,

$$S^{ba}_{n_f n_i} = (\frac{4i}{\hbar}) \sum_{nn'n''n'''} (\delta_{mm'} - i^o K^{bb}_{mm'})^{-1}_{n_f n''} <^o f^b_{n''n}|\hat{V}^{ba}_{nn'}|^o f^a_{n'n'''}>$$

$$(\delta_{mm'} - i^o K^{aa}_{mm'})^{-1}_{n'''n_i}.$$

Making use of eqn. (II.17), we obtain,

$$S^{ba}_{n_f n_i} = (\frac{4i}{\hbar}) \sum_{nn'n''n'''} (\delta_{mm'} - i^o K^{bb}_{mm'})^{-1}_{n_f n''} <^o f^b_{n''n}|W^{ba}_{nn'}|^o f^a_{n'n'''}>$$

$$(\delta_{mm'} - i^o K^{aa}_{mm'})^{-1}_{n'''n_i}. \tag{II.44}$$

Now, based on the reactive part of eqn. (II.35), eqn. (II.44) becomes,

$$\text{DWBA}_{S}{}^{ba}_{n_f n_i} = 2i \sum_{n'' n'''} (\delta_{mm'} - i^{o}K^{bb}_{mm'})^{-1}_{n_f n''} \ R_{K}{}^{ba}_{n'' n'''}$$

$$(\delta_{mm'} - i^{o}K^{aa}_{mm'})^{-1}_{n''' n_i} , \tag{II.45}$$

where based on the definition of S, the channel indices only vary over the open channels. Comparing eqn. (II.45) with eqn. (II.39), we see that we have shown how this development of a multichannel DWBA formalism is, as expected, equivalent to the DWBA limit of the scattering formalism developed in sections a–c above.

2. Coupled channel DWBA for three dimensional $H + H_2$ reactive scattering

In section ld we developed the general formalism for coupled channel DWBA. In this section we will give the specific representation of this formalism appropriate for three dimensional atom – diatom scattering. We will then show the symmetry decoupling for the symmetric $H + H_2$ reaction. We also develop an approximate method based on the coupled states approximation.

a. Three dimensional representation of coupled channel DWBA using body fixed coordinates

Six coordinates are needed to describe the atom – diatom system. To define our six coordinates, for each arrangement we pick $\vec{R}'_a$, the vector from atom A to the center of mass of the diatom BC, and $\vec{r}'_a$, the vector between atoms B and C. Next, it is convenient to mass weight the coordinates, so using the Delves[82,32] mass scaling, we define,

$$\vec{r}_a = c_a^{-1} \ \vec{r}'_a,$$
$$\vec{R}_a = c_a \ \vec{R}'_a,$$

(II.46)

where,

$$c_a = (\mu_{abc}/\mu_{bc})^{1/4}.$$

μ_{abc} is the reduced mass for the motion of atom A relative to the center of mass of the diatom BC, and μ_{bc} is the reduced mass of the relative motion of atom B to atom C,

$$\mu_{abc} = m_a (m_b + m_c)/(m_a + m_b + m_c),$$
$$\mu_{bc} = m_b m_c / (m_b + m_c),$$
(II.47)

where m_a, m_b, and m_c are the masses of atoms A, B, and C respectively.

The J^2 and J_z operators, where J^2 is the square of the total angular momentum operator and J_z is the operator for the projection of the total angular momentum on a space fixed z axis, commute with the Hamiltonian. We perform a standard partial wave analysis[81] of the wavefunction where we expand the wavefunction in terms of states with fixed J and M, the quantum numbers for the total angular momentum and the z axis projection of the total angular momentum,

$$\left| \Psi_{n_i b} \right> = \sum_{J=0}^{\infty} \sum_{M=-J}^{J} c_{JM} \left| \Psi_{n_i b}^{JM} \right>.$$
(II.48)

$\left| \Psi_{n_i b}^{JM} \right>$ is a simultaneous eigenfunction of J^2, J_z, and H which is possible since the operators commute. While it will not be explicitly shown, the c_{JM} are determined from the plane wave incoming flux which we use implicitly in section 2f when we give expressions for the differential and integral cross sections.

Now we are ready to express our wavefunction in terms of a

coordinate system. If we define a randomly oriented space fixed
coordinate system (x,y,z) with the origin at the center of mass of the
three atom system, the vectors, $\vec{r}_a$ and $\vec{R}_a$, defined in eqn. (II.46),
represent the six coordinates which are needed to describe the system.
We take the coordinate representation of our wavefunction in terms of
this coordinate system,

$$\langle \vec{r}_a \; \vec{R}_a | \Psi^{JM}_{n_i b} \rangle = \Psi^{JM}_{n_i b}(\vec{r}_a, \vec{R}_a).$$

(II.49)

Rather than now expanding our wavefunction in terms of complete sets of
eigenfunctions of the orbital and rotational angular momentum operators,
it is more convenient to rotate our coordinate system to a body fixed
coordinate system and to express the wavefunction and the projection of
the angular momentum in terms of this coordinate system following Schatz
and Kuppermann[32].

   We will rotate the space fixed coordinate system to a body fixed
coordinate system (X,Y,Z) again with its origin at the center of mass.
This body fixed coordinate system will have its Z axis oriented along
th\: R_a vector. It requires two angles θ_a and ϕ_a, the polar and
azimuthal angles of the Z axis in the (x,y,z) coordinate system, to
uniquely describe the rotation of the space fixed coordinate system into
the body fixed coordinate system. We are assuming that we do not
reorient the X and Y axes about the Z axis. In the body fixed
coordinate system the vector $\vec{R}_a$ becomes a single component R_a which is
the distance of atom A to the center of mass of the diatom BC.
Therefore, the wavefunction in this body fixed coordinate system is only
a function of four variables. Performing this rotation, the

wavefunction from eqn. (II.49) becomes,

$$\Psi^{JM}_{\substack{b\\n_i}}(\vec{r}_a,\vec{R}_a) = \sum_{\Omega_a=-J}^{J} (\frac{2J+1}{8\pi^2})^{1/2} D^J_{M\Omega_a}(\phi_a,\theta_a,0) \; \Psi^{J\Omega_a}_{\substack{b\\n_i}}(\vec{r}_a,R_a), \quad (II.50)$$

where $\Psi^{J\Omega_a}_{\substack{b\\n_i}}(\vec{r}_a,R_a)$ is the body fixed wavefunction, $D^J_{M\Omega_a}(\phi_a, \theta_a, 0)$ is a Wigner rotation matrix, the factor $[(2J+1)/8\pi^2]^{1/2}$ normalizes the Wigner rotation matrix, and Ω_a is the projection quantum number for the total angular momentum along the body fixed Z_a axis. In the rotating coordinate system the Z_a component of the orbital angular momentum is zero. So, Ω_a is also the Z_a axis projection quantum number for the rotational angular momentum of the diatom BC.

Next we expand our body fixed wavefunction in terms of a complete set of states representing the vibrational and rotational motion of the diatom in body fixed coordinates,

$$\Psi^{J\Omega_a}_{\substack{b\\n_i}}(\vec{r}_a,R_a) = \sum_{v_a=0}^{\infty} \sum_{j_a=|\Omega_a|}^{\infty} Y_{j_a\Omega_a}(\gamma_a,\psi_a) \frac{\phi_{v_aj_a}(r_a)}{r_a R_a} f^{Jv_aj_a\Omega_a}_{\substack{b\\n_i}}(R_a), \quad (II.51)$$

where v_a is the vibrational quantum number and j_a is the rotational quantum number. The sum over j_a begins at $|\Omega_a|$ since Ω_a is the projection of j_a along Z, so j_a cannot be smaller than this. $Y_{j_a\Omega_a}(\gamma_a,\psi_a)$ is a spherical harmonic which is the eigenfunction of j^2 and j_Z. γ_a is the angle between the $\vec{r}_a$ and $\vec{R}_a$ vectors, and ψ_a is the angle which orients the diatom about the Z axis. The $\phi_{v_aj_a}(r_a)$ are the vibrational eigenfunctions of the isolated diatom.

Based on this development, the position representation of the wavefunction defined in section 1, $|\phi^a_n\rangle|f^a_{n+n_i^b}\rangle$, is,

$$\langle \vec{r}_a \vec{R}_a | \phi_n^a \rangle | f^a_{n \leftarrow n_i^b} \rangle = (\frac{2J+1}{8\pi^2})^{1/2} \quad D^J_{M\Omega_a}(\phi_a,\theta_a,0) \quad Y_{j_a\Omega_a}(\gamma_a,\psi_a)$$

$$\frac{\phi_{v_a j_a}(r_a)}{r_a R_a} f^{J v_a j_a \Omega_a}_{n_i^b}(R_a), \quad \text{(II.52a)}$$

$$\phi_n^a(\phi_a,\theta_a,\gamma_a,\psi_a,r_a) = (\frac{2J+1}{8\pi^2})^{1/2} D^J_{M\Omega_a}(\phi_a,\theta_a,0) Y_{j_a\Omega_a}(\gamma_a,\psi_a) \frac{\phi_{v_a j_a}(r_a)}{r_a} ,$$

$$\text{(II.52b)}$$

$$f^a_{n \leftarrow n_i^b}(R_a) = f^{J v_a j_a \Omega_a}_{n_i^b}(R_a)/R_a , \quad \text{(II.52c)}$$

where we have assumed that the wavefunction represents only one partial wave. Our collective index, n^b, of section 1 becomes,

$$n^b \rightarrow \dot{v}_b, j_b, \Omega_b, \quad \text{(II.53)}$$

and we will often interchange the collective index for the complete set of indices throughout this section.

b. The Hamiltonian in body fixed coordinates and the solution for the nonreactive wavefunction

The derivation of the Hamiltonian in body fixed coordinates is given in detail by Schatz and Kuppermann[32] and Pack[83]. The complications come from the angular momentum terms of the kinetic energy. The angular momentum contribution to the kinetic energy in mass weighted, space fixed coordinates is,

$$\hat{K}_{Ang} = \frac{\hat{l}_a^2}{2\mu R_a^2} + \frac{\hat{j}_a^2}{2\mu r_a^2} , \quad \text{(II.54)}$$

where $\hat{l}_a$ is the orbital angular momentum operator for arrangement a, and $\hat{j}_a$ is the diatomic rotational angular momentum operator for arrangement a. First, we need to convert from a representation in terms of $\hat{l}_a$ and $\hat{j}_a$ to a representation in terms of $\hat{j}_a$ and $\hat{J}$ where $\hat{J}$ is the total angular momentum operator. The $\hat{l}_a$ operator can be written in terms of the $\hat{J}$ and

$\hat{j}_a$ operators,

$$\hat{l}_a^2 = |\hat{J} - \hat{j}_a|^2 = \hat{J}^2 + \hat{j}_a^2 - (\hat{J} \cdot \hat{j}_a + \hat{j}_a \cdot \hat{J}).$$

Next $\hat{J}$ and $\hat{j}_a$ need to be expressed in terms of the body fixed coordinates. Schatz and Kuppermann[32] give a detailed table of angular momentum operators in both space fixed and body fixed coordinates. The result is that the angular momentum contribution to the kinetic energy becomes,

$$\hat{K}_{Ang}^{BF} = \frac{\hat{j}_a^2}{2\mu r_a^2} + \frac{1}{2\mu R_a^2} [\hat{J}^2 + \hat{j}_a^2 - 2\hat{j}_{aZ}\hat{J}_Z - (\hat{j}_a^- \hat{J}_a^+ + \hat{j}_a^+ \hat{J}_a^-)], \tag{II.55}$$

where the + and − indicate raising and lowering operators in terms of the body fixed coordinates. The terms with the raising and lowering operators, which connect adjacent Ω_Z states, are due to centrifugal coupling from our conversion to a rotating body fixed coordinate system.

The potential energy is only a function of the relative positions of the three atoms determined by the variables r_a, R_a, and γ_a; i.e. the potential only depends on the shape and size of the triangle formed by the three atoms not on the orientation of the triangle in space. As a result, V does not couple different Ω_a. The fact that the only off diagonal contribution in Ω_a of the body fixed Hamiltonian is due to the centrifugal coupling is the basis for the coupled states approximation to be discussed below.

Now, we are ready to give the body fixed three dimensional representation for the coupled equations for the nonreactive wavefunction given in eqn. (II.6). Starting with eqn. (II.6), we first express the body fixed position representation,

$$\int dr_a^3 dR_a^3 dr_a'^3 dR_a'^3 \sum_n \langle R_a'' | \langle \phi_{n_f}^a | r_a'^3 R_a'^3 \rangle \langle r_a'^3 R_a'^3 | \hat{H} - E | R_a^3 r_a^3 \rangle$$

$$\langle R_a^3 r_a^3 | \phi_n^a \rangle | {}^o f_{n+n_i}^a \rangle = 0, \qquad (II.56a)$$

where the superscript 3 indicates the entire three dimensional space spanned by the vector, and using eqns. (II.52) and (II.53),

$$\langle R_a'' | \langle \phi_{n_f}^a | r_a'^3 R_a'^3 \rangle = \delta(R_a'' - R_a') \left(\frac{2J+1}{8\pi^2}\right)^{1/2} D_{M\Omega_a'}^J(\phi_a, \theta_a, 0)$$

$$Y_{j_a' \Omega_a'}(\gamma_a', \psi_a') \frac{\phi_{v_a' j_a'}(r_a')}{r_a'} ,$$

$$\langle r_a'^3 R_a'^3 | \hat{H} - E | R_a^3 r_a^3 \rangle = \delta(\vec{r}_a - \vec{r}_a')\delta(\vec{R}_a - \vec{R}_a')\{ -\frac{\hbar^2}{2\mu}(\frac{1}{R_a}\frac{\partial^2}{\partial R_a^2} R_a + \frac{1}{r_a}\frac{\partial^2}{\partial r_a^2} r_a)$$

$$+ \frac{\hat{j}_a^2}{2\mu r_a^2} + \frac{1}{2\mu R_a^2}[\hat{J}^2 + \hat{j}_a^2 - 2\hat{j}_{aZ}\hat{J}_Z - (\hat{j}_a^- \hat{J}_a^+ + \hat{j}_a^+ \hat{J}_a^-)] + V(r_a, R_a, \gamma_a),$$

$$\langle R_a^3 r_a^3 | \phi_n^a \rangle | {}^o f_{n+n_i}^a \rangle = \left(\frac{2J+1}{8\pi^2}\right) D_{M\Omega_a}^J(\phi_a, \theta_a, 0) \, Y_{j_a \Omega_a}(\gamma_a, \psi_a)$$

$$\frac{\phi_{v_a j_a}(r_a)}{r_a R_a} \, {}^o f_{n_i}^{Jv_a j_a \Omega_a}(R_a). \qquad (II.56b)$$

Substituting eqn. (II.56b) into eqn. (II.56a), we obtain,

$$\int dr_a^3 dR_a^2 \left(\frac{2J+1}{8\pi^2}\right) D_{M\Omega_a'}^J(\phi_a, \theta_a, 0) \, Y_{j_a' \Omega_a'}(\gamma_a, \psi_a) \frac{\phi_{v_a' j_a'}(r_a)}{r_a}$$

$$\{ -\frac{\hbar^2}{2\mu}(\frac{1}{R_a}\frac{\partial^2}{\partial R_a^2} R_a + \frac{1}{r_a}\frac{\partial^2}{\partial r_a^2} r_a) + \frac{\hat{j}_a^2}{2\mu r_a^2} [\hat{J}^2 + \hat{j}_a^2 - 2\hat{j}_{aZ}\hat{J}_Z$$

$$- \hat{j}_a^- \hat{J}_a^+ + \hat{j}_a^+ \hat{J}_a^-)] + V(r_a, R_a, \gamma_a) - E\} D_{M\Omega_a}^J(\phi_a, \theta_a, 0)$$

$$Y_{j_a \Omega_a}(\gamma_a, \psi_a) \frac{\phi_{v_a j_a}(r_a)}{r_a R_a} \, {}_o f_{v'_a j'_a \Omega'_a}^{Jv_a j_a \Omega_a}(R_a) = 0 \ , \tag{II.57}$$

where dR_a^2 indicates integration over only the angles ϕ_a and θ_a not over the radial distance R_a. Now, we define the centrifugal coupling matrix,

$$(\mathbf{U}^c)_{\Omega_a \Omega'_a}^{j_a v_a} = (\hbar R_a)^{-2} \ \delta_{j_a j'_a, v_a v'_a} \int dR_a^2 \ \left(\frac{2J+1}{8\pi^2}\right) \ D_{M\Omega_a}^J(\phi_a, \theta_a, 0)[\hat{J}^2 + \hat{j}_a^2$$

$$- 2 \ \hat{j}_{aZ}\hat{J}_Z - (\hat{j}_a^- \hat{J}_a^+ + \hat{j}_a^+ \hat{J}_a^-)] \ D_{M\Omega_a}^J(\phi_a, \theta_a, 0)$$

$$= R_a^{-2} \ \delta_{j_a j'_a, v_a v'_a} \ \{\delta_{\Omega_a \Omega'_a}[J(J+1) - 2\Omega_a^2 + j_a(j_a+1)]$$

$$- \delta_{\Omega_a+1\Omega'_a}[J(J+1) - \Omega_a(\Omega_a+1)][j_a(j_a+1) - \Omega_a(\Omega_a+1)]$$

$$- \delta_{\Omega_a-1\Omega'_a}[J(J+1) - \Omega_a(\Omega_a-1)][j_a(j_a+1) - \Omega_a(\Omega_a-1)]. \tag{II.58}$$

The centrifugal coupling term is the only term in the Hamiltonian which couples different Ω_a states, but it does not couple different diatomic vibrational, v_a, or rotational, j_a, states. Next, we define the potential coupling matrix,

$$(\mathbf{U}^p)_{v_a j_a, v'_a j'_a}^{\Omega_a} = \frac{2\mu}{\hbar^2} \ \delta_{\Omega_a \Omega'_a} \int dr^3 \ Y_{j'_a \Omega'_a}(\gamma_a, \psi_a) \frac{\phi_{v'_a j'_a}(r_a)}{r_a} \tag{II.59}$$

$$[V(R_a, r_a, \gamma_a) - v_a(r_a)] \ Y_{j_a \Omega_a}(\gamma_a, \psi_a) \frac{\phi_{v_a j_a}(r_a)}{r_a} \ ,$$

where $v_a(r_a) = V(R_a \to \infty, r_a, \gamma_a)$ which is independent of γ_a. The last matrix that we need to define is diagonal and contains the square of the wavevector for translational motion,

$$(\mathbf{K}^2)^{v_a j_a \Omega_a} = \delta_{v_a j_a \Omega_a, v'_a j'_a \Omega'_a} \ [2\mu(E - \epsilon_{v_a j_a})/\hbar^2] \ , \tag{II.60}$$

where $\varepsilon_{v_a j_a}$ is the eigenvalue for the isolated diatomic motion,

$$[-\frac{\hbar^2}{2\mu r_a}\frac{\partial^2}{\partial r_a^2}r_a + \frac{\hat{j}_a^2}{2\mu r_a^2} + v_a(r_a)] \ Y_{j_a \Omega_a}(\gamma_a,\psi_a) \ \phi_{v_a j_a}(r_a) \ / \ r_a$$

$$= \varepsilon_{v_a j_a} \ Y_{j_a \Omega_a}(\gamma_a,\psi_a) \ \phi_{v_a j_a}(r_a) \ / \ r_a. \qquad (II.61)$$

Now, we write eqn. (II.57) in matrix form using eqns. (II.58) − (II.60) where each matrix is square in the combined indices, i.e., $(v_a j_a \Omega_a)$ by $(v_a' j_a' \Omega_a')$, accounting for the delta functions as needed,

$$\frac{d^2 \ {}^{o}f^J(R_a)}{dR_a^2} = (-\kappa^2 + U^c + U^p) \ {}^{o}f^J(R_a) \ . \qquad (II.62)$$

In section 1c above we outlined how to pick the asymptotic boundary conditions for the open channel part of the wavefunction. Here, we will specify our specific boundary conditions for the closed channel part of the wavefunction. There is some freedom in picking the two linearly independent asymptotic solutions since different linear combinations will work. While not important in the DWBA limit, the particular linear combination will affect the form of the zero order Greens function, see appendix II.a. Based on eqn. (II.24), we specify s_n^a and c_n^a,

$$s_n^a = \frac{\exp(|k_n^a|R_a}{|v|^{1/2}} \ ,$$

$$c_n^a = \frac{\exp(-|k_n^a|R_a)}{|v|^{1/2}} \ , \qquad (II.63)$$

where $|v|$ was defined under eqn. (II.25) and n is now a closed channel.

We solve for the nonreactive wavefunction by numerically integrating the coupled equations, eqn. (II.62). To do this we first divide the R space into a grid of points. We start at the small R

region and integrate the wavefunction outward evaluating the wavefunction at each of the grid points. The wavefunction is integrated between the successive grid points using Gordon's method[84].

Because of numerical problems in the integration, we stabilize the integration at each point. We begin the integration by setting the wavefunction and its derivative to the unit matrix. Then, we integrate the wavefunction outward to the next point. At this point we set the wavefunction back to the identity matrix by dividing out the wavefunction matrix, r_1, and we store the r_1 matrix that we divide out. We propagate the identity matrix to the next point and repeat the process until we have reached the final point. These matrices that are stored are the ratios of the wavefunction at a point p to the wavefunction at a point p-1, $r_p = {}^{o}f_{p-1}^{-1} \; {}^{o}f_p$. At the last point we apply the boundary conditions to determine ${}^{o}K$ which only requires the ratio matrix at the last point. ${}^{o}K$ is used in eqn. (II.24) to generate the normalized wavefunction at the last point, ${}^{o}f_N$. We multiply the wave unction at this final point by the inverse of the ratio matrix at that point to generate the normalized wavefunction at the previous point and so on,

$$
\begin{aligned}
{}^{o}f_{N-1} &= R_N^{-1} \; {}^{o}f_N \\
&\vdots \\
{}^{o}f_{p-1} &= R_p^{-1} \; {}^{o}f_p \\
&\vdots \\
{}^{o}f_1 &= R_2^{-1} \; {}^{o}f_2 \; .
\end{aligned}
$$

$$(II.64)$$

This process of propagating the identity at each point and storing the

ratio matrix is much stabler for integrating the wavefunction which has exponential contributions which are inherently unstable to integrate.

c. Explicit form for the DWBA - CC scattering matrix

In section 1d we derived an expression for the DWBA limit of the S matrix. Here we will write the explicit expression for three dimensional A + BC scattering. In the following section the symmetry decoupling for the H + H_2 reaction is discussed.

The expression for the DWBA limit S matrix is given in eqn. (II.45),

$$\text{DWBA}S^{ba\ J}_{n_f n_i} = 2i \sum_{n' \cdot n' \cdot \cdot} (\delta_{mm'} - i\, {}^{o}K^{bb}_{mm'})^{-1}_{n_f n'}\, \cdot R K^{ba}_{n' \cdot n' \cdot \cdot}\, (\delta_{mm'} - i\, {}^{o}K^{aa}_{mm'})^{-1}_{n' \cdot \cdot n_i}$$

where n and m now represent the collective index (v,j,Ω). We discussed in the previous section how the zero order K matrices, ${}^{o}K^{bb}_{mm'}$, and ${}^{o}K^{aa}_{mm'}$, are calculated from the solution for the zero order wavefunction. What remains is to give an explicit expression for the evaluation of the reactive DWBA K matrix which is defined in eqn. (II.35). Taking the position representation of the reactive part of eqn. (II.35) and using eqn. (II.18), we obtain,

$${}^{R}K^{ba}_{n' \cdot n' \cdot \cdot} = \frac{2}{\hbar} \sum_{nn'} \langle {}^{o}f^{b\ J}_{n' \cdot +n} | W^{ba}_{nn'} | {}^{o}f^{a\ J}_{n'+n' \cdot \cdot} \rangle$$

$$= \frac{2}{\hbar} \sum_{nn'} \langle {}^{o}f^{b\ J}_{n' \cdot +n} | \langle \phi^{b}_{n} | [\hat{v}_a | \phi^{a}_{n'} \rangle - \sum_{n^0} |\phi^{a}_{n^0} \rangle\, v^{a}_{n^0 n'}] | {}^{o}f^{a\ J}_{n'+n' \cdot \cdot} \rangle$$

$$= \frac{2}{\hbar} \int dR^{3}_{b}\, dr^{3}_{b}\, dR^{3}_{a}\, dr^{3}_{a} \sum_{nn'} \langle R^{3}_{b}r^{3}_{b} | R^{3}_{a}r^{3}_{a} \rangle {}^{o}f^{b\ J}_{n' \cdot +n}(R_b) \phi^{b}_{n}(R^{2}_{b}r^{3}_{b})$$

$$[v_a(R_a, r_a, \gamma_a) \phi^{a}_{n'}(R^{2}_{a}r^{3}_{a}) - \sum_{n^0} \phi^{a}_{n^0}(R^{2}_{a}r^{3}_{a}) v^{a}_{n^0 n'}] {}^{o}f^{a\ J}_{n' \cdot +n' \cdot \cdot}(R_a)$$

$$= \frac{2}{\hbar} \int dR_a^3 \, d\vec{r}_a^3 \sum_{nn'} \, {}^0f_{n',+n}^{b \ J}(R_b) \{\phi_n^b(R_b^2 r_b^3) \, V_a(R_a,r_a,\gamma_a)$$

$$\phi_{n'}^a(R_a^2 r_a^3) - \sum_{n0} \phi_n^b(R_b^2 r_b^3)\phi_{n0}^a(R_a^2 r_a^3)V_{n0n'}^a \} \, {}^0f_{n',+n \cdots}^{a \ J} \, , \qquad \text{(II.65)}$$

where we have made use of $\langle R_b^3 r_b^3 | R_a^3 r_a^3 \rangle = \delta(R_b^3 r_b^3 - R_a^3 r_a^3)$. The coordinates $\langle R_b^3 r_b^3 |$ and $\langle R_a^3 r_a^3 |$ are not independent since only 6 coordinates are required to specify the entire space.

If we explicitly write the differential in eqn. (II.65) in terms of polar coordinates for our body fixed coordinate system, we obtain,

$$\int R_a^2 \, dR_a \int r_a^2 \, dr_a \int \sin \theta_a d\theta_a \int d\phi_a \int \sin \gamma_a \, d\gamma_a \int d\psi_a \, . \qquad \text{(II.66)}$$

The coordinates R_a, r_a, and γ_a specify the size and shape of the triangle formed by the three atoms while θ_a, ϕ_a, and ψ_a specify the orientation of the triangle. Since the potential V_a depends only on the coordinates R_a, r_a, and γ_a, the integral over the θ_a, ϕ_a, and ψ_a coordinates can be done analytically. Let us consider the part of the integral over the θ_a, ϕ_a, and ψ_a coordinates,

$$\int \sin \theta_a \, d\theta_a \, d\phi_a \, d\psi_a \, (\frac{2J+1}{8\pi^2}) \, D_{M\Omega_b}^J(\phi_a,\theta_a,0) \, Y_{j_b\Omega_b}(\gamma_b,\psi_b)$$

$$D_{M\Omega_a}^J(\phi_a,\theta_a,0) \, Y_{j_a\Omega_a}(\gamma_a,\psi_a) = P_{j_b\Omega_b}(\cos\gamma_b) \, P_{j_a\Omega_a}(\cos\gamma_a) \, (\frac{2J+1}{8\pi^2})$$

$$\int \sin \theta_a \, d\theta_a \, d\phi_a \, d\psi_a \, D_{M\Omega_b}^J(\phi_b,\theta_b,\psi_b) \, D_{M\Omega_a}^J(\phi_a,\theta_a,\psi_a), \qquad \text{(II.67)}$$

where $P_{j\Omega}(\cos\gamma)$ is the associated Legendre polynomial which is related to the spherical harmonics by,

$$P_{j\Omega}(\cos\gamma) = (2\pi)^{1/2} \exp(-i\Omega\psi) \; Y_{j\Omega}(\gamma,\psi),$$

and we have used a relationship for the rotation matrices that follows from their definition. By converting the rotation matrix in the b coordinates to one in the a coordinates and using ortogonality of the rotation matrices, the intergral in eqn. (II.67) can be done analytically,

$$(II.68)$$

$$(\frac{2J+1}{8\pi^2}) \int \sin\theta_a \, d\theta_a \, d\phi_a \, d\psi_a \; D_{M\Omega_b}^J(\phi_b,\theta_b,\psi_b) D_{M\Omega_a}^J(\phi_a,\theta_a,\psi_a) = d_{\Omega_b\Omega_a}^J(\Delta_{ba}),$$

where $d_{\Omega_b\Omega_a}^J(\Delta) = D_{\Omega_b\Omega_a}^J(0,\Delta,0)$ and Δ_{ba} is the angle between the $\vec{R}_b$ and $\vec{R}_a$ vectors.

We also will, for convenience, change the integration in terms of R_a, r_a, and Y_a to an integration in terms of R_a, R_b, and Δ_{ba}. the transformation between these coordinates is,

$$r_a = (R_b^2 + \cos\alpha_{ba} \; R_a^2 - 2 \cos\alpha_{ba} \cos\Delta_{ba} \; R_b \; R_a)^{1/2}/\cos\alpha_{ba},$$

$$\cos Y_a = (R_a \cos\alpha_{ba} - R_b \cos\Delta_{ba})/(r_a \sin\alpha_{ba}),$$

$$(II.69)$$

where

$$\cos\alpha_{ba} = -\{m_b \, m_a/[(m_a + m_c) \, (m_b + m_c)]\}^{1/2},$$

with α_{ba} between $\pi/2$ and π. Using this transformation, we obtain,

$$(II.70)$$

$$\int R_a^2 \, dR_a \; r_a^2 \, dr_a \; \sin Y_a \; dY_a \rightarrow \sin^{-3}\alpha_{ba} \int R_a^2 \, dR_a R_b^2 \, dR_b \; \sin\Delta_{ba} \; d\Delta_{ba}.$$

Using the analytic integration given in eqns. (II.68) and the transformation given in eqns. (II.69) and (II.70), we can now write $R_K^{ba}{}_{n''n'''}$ from eqn. (II.65) as,

$$R_{K_{n''},_{n'''}}^{ba} = (\frac{1}{\hbar}) \sin^{-3}\alpha_{ba} \sum_{nn'} \int_0^\infty R_a \, dR_a \int_0^\infty R_b \, dR_b \tag{II.71}$$

$$^{o}f_{n'',_{+n}}^{b \ J}(R_b) \ W_{nn'}^J(R_b,R_a) \ ^{o}f_{n',_{+n'''}}^{a \ J}(R_a) \ ,$$

with

$$W_{nn'}^J(R_b,R_a) = \int_0^\pi \sin \Delta_{ba} \, d\Delta_{ba} \ \{d_{\Omega_b\Omega_a}^J(\Delta_{ba}) \ P_{j_b\Omega_b}(\cos \gamma_b) \tag{II.72}$$

$$\phi_{v_b j_b}(r_b)/r_b[[V(R_a,r_a,\gamma_a) - v_a(r_a)] \ P_{j_a\Omega_a}(\cos \gamma_a)$$

$$\frac{\phi_{v_a'j_a'}(r_a)}{r_a} - \sum_n 0 \ \frac{\hbar^2}{2\mu} \ P_{j_a\Omega_a}0(\cos \gamma_a) \ \frac{\phi_{v_a'0}0(r_a)}{r_a} \ v_{n 0_{n'}}^a]\},$$

where the transformation for the b channel variables to R_a, R_b, Δ_{ba} is
analogous to that above in eqn. (II.69) for the a channel.

d. Symmetry decoupling

For a collision of an atom with a homonuclear diatomic molecule,
there is no coupling in the nonreactive wavefunction between the even
and odd rotational states. Thus, one can solve the nonreactive coupled
equations separately for the even rotational states and the odd
rotational states. This uncoupling does not hold for the full
wavefunction though. So, after solving for the even and odd nonreactive
wavefunction, the DWBA calculation is performed with the even – even,
odd – odd, even – odd pairs of wavefunctions. Because of the reduced
dimensionality of the three separate calculations, this represents a
considerable savings in computational effort.

Parity decoupling is another important property which results in a
considerable savings in computer effort. The parity operator P inverts
all of the coordinates through the center of mass,

$$\hat{P} \ \Psi(\vec{r}_a, \vec{R}_a) = \Psi(-\vec{r}_a, -\vec{R}_a) \ ,$$

(II.73)

where Ψ is the wavefunction. For a triatomic system the parity operator commutes with the Hamiltonian, so we can construct simultaneous eigenfunctions of H and P. This is somewhat complicated since the wavefunction in eqn. (II.50) is not an eigenfunction of the parity operator except for $J = 0$. We will only outline here how the parity eigenfunctions are constructed. More details are given by Schatz and Kuppermann[32].

Parity eigenfunctions are constructed by taking a linear combination of our previous solutions from eqn. (II.59),

$$\Psi^{\pm}_{JM}(\vec{r}_a, \vec{R}_a) = \frac{1}{\sqrt{2}} \ \{\Psi^{JM}(\vec{r}_a, \vec{R}_a) \pm (-1)^J \ \Psi^{JM}(-\vec{r}_a, -\vec{R}_a)\},$$

(II.74)

such that

$$\hat{P} \ \Psi^{\pm}_{JM}(\vec{r}_a, \vec{R}_a) = \pm (-1)^J \ \Psi^{\pm}_{JM}(\vec{r}_a, \vec{R}_a).$$

This is equivalent to taking linear combinations of the Ω_a and $-\Omega_a$ radial solutions with the identical expansion functions as in eqns. (II.50) and (II.51)[32]. In the coupled equations for these parity eigenfunctions, the centrifugal coupling matrix, eqn. (II.58), needs to be replaced by,

$$(\overline{U}^c)^{j_a v_a}_{\Omega_a \Omega'_a} = R_a^{-2} \ \delta_{j_a j'_a, v_a v'_a} \{\delta_{\Omega_a \Omega'_a}[J(J+1) - 2\Omega_a^2 + j_a(j_a+1)]$$

(II.75)

$$- b_a \ \delta_{\Omega_a + 1 \Omega'_a}[J(J+1) - \Omega_a(\Omega_a+1)][j_a(j_a+1) - \Omega_a(\Omega_a+1)]$$

$$- c_a \ \delta_{\Omega_a-1\Omega_a'} [J(J+1) - \Omega_a(\Omega_a-1)][j_a(j_a+1) - \Omega_a(\Omega_a-1)],$$

with

$$b_a = \begin{array}{ll} 1 \ , & \Omega_a > 1 \ \text{or} \ \Omega_a < -1; \\ \sqrt{2} \ , & \Omega_a = 0; \\ 0 \ , & \Omega_a = -1; \end{array} \qquad (II.76)$$

and

$$c_a = \begin{array}{ll} 1 \ , & \Omega_a > 1 \ \text{or} \ \Omega_a < -1; \\ \sqrt{2} \ , & \Omega_a = 1; \\ 0 \ , & \Omega_a = 0. \end{array} \qquad (II.77)$$

Then we can proceed as above to generate nonreactive parity eigenstates following our description above in section 2b. Notice from eqns. (II.75) - (II.77) that there is no coupling between states with $\Omega_a > 0$ and $\Omega_a < 0$, so these two sets can be solved independently.

The solution for the parity representation R_∞ matrix is equivalent to that in eqn. (II.71) except that the $d^J_{\Omega_b\Omega_a}(\Delta)$ in eqn. (II.72) is replaced by $\bar{d}^J_{\Omega_b\Omega_a}(\Delta)$,

$$\bar{d}^J_{\Omega_b\Omega_a} = \begin{cases} d^J_{\Omega_b\Omega_a} + (-1)^{\Omega_a} d^J_{\Omega_b-\Omega_a}, & \Omega_b > 0, \ \Omega_a > 0; \\[2mm] \frac{1}{\sqrt{2}} (d^J_{\Omega_b\Omega_a} + (-1)^{\Omega_a} d^J_{\Omega_b-\Omega_a}), & \Omega_b > 0, \ \Omega_a = 0 \ \text{or} \ \Omega_b = 0, \ \Omega_a > 0; \\[2mm] d^J_{\Omega_b\Omega_a}, & \Omega_b = \Omega_a = 0, \\[2mm] d^J_{\Omega_b\Omega_a} - (-1)^{\Omega_a} d^J_{\Omega_b-\Omega_a}, & \Omega_b < 0, \ \Omega_a < 0, \\[2mm] 0, & \Omega_b < 0, \ \Omega_a > 0 \ \text{or} \ \Omega_a < 0, \ \Omega_b > 0. \end{cases}$$

$$(II.78)$$

Note that the matrix element for the parity conserving K matrix is zero
if one of the Ω's is nonnegative and the other Ω is positive. Thus the
uncoupling in the nonreactive parity eigenstate wavefunction also
carries over to the calculation of the K matrix unlike the even – odd
uncoupling discussed above. Finally, linear combinations of the parity
conserving S matrix elements are used to constuct body fixed helicity
scattering matrices,

$$
S_{n_f n_i}^{ba\ J} = \begin{cases}
\frac{1}{2}\,(\bar{S}_{v_a j_a \Omega_a}^{Jv_b j_b \Omega_b} + \bar{S}_{v_a j_a \Omega_a}^{Jv_b j_b -\Omega_b}), & \Omega_a \Omega_b > 0, \\[2mm]
\frac{1}{2}\,(\bar{S}_{v_a j_a |\Omega_a|}^{Jv_b j_b |\Omega_b|} - \bar{S}_{v_a j_a -|\Omega_a|}^{Jv_b j_b -|\Omega_b|}), & \Omega_a \Omega_b < 0, \\[2mm]
\frac{1}{\sqrt{2}}\,\bar{S}_{v_a j_a \Omega_a}^{Jv_b j_b \Omega_b}, & \Omega_a = 0,\ \Omega_b \neq 0 \text{ or } \Omega_b = 0,\ \Omega_a \neq 0, \\[2mm]
\bar{S}_{v_a j_a \Omega_a}^{Jv_b j_b \Omega_b}, & \Omega_a = \Omega_b = 0.
\end{cases}
$$

(II.79)

e. Coupled states approximation

The coupled states or j_z conserving approximation is based on the
body fixed Hamiltonian being nearly diagonal in Ω, see eqns. (II.57) and
(II.58). Several authors[85-87] have shown that accurate reactive
scattering cross sections can be obtained from the j_z conserving
approximation while saving a large amount of computational effort. Its
success seems to rely more on the dominance of the $\Omega = 0$ states than to
the decoupling of different Ω states. $\Omega = 0$ states dominate in systems
with collinear minimum energy paths, since only $\Omega = 0$ states are nonzero
along the collinear path, which leads to much larger reactive
contributions for $\Omega_b = \Omega_a = 0$ than other transitions. Our application

of the coupled states approximation uses a basis with only $\Omega_b = \Omega_a = 0$ following Schatz[87]. This gives basis sets which grow linearly rather than quadratically with the value for total J. The transition probabilities which we obtain with this basis are assumed to equal the values of the degeneracy averaged transition probabilities defined below. It would probably be more accurate to calculate transition probabilities for other fixed Ω's assuming no coupling between different Ω's as some previous calculations have been done[85,86]. This would give a full set of transition probabilities to degeneracy average but would be much more time consuming.

f. Calculation of differential and integral cross sections

Here we outline the derivation of the formulas for the differential and integral cross sections in terms of the body fixed S matrix elements. More details can be found in ref. 32. Here we will ignore the antisymmetrization for the identical nuclei of the diatom. We will use an axis for projecting the angular momentum that points toward the incoming or outgoing atom for the reactants and products respectively rather than using the initial or final wave vectors as is done in ref. 32.

In order to obtain cross sections, we need to relate our solution to a space fixed scattering amplitude, F. The differential cross section, which is the ratio of the outgoing radial flux per unit solid angle to the incoming plane wave flux, is given by,

$$\sigma_{n'n}^{ba}(\theta) = \frac{v_{n'}^b}{v_n^a} \left| F_{n'n}^{ba} \right|^2 , \tag{II.80}$$

where v is the velocity in the physical, non-mass weighted coordinates,

$$v_n^a = \left| \frac{\hbar \overline{k}_n^a}{\mu_{abc}} \right| , \quad \overline{k}_n^a = k_n^a / c_a , \tag{II.81}$$

where c_a and μ_{abc} are defined in eqn. (II.47). Schatz and Kuppermann[32] go into great detail relating the wavefunctions for a space fixed helicity formulation to the body fixed wavefunctions. The resulting relationship for the scattering amplitude in terms of our body fixed S matrix is,

$$F_{n'n}^{ba} = \left(\frac{v_n^a}{v_{n'}^b} \right)^{1/2} \frac{e^{i \Omega_a \phi_a}}{2 \overline{k}_n^a} i^{j_a - j_b + 1} \sum_{J=0}^{\infty} (2J+1) \, d_{\Omega_a \Omega_b}^J (\theta_b) \, T_{n'n}^{ba \, J} , \tag{II.82}$$

where

$$T_{n'n}^{ba \, J} = \delta_{n'n} - S_{n'n}^{ba \, J} ,$$

and θ_b is the scattering angle which is measured relative to the body fixed axis in the reactant channel and n is the combined index, $vj\Omega$. Using eqns. (II.80) and (II.82), the formula for the differential cross section is,

$$\sigma_{n'n}^{ba} (\theta_b) = (4 \overline{k}_n^a{}^2)^{-1} \left| \sum_{J=0}^{\infty} (2J+1) \, d_{\Omega_a \Omega_b}^J (\theta_b) \, T_{n'n}^{ba \, J} \right|^2 . \tag{II.83}$$

Integral cross sections are found by integrating eqn. (II.83) over θ_b and ϕ_b. Because of the orthogonality of the d^J functions, the formula for the integral cross section is quite simple,

$$Q_{n'n}^{ba} = (\pi / \overline{k}_n^2) \sum_{J=0}^{\infty} (2J+1) \left| T_{n'n}^{ba \, J} \right|^2 . \tag{II.84}$$

We also present transition probabilities which are just squares of the S matrix elements,

$$P_{n'n}^{ba \, J} = \left| S_{n'n}^{ba \, J} \right|^2 . \tag{II.85}$$

Degeneracy averaged values are defined as sums over final Ω_j and averages over initial Ω_j,

$$\mathscr{P}^J_{v'j',vj} = (2j+1)^{-1} \sum_{\Omega_j} \sum_{\Omega'_j} P^J_{v'j'\Omega',vj\Omega}, \qquad (II.86)$$

with $\left|\Omega_j\right| \leqslant \min(j,J)$ and $\left|\Omega'_j\right| \leqslant \min(j',J)$. There are similar expressions for degeneracy averaged differential and integral cross sections.

3. Details of the formalism for the collinear exact studies on $H + H_2$

a. Coordinate representation for collinear $H + H_2$ scattering

Two coordinates are needed to describe a collinear $A + BC$ system. For each arrangement we pick for our coordinates R_a, the distance of atom A to the center of mass of BC, and r_a, the distance of atom B to atom C. Based on these coordinates, the position representation of our wavefunction becomes,

$$\Psi_{b}(R,r) = \langle rR | \Psi_{b} \rangle = \sum_{n} \phi^1_n(r_1) \; f^1_{n+n_i}(R_1) + \sum_{n'} \phi^2_{n'}(r_2) \; f^2_{n'+n_i}(R_2) \qquad (II.87)$$

where ϕ^a_n is the asymptotic n th vibrational eigenfunction for arrangement a. Note that each term of the expansion for the wavefunction has the appropriate coordinates for the particular arrangement. For collinear $A + BC$ there are only two asymptotic arrangements possible, $A + BC$ and $AB + C$. The two sets of coordinates $(r_1 R_1)$ and $(r_2 R_2)$ are not independent. They are related by,

$$r_c = R_a - \left(\frac{m_c}{m_b + m_c}\right) r_a \; ,$$

$$R_c = (\frac{m_a}{m_a+m_b}) R_a + \frac{m_b(m_a+m_b+m_c)}{(m_a+m_b)(m_b+m_c)} r_a \, ,$$

(II.88),

where atom a or atom c is the asymptotic free atom for that arrangement. Therefore, we may pick any pair of the four coordinates to be the independent variables. Later we will find it convenient to pick R_1 and R_2 as the independent variables.

The position representation of the collinear Hamiltonian is,

$$\hat{H}(r_a,R_a) = \langle R_a, r_a, |\hat{H}|R_a r_a\rangle = \langle R_a, r_a, |R_a r_a\rangle \, [\frac{-\hbar^2}{2\mu_{abc}} \frac{\partial^2}{\partial R_a^2}$$

$$- \frac{\hbar^2}{2\mu_{bc}} \frac{\partial^2}{\partial r_a^2} + V(R_a,r_a)] ,$$

(II.89)

where μ_{abc} and μ_{bc} are defined in eqn. (II.47). The position representation of the various parts of the Hamiltonian defined in eqn. (II.13) are,

$$\hat{K}(R_a) = \frac{-\hbar^2}{2\mu_{abc}} \frac{\partial^2}{\partial R_a^2} \, ,$$

$$V_a(R_a,r_a) = V(R_a,r_a) - v(r_a) ,$$

$$h(r_a) = \frac{-\hbar^2}{2\mu_{bc}} \frac{\partial^2}{\partial r_a^2} + v(r_a) ,$$

(II.90)

where $v(r_a) = V(R_a+\infty,r_a)$ and $\phi_n^a(r_a)$ is an eigenfunction of $h(r_a)$ with eigenvalue ϵ_n^a.

b. Solving for the nonreactive wavefunction

The coordinate representation of the coupled equations for the nonreactive wavefunction, eqn. (II.6), is,

$$\int dr_a' \, dR_a' \, dr_a \, dR_a \, \langle R_a''|\langle\phi_{n_f}^a|r_a'R_a'\rangle \, \langle r_a'R_a'|\hat{H} - E|r_a R_a\rangle$$

$$\langle r_a R_a | \phi_n^a \rangle |^o f_{n+n_1}^a \rangle = 0. \tag{II.91}$$

Making use of eqn. (II.89), eqn. (II.91) becomes,

$$\int dr_a \sum_n \phi_{n_f}^a (r_a) \left[\frac{-\hbar^2}{2\mu_{abc}} \frac{\partial^2}{\partial R_a^2} - \frac{\hbar^2}{2\mu_{bc}} \frac{\partial^2}{\partial r_a^2} + V(R_a, r_a) - E \right]$$

$$\phi_n^a (r_a) \; ^o f_{n+n_1}^a (R_a) = 0, \tag{II.92}$$

or making use of the fact that $\phi(r_a)$ is an eigenfunction of $h(r_a)$ given in eqn. (II.90) and of the definition of $V_{n'n}^a$ in eqn. (II.16), we have,

$$\left[\frac{-\hbar^2}{2\mu_{abc}} \frac{d^2}{dR_a^2} - E_n^a \right] \; ^o f_{n_f+n_1}^a (R_a) + \sum_n V_{n_f n}^a \; ^o f_{n+n_1}^a (R_a) = 0, \tag{II.93}$$

with $E_n^a = E - \varepsilon_n^a$. We numerically integrate the coupled equations in eqn. (II.93) to obtain $^o f$, by dividing the R_a axis into an evenly spaced grid and integrating the wavefunction from point to point. In order to calculate the Greens function matrix, we need both the regular and irregular nonreactive wavefunctions. The regular solution goes to zero at the origin while the irregular solution exponentially grows as it approaches the origin. Also, because of the way we pick our asymptotic boundary conditions, the closed channel part of the nonreactive regular wavefunction grows exponentially as it approaches the asymptotic region while the irregular wavefunction exponentially decays in the asymptotic region. For stability the regular solution is integrated outward starting near the origin, and the irregular solution is integrated inward starting in the asymptotic region.

Our integration method is based on the renormalized Numerov algorithm[88,89]. Before giving the details of this integration

procedure, it is convenient to first write eqn. (II.93) in matrix form for the vibrational state indices,

$$(\mathbf{I} \frac{d^2}{dR^2}) \; {}^o\underline{f}(R) = \underline{Q}(R) \; {}^o\underline{f}(R),$$

(II.94)

where

$$\underline{Q}(R) = (\frac{2\mu_{abc}}{\hbar^2}) \; (\underline{V}^a - \underline{E}^a),$$

and $\mathbf{I}$ is the identity matrix. A three term recurrance relation provides the basis for Numerov integration[88],

$$(\mathbf{I} - \underline{T}_n) \; {}^o\underline{f}_n - (2\mathbf{I} + 10\underline{T}_{n-1}) \; {}^o\underline{f}_{n-1} + (\mathbf{I} - \underline{T}_{n-2}) \; {}^o\underline{f}_{n-2} = 0,$$

(II.95)

with

$${}^o\underline{f}_n = {}^o\underline{f}(r_n),$$

and

$$\underline{T}_n = (\frac{h^2}{12}) \; \underline{Q}(r_n),$$

where h is the spacing between the grid points and r_n is the value of R at the n th grid point. We define a matrix F,

$$\underline{F}_n = \underline{I} - \underline{T}_n \; .$$

(II.96)

Substituting eqn. (II.96) into eqn. (II.95), we obtain,

$$\underline{F}_n \; {}^o\underline{f}_n - (12\underline{I} - 10\underline{F}_{n-1}) \; {}^o\underline{f}_{n-1} + \underline{F}_{n-2} \; {}^o\underline{f}_{n-2} = 0.$$

(II.97)

If we multiply eqn. (II.97) from the right by ${}^o\underline{f}_{n-1}^{-1}$ and rearrange, the resulting equation is,

$$\underline{R}_n = (12\underline{I} - 10\underline{F}_{n-1} - \underline{F}_{n-2} \; \underline{R}_{n-1})^{-1} \; \underline{F}_n \; ,$$

(II.98)

wnere

$$R_n = {}^0f_{n-1} \; {}^0f_n^{-1} .$$

Eqn. (II.98) is the algorithm we use to propagate the regular solution outward from the origin. At each grid point we calculate and store the ratio matrix, R_n. As in the case for the three dimensional DWBA calculation described in section 2b, where we also calculate a ratio matrix using a different algorithm, this integration can be quite stable if enough grid points are used. With the boundary conditions and the ratio matrix in the asymptotic region, the ${}^0K$ matrix can be calculated. We can then calculate the normalized wavefunction from eqn. (II.24) at this final point, N. By multiplying with the ratio matrix at this point, we get the wavefunction at the previous point and so on until we have generated the normalized wavefunction at all of the grid points,

$$
\begin{aligned}
{}^0f_{N-1} &= R_N \; {}^0f_N \; , \\
&\vdots \\
{}^0f_1 &= R_2 \; {}^0f_2 \; .
\end{aligned}
\tag{II.100}
$$

As we show below, we only need the inverse of the ratio matrices of the irregular solution to calculate the Greens function matrix rather than the normalized wavefunction. Rearranging eqn. (II.98), we obtain,

$$R_{n-1}^{I \; -1} = (12I - 10F_{n-1} - F_n \; R_n^{I \; -1})^{-1} \; F_{n-2} \; ,
\tag{II.101}$$

where the I indicates the irregular solution. The algorithm in eqn. (II.101) is used for the integration of the irregular solution inward from the asymptotic region. The initial ratio matrix R_N^{-1} is obtained from the boundary conditions which we discuss below.

To calculate the Greens function matrix we also need the log

derivative matrix at each of the grid points. The log derivative matrix
is defined as,

$$\underset{\sim}{y}(r_n) = \underset{\sim}{f}'(r_n) \; \underset{\sim}{f}^{-1}(r_n),$$
(II.102)

where $\underset{\sim}{f}'(r_n)$ is the derivative of f with respect to R evaluated at r_n.
We calculate the log derivative matrix for the regular and irregular
wavefunctions as we propagate the ratio matrices. Making use of
quantities which are already calculated, the log derivative matrix is
calculated from[88],

$$\underset{\sim}{y}(r_n) = h^{-1}(\underset{\sim}{A}_{n+1}\underset{\sim}{R}_n - \underset{\sim}{A}_{n-1}\underset{\sim}{R}_{n-1}^{-1}) \; \underset{\sim}{E}_n,$$
(II.103)

where $\underset{\sim}{y}(r_n)$ is the log derivative matrix and ,

$$\underset{\sim}{A}_n = \underset{\sim}{I} - 0.5 \; \underset{\sim}{E}_n \; .$$

In section 1c we derived the asymptotic form for the open channel
part of the nonreactive wavefunction which is given in eqns. (II.24) —
(II.26). Here, we specify that for the closed channels,

$$s_n^a = \frac{e^{k_n^a R_a}}{|2v|^{1/2}} \; ,$$

$$c_n^a = \frac{e^{-k_n^a R_a}}{|2v|^{1/2}} \; ,$$
(II.104)

where eqns. (II.24) and (II.26) still hold and k_n^a and v are defined
under eqn. (II.25). We were free to pick various linear combinations of
these two linearly independent asymptotic wavefunctions, but this
particular choice yields a convenient form for the Greens function

matrix as we show in appendix II.A.

c. Calculation of the S matrix

The form of the S matrix in terms of the reactance matrix, K, is given in eqn. (II.33b),

$$\underset{\sim}{S} = (\underset{\sim}{1} + i\underset{\sim}{K}^{oo}) \ (\underset{\sim}{1} - i\underset{\sim}{K}^{oo})^{-1},$$

where these are matrices in the combined indices of the arrangement and diatomic vibrational state, and the oo lable on the K matrix indicates that the indices only range over the asymptotically open channels. It remains to explicitly specify how the K matrix is calculated. We begin by taking the position representation of eqn. (II.29),

$$K_{ana_i n_i} = {}^oK_{ana_i n_i} + \frac{2}{\hbar} \int dR_{a''} dR_{a0} \sum_{\substack{n'n''n^0 \\ a'a''a^0}} \langle {}^of_{ana''n''} | R_{a''} \rangle$$

$$\langle R_{a''} | (\delta_{bmb'm'} + S_{bmb'm'} - \sum_{b^0_m 0} W_{bmb^0_m 0} \ {}^oG_{b^0_m 0 b'm'})^{-1}_{a''n''a^0n^0} | R_{a^0} \rangle$$

$$\langle R^0_a | W_{a^0_n 0 a'n'} | {}^of_{a'n'a_i n_i} \rangle, \qquad (II.105)$$

where a's anc b's are arrangement indices and n and m are indices for vibrational expansion functions. We have discussed in sec. 3b how to calculate ${}^oK$. While we will not indicate it with our notation, it should be remembered that ${}^oK$, ${}^of$, and ${}^oG$ are diagonal in arrangement index and W and S are off diagonal in arrangement index. Let us first consider more explicitly the final term of eqn. (II.105) making use of the definition of the W kernal in eqn. (II.18),

$$\langle R' | W_{a^0_n 0 a'n'} | {}^of_{a'n'a_i n_i} \rangle = \langle R^0_a | \langle \phi^{a^0}_{n_f} | [\hat{V}_a | \phi^{a'}_n \rangle | {}^of^{a'}_{a'n'a_i n_i} \rangle$$

$$\cdot \quad - \sum_{n'} \; |\phi_{n'}^{a'}\rangle \; v_{n'n}^{a'} \; |^o f_{ana_i n_i}\rangle] \; ,$$

$$= \int dR_{a0} \; dr_{a0} \; dR_{a'} \; dr_{a'} \langle R_{a0}'| \langle \phi_{n_f}^{a0} |R_{a0} r_{a0}\rangle \langle R_{a0} r_{a0} | [\hat{v}_{a'}|R_{a'} r_{a'}\rangle$$

$$\langle R_{a'} r_{a'} | \phi_n^{a'}\rangle - \sum_{n'} \; |R_{a'} r_{a'}\rangle \langle R_{a'} r_{a'} | \phi_{n'}^{a'}\rangle \; v_{n'n}^{a'}] \; |^o f_{n'n_i}^{a'}\rangle$$

$$= \int dr_{a0} \; \delta(R_{a0}' - R_{a0}) \; \phi_{n_f}^{a0}(r_{a0}) \; [\hat{v}_{a'}(R_{a'}, r_{a'}) \; \phi_n^{a}(r_{a'})$$

$$- \sum_{n'} \; \phi_{n'}^{a'}(r_{a'}) \; v_{n'n}^{a'}] \; {}^o f_{a'na_i n_i}(R_{a'})$$

$$= \int dR_{a'} \; \frac{\partial r_{a0}}{\partial R_{a'}} \; \phi_{n_f}^{a0}[r_{a0}(R_{a0}, R_{a'})] \{V_{a'}(R_{a'}, R_{a0})\phi_n^{a'}[r_{a'}(R_{a0}, R_{a'})]$$

$$- \sum_{n'} \; \phi_{n'}^{a'}[r_{a'}(R_{a0}, R_{a'})] \; v_{n'n}^{a'}\} \; {}^o f_{a'na_i n_i}(R_{a'}), \qquad \text{(II.106)}$$

where

$$\frac{\partial r_{a0}}{\partial r_{a'}} = \frac{m_b \; (m_{a0} + m_b + m_{a'})}{(m_{a0} + m_b)(m_b + m_{a'})}$$

which follows from eqn. (II.88). Now we define a W matrix by,

$$W_{ana'n'}(R,R') = \phi_n^a[r_a(R,R')] [V_{a'}(R,R') \; \phi_{n'}^{a'}[r_{a'}(R,R')]$$

$$- \sum_{n0} \; \phi_{n0}^{a'}[r_{a'}(R,R')] \; v_{n0n'}^{a'}] \; . \qquad \text{(II.107)}$$

Next, we consider the position representation of the inverse operator. We construct a grid for $R_{a'}$ and R_{a0} with indices, i'' and i^o, respectively. Then we can consider the position representation as an i, i' element of a matrix representation in R space. By considering the summation in eqn. (II.10) from which the inverse operator is defined it

can be shown that,

$$\langle R_{a''}^{1''} | (\delta_{bm,b'm'} + S_{bmb'm'} - \sum_{b0_m0} W_{bmb0_m0} \, {}^{o}G_{b0_m0b'm'})_{a''n''a0n0}^{-1} | R_{a0}^{10}\rangle$$

$$= (\delta_{bmjb'm'j'} + S_{bmjb'm'j'} - \sum_{b0_m0}\langle R_b^j | W_{bmb0_m0} \, {}^{o}G_{b0_m0b'm'} | R_b^{j'}\rangle)_{a''n''j''}^{-1}$$
$$a0_n0_10$$

$$(II.108)$$

where the matrix inverse of the right hand side of eqn. (II.108) is over
the combined index, bmj, where b is the arrangement index, m is the
vibrational state expansion function, and j is the index for the R
grid. Looking at the overlap matrix in the second term of eqn.
(II.108), it can be written more explicitly using its definition in eqn.
(II.22) as,

$$S_{bmjb'm'j'} = \langle R_b^j | \langle \phi_m^b | \phi_{m'}^{b'}\rangle | R_{j'}^{b'}\rangle$$

$$= \int dR_b \, dr_b \, dR'_{b'} \, dr'_{b'} \langle R_b^j | \langle \phi_m^b | R_b r_b\rangle \langle R_b r_b | R_{b'}, r_{b'}\rangle$$

$$\langle R_{b'}, r_{b'} | \phi_{m'}^{b'}\rangle | R_{j'}^{b'}\rangle$$

$$= \int dr_b \, \phi_m^b(r_b) \, \phi_{m'}^{b'}(r_{b'}) \, \langle R_{b'} | R_{b'}^{j'}\rangle$$

$$S_{bmjb'm'j'} = \frac{\partial r_b}{\partial R_{b'}} \, \phi_m^b[r_b(R_b^j, R_{b'}^{j'})] \, \phi_{m'}^{b'}[r_{b'}(R_b^j, R_{b'}^{j'})],$$

$$(II.109)$$

where $\partial r^b / \partial R^{b'}$ is given below eqn. (II.106). Lastly, needing a more
explicit form for the last term in eqn. (II.108), we obtain,

$$\langle R_b^j | W_{bmb0_m0} \, {}^{o}G_{b0_m0b'm'} | R_b^{j'}\rangle = \int dR_b, \frac{\partial r_b}{\partial R_{b'}} \, W_{bmb0_m0}(R_b^i, R_{b'})$$

$$^oG_{b_0m_0b'_m{}'}(R_{b'}, R_{b'}^{j'}) \ ,$$

$$(II.110)$$

following similar steps as those in eqn. (II.106) where $\partial r_b / \partial R_{b'}$ is given below eqn. (II.106). The Greens function matrix element,

$$^oG_{b_0m_0b'_m{}'}(R_{b'}, R_{b'}^{j'}) = \langle R_{b'}|^oG_{b_0m_0b'_m{}'}|R_{b'}^{j'}\rangle \ ,$$

will be discussed more below.

The variables, R_1, defined in eqn. (II.110) and R_a, defined in eqn. (II.106) will also be placed on the same grid as discussed above. The four intergrals in eqns. (II.105), (II.106), and (II.110) are all over variables defined on a grid. We will perform these integrals using the trapazoidal rule which seems adequate although other quadrature methods could be used. We can rewrite eqn. (II.105) in explicit form,

$$K_{ana_in_i} = {}^oK_{ana_in_i} + \frac{2}{\hbar} \sum_{\substack{n'n''n^0 \\ a'a''a^0 \\ i'i''i^0}} {}^of_{ana''n''i''} \ (\delta_{bmjb'm'j'} + S_{bmjb'm'j'}$$

$$(II.111)$$

$$- \sum_{b_0m_0j_0} W_{bmjb_0m_0j^0} \ {}^oG_{b_0m_0j_0b'm'j'})_{\substack{a''n''i'' \\ a^0n^0i^0}}^{-1} \ W_{a_0n_0i_0} \ {}^of_{a'n'i'a_in_i}.$$

We have found that the grid to do these integrals need not be as fine as the grid for the integration of the nonreactive wavefunction. We therefore have two grid sizes with an integer factor relating them. Also, W is localized in the interaction region, so these integrals need not extend out to the asymptotic regon. We cut off the integrations at a point where there appears to be no further contribution to the integral. We give the details about the grid sizes with the results below.

All that remains to be specified about the calculation is the computation of the Greens function matrix. The derivation of the

equation for the calculation of the Greens function matrix is given in appendix II.A. The result from eqn (II.A.20) is that the distorted wave Greens function matrix can be found from,

$$^o\underline{G}(r_n, r_{n'}) = \frac{-2\mu}{\mu^2} \underline{R}_{n+1} \underline{R}_{n+2} \cdots \underline{R}_{n'} [^o\underline{f}'(r_{n'}) \, ^o\underline{f}^{-1}(r_{n'})$$

$$- \,^o\underline{g}'(r_n) \, ^o\underline{g}^{-1}(r_n)]^{-1} \, , \quad r_n < r_{n'}$$

and

$$^o\underline{G}(r_n, r_{n'}) = \frac{-2\mu}{\mu^2} \underline{R}_n^{I \, -1} \cdots \underline{R}_{n'+1}^{I \, -1} [^o\underline{f}'(r_{n'}) \, ^o\underline{f}^{-1}(r_{n'})$$

$$- \,^o\underline{g}'(r_{n'}) \, ^o\underline{g}^{-1}(r_{n'})]^{-1} \, , \qquad r_n > r_{n'} \tag{II.112}$$

where $^o\underline{g}$ is the irregular nonreactive wavefunction. We have discussed the calculation of the ratio matrices, $\underline{R}_n$, for the regular nonreactive wavefunction in eqn. (II.98) and the inverse of the ratio matrices, $\underline{R}_n^{I-1}$, for the irregular nonreactive wavefunction in eqn. (II.101). The quantity in square brackets in eqn. (II.112) is the difference between the log derivative matrices for the regular and irregular solutions which we show how to calculate in eqn. (II.103). We could also have calculated the distorted wave Greens function matrix from the normalized regular and irregular nonreactive wavefunctions rather than from the ratio matrices and the log derivative matrices. The formula for calculating the Greens function matrix in eqn. (II.112) without the nonmalized wavefunctions is numerically much better behaved.

C. Results and Discussion

1. Multichannel DWBA for three dimensional $H + H_2$

a. Transition Probabilities

In this section we present the degeneracy averaged reactive transition probabilities for the $H + H_2 (v,j) \to H_2 (v',j') + H$ reaction on the Porter - Karplus[80] potential energy surface, and below we give the cross section results. Exact quantum calculations[16] are available for comparison which makes this a convenient test problem. First we present the transition probabilities for total angular momentum, $J = 0$ to show how well the results converge with respect to basis functions at different energies. Then we present the transition probabilities as a function of J.

Using coupled channel DWBA, it was found for collinear $H + H_2$[34] that accurate converged results were obtained when the reaction probabilities were sufficiently small (< 0.1). Our results here are very reminiscent of the collinear results. Table II.1 contains our results with $J = 0$ for the reactive transition probabilities $v=0, \ j=0 \to v'=0, \ j'=0; \ v'=0, \ j'=1$ and $v=0, \ j=1 \to v'=0, \ j'=1$. The results for $E < 0.6$ eV converge with 18 basis functions (the specific basis used is explained in the table). For larger energies the results show the same growing oscillations as the collinear results. This can be seen in Fig. II.1 where $P_{00 \to 00}^{J=0}$ is plotted as a function of basis functions for $E = 0.65$ eV. The DWBA results are expected to break down at higher energies where reaction probabilities become larger since the perturbation assumptions are no longer valid. It is not clear, though, that the growing instability is purely a result of this breakdown in the

perturbation theory. The fact that, as we see in the next section, for collinear $H + H_2$ the full, the nonperturbative solution converges at higher energies supports the argument that it is a breakdown of the perturbation approximation. It also seems possible that there is some nonconvergence in the nonreactive wavefunction that is causing the large oscillations.

The "exact" quantum results are also shown in Table II.1 for comparison. The transition probabilities from $v=0$, $j=0 \rightarrow v'=0$ summed over final rotational levels are shown in Fig. II.2. These transition probabilities also show good agreement and similar trends at high energies. Other transition probabilities, not shown, have about equivalent agreement. In Fig. II.3 the transition probabilities multiplied by $(2J+1)$ at 0.5 eV as a function of J along with the exact quantum and coupled states distorted wave results. The DWBA results are converged to within several percent with the given basis. Both the DWBA-CC and DWBA-CS results agree well with the exact quantum results. The DWBA transition probabilities, though, decay less quickly as J becomes larger. In Fig. II.4, transition probabilities within the coupled states approximation at $E = 0.4$ and 0.6 eV are plotted as a function of J. The DWBA-CS results at these energies also agree well with the "exact" quantum results although they seem to deviate slightly more near the peak maximum. Again the DWBA results decay slightly more slowly with increasing J.

It is interesting to note that the DWBA transition probabilities as a function of J agree better with the "exact" results at 0.5 eV than 0.4 or 0.6 eV. We would expect the agreement to be worse at 0.6 eV since

the perturbation assumption could be beginning to break down. It is more difficult to understand the discrepancy between the DWBA-CS and the "exact" quantum results at 0.4 eV except that possibly the "exact" quantum results are not fully converged. We have actually used a larger basis at this energy than in the "exact" quantum results. If we use a smaller basis in our calculation the agreement improves. It is difficult though to really compare basis sets in the two different methods.

b. Cross sections

In Fig. II.5 the differential cross sections are plotted as a function of scattering angle for a total energy of 0.5 eV. The solid line indicates the exact quantum results. The DWBA-CC and DWBA-CS results are plotted using the indicates dots. One can see that the DWBA results agree very well with the "exact" quantum results. In Fig. II.6, the differential cross sections are shown as a function of scattering angle for total energies 0.4 and 0.6 eV. The solid line indicates the "exact" quantum results, and the dots are the DWBA-CS results. The DWBA results at these energies are also in quite good agreement with the "exact" quantum results. At E = 0.6 eV the DWBA-CS differential cross section seems to die off a little too slowly at small angles and to peak somewhat too high at 180°. It should be noted that we obtain quantitative agreement in the differential cross section without any normalization to the "exact" results.

In Table II.2 some integral cross sections are given for total energies of 0.4, 0.5, and 0.6 eV. The integral cross section results show good agreement between the "exact" quantum and DWBA results.

Almost all of the DWBA integral cross sections are higher than the corresponding "exact" quantum results which may again indicate some lack of convergence in the "exact" quantum results with respect to basis sets.

For comparison, we will give relative computer times for the DWBA and the exact calculations. Most of the computer time in the DWBA calculation is involved in performing the integrals in eqns. (II.71) and (II.72). We have not put much effort into optimizing these integrations so that we avoid regions where there is little contribution to the integral. With 16 basis functions, described in Table II.1, and $J = 0$, DWBA-CC required 19 minutes of computer time on a Harris H800 computer to evaluate the entire probability matrix. The "exact" quantum calculation with the same basis required 21 minutes , but the exact quantum program is highly optimized to be as efficient as possible. The DWBA-CS calculations is identical for $J = 0$ with the DWBA-CC calculation, but for an entire cross section calculation it requires about 1/5 the time needed for DWBA-CC at 0.5 eV.

2. "Exact" collinear $H + H_2$ reactive scattering

Here we present reactive scattering transition probabilities for collinear $H + H_2$ with the Porter - Karplus[80] potential energy surface. The asymptotic form for the vibrational potential energy is a Morse function, so we therefore use Morse eigenstates for our expansion of the vibrational motion. We perform calculations over a large range of energies from the deepest tunneling region to energies with 3 open channels. We also present a comparison of our results with previous

"exact" results on this same system.

We perform calculations with up to 6 vibrational states in our expansion. Table II.3 shows convergence with respect to basis set size. Unlike the DWBA case described in the previous section, the results here converge with respect to basis size quite well with 6 basis functions even at higher energies. The convergence at the very lowest energies and at 1.6466 eV is not as good as at the other energies. This is still being investigated. At no energies, though, do we observe the oscillations that we found for the DWBA calculations.

We integrate the nonreactive wavefunction from 1.0 Bohr to 10.0 Bohr using about 500 grid points. The convergence of the integration for the nonreactive wavefunction can be checked from the symmetry of the nonreactive Greens function matrix. For the integration to obtain the S matrix in eqn. (II.111), we find that because of the limited range of the exchange interaction, only the innermost 40 % of the region contributes significantly to the integrals, and the rest of the region can be ignored. Within this region we have used from 40 – 60 grid points. In table II.4 we present results to show the convergence with respect to this grid size. We see that for convergence to 1 – 2 % that about 50 grid points are sufficient.

In table II.5 we present a comparison of our results with previous "exact" quantum calculations. Throughout the entire energy range, our results show excellent agreement with the previous calculations usually within a few percent. We see that this method performs well with more than one open channel, and describes the resonance region correctly.

D. Conclusions

We have presented a formalism for performing "exact" scattering calculations and coupled channel distorted wave Born approximation calculations for reactive atom – diatom systems. Calculations are presented for "exact" collinear $H + H_2$ reactive scattering and for three dimensional $H + H_2$ reactive scattering using multichannel DWBA. We have shown that accurate reactive probabilities and cross sections are obtained using this multichannel DWBA method for three dimensional $H + H_2$. For total energies up to 0.6 eV, the DWBA transition probabilities, differential cross sections, and integral cross sections agree quantitatively with the exact quantum results. We also introduce an approximate method for obtaining the nonreactive wavefunction using the coupled states approximation which saves considerable computational effort with very good results. Above 0.6 eV, where the reaction probabilities become larger than about 0.1, the DWBA results do not converge with respect to the addition of vibrational basis functions. The convergence problem here is analogous to the equivalent problem observed by Hubbard, Shi, Miller[34] using coupled channel DWBA for collinear $H + H_2$. For our "exact" collinear $H + H_2$ calculations we obtain excellent agreement with previous calculations over a very large range of energies. Over most of the energy range we obtain convergence with 6 vibrational expansion functions.

The reactive scattering formalism which we present is straightforward to extend to any atom – diatom scattering problem but numerical limitations need to be investigated further. Based on an over

complete basis, this method avoids all of the problems of finding an appropriate coordinate system for the rearranging atoms. Our accurate results for collinear $H + H_2$ are encouraging. Using a DWBA version of this formalism, we have obtained for the first time quantitative agreement with the three dimensional $H + H_2$ results of Schatz and Kuppermann[16] at low energies. These methods appear very promising for obtaining quantitative reactive scattering results for atom – diatom systems other than $H + H_2$.

Appendix II.A. Nonreactive coupled channel Greens function for collinear $H + H_2$ scattering

1. Form of the coupled channel Greens function matrix

Here we present a derivation of the nonreactive Greens function matrix specific for our calculation on collinear $H + H_2$ reactive scattering. A more general discussion of coupled channel Greens functions can be found in reference 90. The nonreactive coupled channel Greens function matrix satisfies the following equation,

$$[\underline{I} \, (\frac{-\hbar^2}{2\mu} \frac{d^2}{dR^2}) + \underline{V}(R) - \underline{E}] \; ^o\underline{G}(R,R') = -\underline{I} \, \delta(R - R'),$$
(II.A.1)

where these are matrices indexed by the asymptotic vibrational expansion functions and $\underline{V}(R)$ is defined under eqn. (II.16). The Greens function matrix is everywhere finite. The nonreactive Greens function, like the nonreactive wavefunctions, are solved for each arrangement separately. Later, when put in a matrix in the combined index of arrangement and expansion functions, the nonreactive Greens function matrix will be diagonal in arrangement index.

The nonreactive regular, $^o f$, and irregular, $^o g$, wavefunctions are solutions of the following coupled equations,

$$[\underline{I} \, (\frac{-\hbar^2}{2\mu} \frac{d^2}{dR^2}) + \underline{V}(R) - \underline{E}] \; \{ \begin{array}{c} ^o\underline{f}(R) \\ ^o\underline{g}(R) \end{array} = 0,$$
(II.A.2)

with the asymptotic boundary conditions from eqns. (II.24) and (II.26),

$$^o\underline{f}(R) \sim \underline{s}(R) + \underline{c}(R) \; ^o\underline{K},$$

and

$$^{o}\underset{\sim}{g}(R) \sim \underset{\sim}{c}(R),$$

$$(II.A.3)$$

where $\underset{\sim}{g}$ and $\underset{\sim}{c}$ are defined in eqns. (II.25) and (II.104).

For $R' \neq R$, it follows from eqn. (II.A.1) that $^{o}\underset{\sim}{G}$ is a solution of the homogeneous equation,

$$[\underset{\sim}{I} \ (\frac{-\hbar^2}{2\mu} \ \frac{d^2}{dR^2}) + \underset{\sim}{V}(R) - \underset{\sim}{E}] \ ^{o}\underset{\sim}{G}(R,R') = 0.$$

For ^{o}G to remain everywhere finite, it follows from the boundary conditions that,

$$^{o}\underset{\sim}{G}(R,R') = \ ^{o}\underset{\sim}{f}(R) \ \underset{\sim}{A}(R'), \ R < R' \ ,$$

and

$$^{o}\underset{\sim}{G}(R,R') = \ ^{o}\underset{\sim}{g}(R) \ \underset{\sim}{B}(R'), \ R > R' \ ,$$

$$(II.A.4)$$

where $\underset{\sim}{A}(R')$ and $\underset{\sim}{B}(R')$ will be determined by matching the solutions at $R = R'$. $^{o}\underset{\sim}{G}$ is continuous at $R = R'$ so that,

$$^{o}\underset{\sim}{f}(R') \ \underset{\sim}{A}(R') = \ ^{o}\underset{\sim}{g}(R') \ \underset{\sim}{B}(R') \ ,$$

or

$$\underset{\sim}{B}(R') = \ ^{o}\underset{\sim}{g}^{-1}(R') \ ^{o}\underset{\sim}{f}(R') \ ^{o}\underset{\sim}{A}(R').$$

$$(II.A.5)$$

Next, we integrate eqn. (II.A.1) from an ε on either side of R' to obtain,

$$\lim_{\varepsilon \to 0} \int_{R'-\varepsilon}^{R'+\varepsilon} dR \ [\underset{\sim}{I} \ (\frac{-\hbar^2}{2\mu} \frac{d^2}{dR^2}) + \underset{\sim}{V}(R) - \underset{\sim}{E}] \ ^{o}\underset{\sim}{G}(R,R') = -\underset{\sim}{I} \ .$$

$$(II.A.6)$$

The terms involving $\underset{\sim}{V}(R)$ and $\underset{\sim}{E}$ go to zero as ε goes to zero since $^{o}\underset{\sim}{G}$ and $\underset{\sim}{V}$ are continuous in R, but since the derivatives of $^{o}\underset{\sim}{G}$ are not continuous at $R = R'$, the term involving the second derivative of $^{o}\underset{\sim}{G}$ does not go to zero. So, eqn. (II.A.6) becomes,

$$\lim_{\epsilon \to 0} \int_{R-\epsilon}^{R+\epsilon} \frac{-\hbar^2}{2\mu} \frac{d^2}{dR^2} \, {}^o\underline{\underline{G}}(R,R') = -\underline{I} \, ,$$

$$\lim_{\epsilon \to 0} \, [\frac{d\,{}^o\underline{\underline{G}}(R,R')}{dR} \Big|_{R=R'+\epsilon} - \frac{d\,{}^o\underline{\underline{G}}(R,R')}{dR} \Big|_{R=R'-\epsilon}] = \frac{2\mu}{\hbar^2} \underline{I} \, .$$

Making use of eqns. (II.A.4) and (II.A.5), this becomes,

$$[{}^o\underline{g}'(R') \, {}^o\underline{g}^{-1}(R') \, {}^o\underline{f}(R') - {}^o\underline{f}'(R')] \, \underline{\underline{A}}(R') = \frac{-2\mu}{h^2} \underline{I} \, ,$$

or

$$\underline{\underline{A}}(R') = \frac{-2\mu}{\hbar^2} [{}^o\underline{g}'(R') \, {}^o\underline{g}^{-1}(R') \, {}^o\underline{f}(R') - {}^o\underline{f}'(R')]^{-1} \tag{II.A.7}$$

where a primed function indicates the derivative with respect to R evaluated at the indicated value. Combining eqns. (II.A.4), (II.A.5), and (II.A.7), the expression for ${}^o\underline{\underline{G}}$ becomes,

$$\tag{II.A.8a}$$
$${}^o\underline{\underline{G}}(R,R') = \frac{-2\mu}{\hbar^2} \, {}^o\underline{f}(R) \, [{}^o\underline{f}'(R') - {}^o\underline{g}'(R') \, {}^o\underline{g}^{-1}(R') \, {}^o\underline{f}(R')]^{-1}, \, R < R',$$

$$\tag{II.A.8b}$$
$${}^o\underline{\underline{G}}(R,R') = \frac{-2\mu}{\hbar^2} \, {}^o\underline{g}'(R) \, [-{}^o\underline{g}(R') + {}^o\underline{f}'(R') \, {}^o\underline{f}^{-1}(R') \, {}^o\underline{g}(R')]^{-1}, \, R > R'.$$

Starting with eqn. (II.A.8a), we define,

$$\underline{\underline{U}}(R') = [{}^o\underline{f}'(R') - {}^o\underline{g}'(R') \, {}^o\underline{g}^{-1}(R') \, {}^o\underline{f}(R')]^{-1}. \tag{II.A.9}$$

Differentiating $\underline{\underline{U}}$ twice, it can be shown that,

$$\underline{\underline{U}}''(R') = \underline{\underline{U}}(R') \, {}^o\underline{g}''(R') \, {}^o\underline{g}^{-1}(R'), \tag{II.A.10}$$

where we have made use of the fact that,

$${}^o\underline{f}''(R') \, {}^o\underline{f}^{-1}(R') = {}^o\underline{g}''(R') \, {}^o\underline{g}^{-1}(R') = \frac{-2\mu}{\hbar^2} [\underline{\underline{E}} - \underline{\underline{V}}(R')],$$

which follows directly from the coupled equations, (II.A.2). It follows

from eqn. (II.A.10) that,

$$\underline{U}^{-1}(R') \ \underline{U}''(R') = {}^{o}\underline{g}''(R') \ {}^{o}\underline{g}^{-1}(R') = \frac{-2\mu}{\hbar^2} \ [\underline{E} - \underline{V}(R')],$$

or

$$[\underline{I} \ (\frac{-\hbar^2}{2\mu} \frac{d^2}{dR^2}) + \underline{V}(R') - \underline{E}] \ \underline{U}^{\dagger}(R') = 0. \tag{II.A.11}$$

So, $\underline{U}^{\dagger}(R')$ is a solution of the coupled equations, and therefore it must be a linear combination of the regular and irregular solutions,

$$\underline{U}^{\dagger}(R') = {}^{o}\underline{f}(R') \ \underline{c}_1 + {}^{o}\underline{g}(R') \ \underline{c}_2 \ , \tag{II.A.12}$$

where $\underline{c}_1$ and $\underline{c}_2$ are constant matrices. To determine $\underline{c}_1$ and $\underline{c}_2$, we compare the asymptotic forms of eqns. (II.A.9) and (II.A.12). Making use of eqns. (II.A.3), (II.25), and (II.104), one can show that,

$$\underline{c}_1 = 0 \quad \text{and} \quad \underline{c}_2 = \frac{\hbar}{\mu} \ \underline{I} \ ,$$

so that,

$$\underline{U}^{\dagger}(R') = \frac{\hbar}{\mu} \ {}^{o}\underline{g}(R'). \tag{II.A.13}$$

Combining eqn. (II.A.13) with eqn. (II.A.8a), we obtain,

$${}^{o}\underline{G}(R,R') = \frac{-2}{\hbar} \ {}^{o}\underline{f}(R) \ {}^{o}\underline{g}^{\dagger}(R'), \ R < R' \ . \tag{II.A.14}$$

Following a similar development for eqn. (II.A.8b), it can be shown that,

$${}^{o}\underline{G}(R,R') = \frac{-2}{\hbar} \ {}^{o}\underline{g}(R) \ {}^{o}\underline{f}^{\dagger}(R') \ , \ R > R'. \tag{II.A.15}$$

2. *Computational aspects*

Eqn. (II.A.14) and (II.A.15) provide a simple form for calculating

the nonreactive Greens function matrix from the normalized regular and irregular nonreactive wavefunctions. Unfortunately, though, the calculation of the Greens function matrix from the normalized wavefunctions is not numerically very stable. Now, we develop an alternative formula for calculating the Greens function matrix.

We begin by rearranging eqns. (II.A.8a) and (II.A.8b) to obtain,

$$^{O}\mathcal{G}(R,R') = \frac{-2\mu}{h^2} {}^{O}\underline{f}(R) \; {}^{O}\underline{f}^{-1}(R')[{}^{O}\underline{f}'(R') \; {}^{O}\underline{f}^{-1}(R')-{}^{O}\underline{g}'(R') \; {}^{O}\underline{g}^{-1}(R')]^{-1},$$
$$R < R', \quad \text{(II.A.16a)}$$

$$^{O}\mathcal{G}(R,R') = \frac{-2\mu}{h^2} {}^{O}\underline{g}(R) \; {}^{O}\underline{g}^{-1}(R')[{}^{O}\underline{f}'(R') \; {}^{O}\underline{f}^{-1}(R')-{}^{O}\underline{g}'(R') \; {}^{O}\underline{g}^{-1}(R')]^{-1},$$
$$R > R', \quad \text{(II.A.16b)}$$

The last factor of both equations above involves the inverse of the difference of the log derivative matrices for the regular and irregular solutions. We have given an algorithm for the calculation of the log derivative matrices in eqn. (II.103) which uses the ratio of the wavefunction at neighboring points.

Next, we express $^{O}\underline{f}(R) \; {}^{O}\underline{f}^{-1}(R')$ and $^{O}\underline{g}(R) \; {}^{O}\underline{g}^{-1}(R')$ in terms of ratio matrices. As is discussed in sec. 3b, the R coordinate is put on a grid, and the ratio matrix is calculated at each of the grid points. To avoid confusion between a point on the grid and the ratio matrices, points on the grid will be indicated with r_n rather than R_n. Using eqn. (II.100) we can show that,

$$^{O}\underline{f}(r_n) = \underline{R}_{n+1} \cdots \underline{R}_N \; {}^{O}\underline{f}_N \; ,$$

and

$$^{O}\underline{f}^{-1}(r_{n'}) = {}^{O}\underline{f}_N^{-1} \; \underline{R}_N^{-1} \cdots \underline{R}_{n'+1}^{-1}, \qquad \text{(II.A.17)}$$

where $^{O}\underline{f}_N$ is the normalized wavefunction at the last point, N, on the

grid and $\underset{\sim}{R}_n$ is a ratio matrix at point n defined under eqn. (II.98). There is an equation equivalent to (II.A.17) for the irregular solution. It follows directly for $r_n < r_{n'}$ that,

$$
{}^o\underset{\sim}{f}(r_n) \, {}^o\underset{\sim}{f}^{-1}(r_{n'}) = \underset{\sim}{R}_{n+1} \, \underset{\sim}{R}_{n+2} \, \cdots \, \underset{\sim}{R}_{n'} \, .
\tag{II.A.18}
$$

Making use of the equation corresponding to (II.A.17) for the irregular solution, with $r_n > r_{n'}$ it can be shown that,

$$
{}^o\underset{\sim}{g}(r_n) \, {}^o\underset{\sim}{g}^{-1}(r_{n'}) = \underset{\sim}{R}_n^{I \, -1} \, \underset{\sim}{R}_{n-1}^{I \, -1} \, \cdots \, \underset{\sim}{R}_{n'+1}^{I \, -1} \, .
\tag{II.A.19}
$$

Combining eqns. (II.A.18) and (II.A.19) with eqn. (II.A.16), the equations for the Greens function matrix becomes,

$$
{}^o\underset{\sim}{G}(r_n, r_{n'}) = \frac{-2\mu}{\not{h}^2} \underset{\sim}{R}_{n+1} \, \underset{\sim}{R}_{n+2} \, \cdots \, \underset{\sim}{R}_{n'} \, [\, {}^o\underset{\sim}{f}'(r_{n'}) \, {}^o\underset{\sim}{f}^{-1}(r_{n'})
$$

$$
- \, {}^o\underset{\sim}{g}'(r_{n'}) \, {}^o\underset{\sim}{g}^{-1}(r_{n'})]^{-1}, \, r_n < r_{n'},
$$

$$
{}^o\underset{\sim}{G}(r_n, r_{n'}) = \frac{-2\mu}{\not{h}^2} \underset{\sim}{R}_n^{I \, -1} \, \underset{\sim}{R}_{n-1}^{I \, -1} \, \cdots \, \underset{\sim}{R}_{n'+1}^{I \, -1} \, [\, {}^o\underset{\sim}{f}'(r_{n'}) \, {}^o\underset{\sim}{f}^{-1}(r_{n'})
$$

$$
- \, {}^o\underset{\sim}{g}'(r_{n'}) \, {}^o\underset{\sim}{g}^{-1}(r_{n'})]^{-1}, \, r_n > r_{n'}.
\tag{II.A.20}
$$

Since the log derivative matrices can be expressed in terms of the ratio matrices, the Greens function matrix can be calculated from eqn. (II.A.20) without using the normalized wavefunction by using instead the ratio matrices for the regular and irregular nonreactive wavefunctions. In section 3b we discuss the calculation of ratio matrices. Eqn. (II.A.20) is the formula used for the calculation of the nonreactive Greens function matrix.

III. Classical and quantum mechanical studies of HF in an intense laser field.

A. Introduction

Since the advent of high power lasers there has been great interest in the use of lasers in chemistry.[91] The uses have ranged from sophisticated forms of spectroscopy[92] to the control of molecular dynamics.[93] Experiments involving multiphoton absorption[94], overtone absorption[95], and radiationless transitions from excited states[96] have allowed the study of new phenomena in molecular dynamics. Also, laser pulses on a picosecond timescale[97] are allowing very fast processes to be observed. Resultingly, theoretical efforts[98] have turned toward understanding highly vibrationally excited molecules which exibit fundamentally different behavior than the harmonic oscillator (normal mode) view of ground state or very low vibrationally excited molecules. High densities of states in even small vibrationally excited molecules present a formidable but very important problem.

Here we examine a diatomic molecule subjected to a picosecond (ps) pulse of a very intense laser radiation. A diatomic molecule has the advantage of a simple and accurate potential energy function and a small number of states. This allows essentially exact quantum and classical calculations to be done. The dynamics of an isolated diatomic molecule is, of coarse, trivial, but here we dynamically account for the absorption of the coherent laser radiation. The disadvantage of studying a diatomic molecule is that the low density of states will have

a fundamentally different behavior than polyatomics at high vibrational energies. The advantage of being able to do exact calculations, though, allows for a good test of the validity of classical mechanics applied to these problems. Assuming that their validity can be established, classical trajectory techniques offer a way of possibly avoiding the problem of the unwieldy densities of states in polyatomic problems. This should be a rather severe test of classical mechanics since there are so few quantum states involved. Also, based on what can be learned from a diatomic molecule, understanding can be gained about the absorption processes in the lower parts of the vibrational manifold of small and moderate size molecules where ther are also well separated states.

Much of the interest in this field, especially towards the application of classical mechanics, was generated by the work of Walker and Preston[99] who performed quantum and classical calculations for a model nonrotating HF molecule. Their results, using laser intensities ≥ 10 TW/cm^2 (1TW = 10^{12} W) indicated good agreement between classical and quantum predictions of energy averaged over laser pulse times, except near multiphoton resonances. Since then there have been many exact classical[99-104] and quantum mechanical[99,102c,105-107] studies of oscillators in intense laser fields. Quantum mechanical studies have made use of Floquet analysis[105,108,109] to simplify the computation. Wyatt et. al.[105] have recently even made progress in studying dissociation of an oscillator in a laser using quantum mechanics. Davis and Wyatt[101], Stein and Noid[102c], and Gray[100] have made significant progress in understanding the classical behavior of nonrotating HF in an

intense laser field through the use of Poincaré surface of section plots. There have been some studies of model polyatomic systems[102d,103] but much remains to be done to get a good understanding of these systems.

Here we present quantum and classical results for HF in an intense laser field. The quantum and classical equations of motion are solved by direct numerical integration. For one and two photon absorption near the fundamental frequency we include results for both rotating and, for comparison, nonrotating HF initially in its ground state at laser intensities of 1.0 and 2.5 TW/cm^2. Calculations are also performed on overtone (v=0 + v=2) absorption for rotating and nonrotating HF and multiphoton absorption for nonrotating HF following a classical study by Christoffel and Bowman[104] for nonrotating HF, at the same laser intensity, 43.68 TW/cm^2. For all the calculations, energy absorption and transition probabilities are calculated as a function of laser pulse time and as an average over pulse time. It is found that classical mechanics does not correctly describe the time behavior of the system in most cases. Furthermore, classical rotational state distributions are completely incorrect for all the cases where rotating HF is studied.

For one photon (v=0 + v=1) absorption classical mechanics does give the correct magnitude of pulse averaged energy absorption. In addition, classical mechanics correctly indicates the presence of increased two photon absorption for frequencies lower than the one photon resonance, although, in agreement with Walker and Preston's[99] nonrotating results, specific resonances are not resolved and only a small amount of two photon absorption is seen. For the frequencies near the fundamental,

the effect of the laser phase is studied and found to have only a small
effect on the quantum results and little or no effect on the classical
results.

For the overtone absorption we find an even greater discrepancy
between the classical and quantum results than the discrepancy found
near the fundamental frequency. At overtone frequencies the classical
and quantum maxima of the pulse time averaged energy absorbed as a
function of laser frequency are shifted by 200 cm^{-1} relative to each
other. Very good agreement between the quantum and classical results is
observed for the multiphoton results. To study multiphoton absorption,
we fix the laser frequency at $\bar{\nu} = 3922$ cm^{-1} and vary the initial
vibrational state from 0 - 10, analogous to Christoffel and Bowman[104].
To get a better understanding of the overtone and multiphoton classical
results for nonrotating HF we construct Poincaré surfaces of section.

B. Methods

1. General information
    The calculations are performed for rotating and nonrotating HF.
The molecular Hamiltonian is

$$H_o = \frac{p_r^2}{2\mu} + \frac{1}{2\mu r^2} \left(p_\theta^2 + \frac{p_\phi^2}{\sin^2\theta} \right) + V(r), \qquad (III.1)$$

where r, θ, ϕ, p_r, p_θ, p_ϕ are spherical coordinates and their conjugate
momenta, and μ is the reduced mass. For the nonrotating case the term
with the angular momentum is excluded. The Born-Oppenheimer potential

is given by a Morse function $V = D\{1-\exp[-\alpha(r-r_e)]\}^2$, with values for the parameters[23] in atomic units of $D = 0.22509$, $\alpha = 1.1741$, and $r_e = 1.7329$ a.u.

The laser field is treated classically through a dipole interaction. This is valid in the limit of high photon density which is certainly true here. For very low intensities the photon field should be quantized[110] and classically the formalism developed by Miller[111] should be used. The full Hamiltonian with an oscillating electric field of frequency ω, z polarization and phase δ is ,

$$H = H_o - d(r) \cos\theta E_o \sin(\omega t+\delta),$$

(III.2)

where E_o is the field strength [in Gaussian units it is related to the intensity by $E_o = (8\pi I/c)^{1/2}$, where c is the speed of light] and $d(r)$ is the molecular dipole function. The $\cos\theta$ factor is omitted for the nonrotating case. A linear and quadratic form of the dipole funciotn are used, $d(r) = d_o + d_1(r-r_e)$, $d_o = 0.716$ and $d_1 = 0.310$ a.u. (1D = 0.39343 a.u.) for one and two photon absorption about the fundamental frequency corresponding to Ref. 105c, $d_o = 0.7362$ and $d_1 = 0.29769$ a.u. for overtone and multiphoton absorption corresponding to Ref. 104; $d(r) = d_o + d_1 r + d_2 r^2$, with[104] $d_o = -0.41010$, $d_1 = 1.04941$, $d_2 = -0.21551$ a.u. Laser intensities of 1.0, 2.5, and 43.68 TW/cm^2 were used which correspond to field strengths of 0.005338, 0.008440, and 0.03528 a.u., respectively (1v/cm = 1.9447×10^{-10} a.u.). The laser field is instantaneously turned on and turned off.

All numerical integrations were back integrated to reproduce all the initial variables to, at least, four significant figures to assure

numerical accuracy. It should be noted that for the quantum calculations, conservation of probability was not a valid criteria for good integration. There was, at least, one case where we obtained qualitatively incorrect results even though probability was conserved to six significant figures.

There is an approximation in using this potential since the electric field would perturb it a nontrivial amount. It would be more correct to use dressed molecular potentials[112]. Since we do not attempt to make our calculations quantitatively comparable to experiment, we avoid this extra complication.

To aid with the interpritation of the results, Table III.1 gives the relevant E_{vj}^o levels for HF, calculated with the rotating Morse oscillator formula[113].

2. Classical mechanics

The classical solution is found through the direct integration of Hamilton's equations of motion for the Hamiltonian given in Eq.(III.2). In the absence of external fields there are three conserved quantities which are the vibrational action N_v,

$$N_v = - \frac{1}{2} + \frac{1}{2\pi} \cdot \oint p_r \, dr,$$

the rotational angular momentum J,

$$[J(J+\hbar)]^{1/2} = (p_\theta^2 + \frac{p_\phi^2}{\sin^2\theta})^{1/2},$$

and the z projection of the angular momentum $M = p_\phi$.

With the interaction present, the vibrational action N_v and rotational angular momentum J are no longer conserved. However, with the present choice of polarization, M is still conserved since H has no ϕ dependence. The complete classical solution involves specification of the appropriate initial conditions and solution of Hamilton's equations:

$$\dot{p}_r = - \frac{\partial H}{\partial r} = \frac{1}{\mu r^3} (p_\theta^2 + p_\phi^2/\sin^2 \theta) - \frac{\partial V}{\partial r}$$
$$+ \frac{\partial d}{\partial r} \cos \theta \ E_o \ \sin(\omega t + \delta),$$

$$\dot{p}_\theta = - \frac{\partial H}{\partial \theta} = p_\phi^2/\mu r^2 \sin^3 \theta - d(r)\sin\theta \ E_o \ \sin(\omega t + \delta), \qquad (III.3)$$

$$\dot{r} = \frac{\partial H}{\partial p_r} = p_r/\mu,$$

$$\dot{\theta} = \frac{\partial H}{\partial p_\theta} = p_\theta/\mu r^2.$$

Approximate analytic orbits have been obtained[113] for a rotating Morse oscillator with no external field, and these are used to determine diatomic initial conditions (see Appendix III.A for details). This approximation is excellent for the vibration − rot? on levels of importance here. The laser phase δ is averaged over in most cases for one and two photon absorption about the fundamental frequency (i.e. each trajectory has δ chosen randomly between 0 and 2π), although it will be shown to be unimportant. It is set to zero for the overtone and multiphoton calculations.

For the rotating HF calculations, 1000 trajectories with random initial conditions (see Appendix III.A) were run for each frequency. Monte Carlo errors in the quantities of interest were between 10% and

15%. For the nonrotating HF calculations, 50 trajectories were run for each frequency. In this case, it is more efficient to increment the vibrational angle variable in a stepwise fashion between 0 and 2π than to pick it randomly. The classical equations of motion were integrated with a standard predictor – corrector algorithm[114] to either 0.9 or 1.5 ps. Integration of the classical equations of motion beyond 1.5 ps. is extremely difficult due to the accumulation of error. The integration of oscillatory nonlinear differential equations over long time periods is still a current problem in numerical analysis[115].

The energy absorbed as a function of pulse length is defined by

$$\langle E(t)\rangle_{CL} = \frac{1}{N} \sum_{i=1}^{N} H_o \, [p_r^i(0), \, p_\theta^i(0), r^i(0), \theta^i(0), \delta^i, t] - E_i \tag{III.4}$$

where N is the number of trajectories and E_i is the initial molecular energy. The final vibrational action N_v after a pulse of length t is also calculated with the rotating Morse oscillator approximation[114]. Appendix III.A shows that this is an excellent approximation for the states of interest here. J is calculated directly from $J(J+K) = p_\theta^2 + p_\phi^2/\sin^2\theta$. (Note: $p_\phi = 0$ in the present study since $J = 0$ initially.) With $K = 1$, N_v and J are boxed according to the nearest integers v,j such that $v-1/2 < N_v < v+1/2$ and $j-1/2 < J < j+1/2$, which is the usual quasiclassical quantization procedure. The transition probability into a particular v,j state, as a function of pulse length is

$$P_{v,j}^{CL}(t) = N_{v,j}(t)/N, \tag{III.5}$$

where $N_{v,j}(t)$ is the number of trajectories with final actions in the v,j box. Of coarse, a single trajectory integrated out to some large

pulse length T contributes to all intermediate pulse time results. Also, pulse averaged energy absorbed and transition probabilities are defined as

$$\bar{E}_{CL}(\omega) = \frac{1}{T} \int_0^T \langle E(t) \rangle_{CL} \, dt,$$

$$\bar{P}_{v,j}^{CL}(\omega) = \frac{1}{T} \int_0^T P_{v,j}^{CL}(t) \, dt. \tag{III.6}$$

By between 0.9 and 1.5 ps., the pulse averaged energy absorption Eq. (III.6) appears to be converging, but has not fully converged. However, reasonable estimates of the converged $\bar{E}_{CL}(\omega)$ can be obtained, since $\langle E(t) \rangle_{CL}$ has either reasonably leveled off or oscillates with a small amplitude. Thus, either the leveled off value or the average of the oscillations in $\langle E(t) \rangle_{CL}$ is taken to be $\bar{E}_{CL}(\omega)$. The error in the averaged quantities is expected to be less than 10%.

3. Quantum Mechanics

    Although Floquet[105,109] analysis has been used as an efficient and stable way to obtain long time quantum solutions for oscillators in a laser field, the time scale of interest here is short enough ($\leq$ 20 ps) that direct integration of the coupled quantum equations is possible.

    The total wavefunction is expanded as

$$\Psi_m(r,\theta,\phi,t) = \sum_{v,j} c_{v,j,m}(t) \, \chi_{v,j,m}(r,\theta,\phi), \tag{III.7}$$

with

$$\chi_{v,j,m}(r,\theta,\phi) = R_v(r) \, Y_{j,m}(\theta,\phi)/r.$$

The $Y_{j,m}$ are spherical harmonics and R_v are Morse eigenfunctions[116]. Strictly speaking, R_v should also depend on j, but in the present

problem, with only small values of j being important, such rotational corrections should be small. As in classical mechanics, the z component of the angular momentum (m$\hbar$) is conserved. Since the present study involves j = 0 initially, m is zero throughout. In all subsequent equations m is understood to be zero. If the molecule had j ≠ 0 initially, it would be necessary to average over transition probabilities for all integer values of m such that −j ≤ m ≤ j.

Inserting Eq. (III.7) into the time dependent Schrödinger equation results in the coupled equations

$$i\hbar\dot{c}_{v,j}(t) = E^o_{v,j}\, c_{v,j} + \sum_{v,j} D_{v'j',vj}\, c_{v',j'}\, E_o\, \sin(\omega t+\delta),$$

(III.8)

where the $E^o_{v,j}$ are eigenvalues of $\hat{H}_o$ are matrix elements

$$D_{v'j',vj} = -\int_0^\infty R_{v'}\, d(r)\, R_v\, dr \times \left\{ \begin{array}{ll} \left[\dfrac{(j+1)^2}{(2j+1)\,(2j+3)}\right]^{1/2} & ,\; j' = j+1 \\[2mm] & \text{or} \\[2mm] \left[\dfrac{j^2}{(2j-1)\,(2j+1)}\right]^{1/2} & ,\; j' = j-1 \end{array} \right.$$

(III.9)

It will be shown later, as with the classical results, that the laser phase δ does not appreciably affect the results. For efficiency, the majority of the quantum calculations are made with a fixed δ of π/2. The coefficients $C_{v,j}$ of Eq. (III.8) must be complex. Thus, writing $C_{v,j} = X_{v,j} + iY_{v,j}$, one obtains the coupled real equations

$$-\hbar\dot{Y}_{v,j} = E^o_{v,j}\, X_{v,j} + \sum_{v',j'} D_{v'j',vj}\, X_{v',j'}\, E_o\, \sin(\omega t+\delta),$$

$$/\hbar\dot{X}_{v,j} = E^o_{v,j}\, Y_{v,j} + \sum_{v',j'} D_{v'j',vj}\, Y_{v',j'}\, E_o\, \sin(\omega t+\delta).$$

(III.10)

The quantum equations of motion were integrated with the same

predictor-corrector algorithm used in the classical calculations. For the one and two photon resonances near the fundamental frequency, an adequate basis for HF with the intensities and time scales of interest consisted of the first five v and first five j states, i.e. a 25 term expansion. The nonrotating quantum solutions were obtained in an analogous fashion, using the first five vibrational states in the wavefunction expansion. About the overtone frequency, basis sets for rotating HF consisted of either seven vibrational states each with seven rotational states or, further from resonance, five vibrational states each with five rotational states. For nonrotating HF, ten states were used in the overtone calculations, and as many as all 24 vibrational states were used in the multiphoton calculations at $\bar{\nu} = 3922$ cm^{-1}.

The transition probabilities are found from the coefficients of the basis functions

$$P_{v,j}^{QM}(t) = \left| c_{v,j}(t) \right|^2.$$
(III.11)

The energy absorbed is defined as

$$\langle E(t) \rangle_{QM} = \sum_{v,j} P_{v,j}^{QM}(t) \; E_{v,j}^{o} - E_{i}^{o},$$
(III.12)

where E_{i}^{o} is the energy of the initial state. The pulse averaged energy absorbed and transition probability are given by

$$\bar{E}_{QM}(\omega) = \frac{1}{T} \int_0^T \langle E(t) \rangle_{QM} \; dt,$$

$$\bar{P}_{v,j}^{QM}(\omega) = \frac{1}{T} \int_0^T P_{v,j}^{QM} \; (t) \; dt.$$
(III.13)

The quantum solutions were integrated from 1 to 10 ps depending on

frequency range and how near resonance, which is long enough to converge
the time averaged quantities to 10%. Note that it was sometimes
necessary to average over small oscillations which had not damped
completely out yet that were apparent in $\bar{E}_{QM}$ as a function of pulse
length T to obtain the best estimate. Interestingly, because the
quantum equations are linear, it is possible to integrate 50 coupled
quantum equations to times exceeding 20 ps, which is much longer than it
is practicle to integrate only four nonlinear classical equations.

4. Poincaré surfaces of section

At least three, essentially equivalent, formalisms have been used
to define the Poincaré surfaces of section for time dependent oscillator
problems. The methods of Stine and Noid[102e] and Gray[100] are exactly
equivalent, and the method of Davis and Wyatt[101] identically reduces to
the other two methods in the limit of strong fields which is certainly
the limit studied here. We will follow the formalism of Gray[100].
First, we define a mapping of a phase space point $[p(t),x(t)]$ to a point
$|p(t+1/\nu),x(t+1/\nu)|$ where ν is the laser frequency and $1/\nu$ is a period of
the laser. (Note that the notation has been changed from above with
(p_r,r) replaced by (p,x) to be consistant with the more ususal one-
dimensional notation.) Beginning at a point in phase space, the surface
of section is generated by repeatedly mapping the point until either a
closed curve is generated or a chaotic trajectory is found.

The surface of section plots are constucted for nonrotating HF
using action-angle variables (n,q) so that the unperturbed Hamiltonian
is only a function of the action. This is convenient since it is easy
to see changes in the molecular energy, and it makes the resolution of

the structure in the high energy region of phase space equivalent to that at low energy. Also, the integration in the chaotic region of phase space seems somewhat stabler. The transformation to action-angle variables is known for a Morse oscillator[117]. The unperturbed Hamiltonian becomes

$$H_o(n) = \left(n + \frac{\gamma}{2}\right)\omega_o - \left(n + \frac{\gamma}{2}\right)^2 \cdot \frac{\omega_o^2}{4D},$$
(III.14)

where $\omega_o = (2d\alpha^2/\mu)^{1/2}$. The equations of motion of the unperturbed oscillator are $\dot{n} = 0$ and $\dot{q} = \omega(n)$, where the oscillator frequency is

$$\omega(n) = \frac{\partial H_o}{\partial n} = \omega_o - \left(n + \frac{\gamma}{2}\right) \omega_o^2/2D.$$
(III.15)

This corresponds to a line in phase space with n = constant and $q = \omega t$. The old variables, expressed in terms of the action-angle variables are

$$x(n,q) = \alpha^{-1} \ln\{[D + (DH_o)^{1/2} \cos q]/(D - H_o)\},$$

$$p(n,q) = \mu\omega(n) \frac{\partial x}{\partial q}$$
(III.16)

$$= \mu\alpha^{-1} \omega(n) \cdot (DH_o)^{1/2} \sin q/[D + (DH_o)^{1/2} \cos q].$$

The total Hamiltonian in terms of the new variables is

$$H(n,q,t) = H_o(n) - \epsilon x(n,q)\cos(\Omega t).$$
(III.17)

The equations of motion are

$$\dot{n} = -\epsilon \cos(\Omega t) \cdot (DH_o)^{1/2}\sin q/\{\alpha[D + (DH_o)^{1/2}\cos q]\}$$

$$\dot{q} = \left[\omega_o - \left(n + \frac{1}{2}\right)\frac{\omega_o^2}{2D}\right]\left(1 - \frac{\epsilon \cos(\Omega t)}{\alpha}\right.$$

$$\left. \times \left\{\frac{\cos q}{2[(DH_o)^{1/2} + H_o \cos q]} + \frac{1}{(D - H_o)}\right\}\right).$$
(III.18)

It should be noted that ... phase convention for the action—angle
variables, here, follows that of Ref. 100.

C. Results and discussion

1. One and two photon absorption about the fundamental frequency

a. Energy absorption spectra

The quantum and classical pulse time averaged energy absorption
spectra are plotted in Fig. III.1(a) for nonrotating HF and Fig. III.1(b)
for rotating HF, with laser intensity 1.0 TW/cm^2. The plot for
nonrotating HF is similar to plots of Walker and Preston[99] for higher
intensities ($\geq$ 10 TW/cm^2). At 1.0 TW/cm^2, though, the quantum structure
is more resolved. The major features are a narrow two photon resonance
at $\bar{\nu}$ = 3879 cm^{-1} (the v=0 to v=2 absorption), and a broad one photon
resonance at 3966 cm^{-1} (the v=0 to v=1 absorption). The classical
spectrum shows just one very broad peak with a maximum at about $\bar{\nu} \approx$ 3940
cm^{-1}. While the classical spectrum does not have any of the quantum
structure, examination of the classical state distribution does show the
presence of a small amount of two photon absorption, as the frequency is
lowered. Details of this will be given later.

For rotating HF, the spectra [Fig. III.1(b)] are qualitatively
similar to the nonrotating case. There are three peaks in the quantum
spectrum: one broad peak near $\bar{\nu}$ = 4006 cm^{-1} [the $(v,j) \equiv (0,0) \rightarrow (1,1)$ one
photon resonance] with a full width at half maximum (FWHM) of $\sim$ 50 cm^{-1},
and two narrow peaks near $\bar{\nu}$ = 3937 cm^{-1} [the $(0,0) \rightarrow (2,2)$ two photon
resonance] and 3879 cm^{-1} [the $(0,0) \rightarrow (2,0)$ two photon resonance], each

with a FWHM of $< 10 \text{ cm}^{-1}$. The classical specrum has one very broad peak which peaks near the $(0,0) \rightarrow (1,0)$ resonance at $\bar{\nu} = 3966 \text{ cm}^{-1}$. Overall, the classical solution for rotating HF gives a general idea of the absorption. As in the nonrotating case, the classical result predicts increased two photon absorption for frequencies red shifted from the one photon resonance, as will be seen below in Sec. C.1.b.

In Fig. III.2, the rotating HF average energy absorption for $I = 2.5 \text{ TW/cm}^2$ is shown. Qualitatively, the quantum peaks become broader and overlap more than the 1.0 TW/cm^2 case. There appears to be a small power shifting of the resonance peaks, toward higher frequencies, but it has not been resolved (see Ref. 105c for a discussion of power shifting). Classically, the absorption also broadens relative to 1.0 TW/cm^2 and the peak maximum appears to shift to lower freuencies, indicating more multiphoton absorption.

b. Transition probabilities

In this section, the approximate time averaged transition probabilities into various states are examined qualitatively to help show the relative amounts of one and two photon absorption. Looking at the classical results, it is clear that classical mechanics does not give the correct rotational state distribution. Classically, there are large probabilities for ending in the $(0,1)$ and $(1,0)$ states, which correspond to high order processes in quantum mechanics. These transitions are not observed to any large extent in the quantum results. To get a meaningful comparison, only the probabilities for ending in a particular vibrational level will be considered, i.e., a sum is taken over rotational states within a vibrational level.

Table III.2 shows the quantum and clasical time averaged probabilities at various frequencies for rotating and nonrotating HF, with $I = 1.0$ TW/cm^2. Each peak of the quantum solution can be seen to be either a one or a two photon absorption, with both processes observed appreciably only where peaks overlap. At high intensities the peaks will broaden and overlap more, but each peak will still correspond to a particular absorption. The classical results do indicate the presence of some two photon absorption as the frequency is decreased. But classically, there is a very gradual change, which results in the very broad single peak in the spectrum (Fig. III.1), rather than the abrupt changes in the quantum results.

To show some intensity effects, average probabilities for rotating HF at 2.5 TW/cm^2 are given in Table III.3. For this larger intensity, both classically and quantum mechanically, the excited states become more populated.

c. Time behavior

The previous two sections were concerned with average quantities. In this section, the energy absorption and transition probabilities as a function of time are examined. The quantum mechanical laser phase used in this section was fixed at $\pi/2$. The effect of laser phase is examined in the next section.

In Fig. III.3, a comparison of classical and quantum energy absorption as a function of time is given for nonrotating HF at $\bar{\nu} = 3966$ cm^{-1} (the one photon v=0 to v=1 resonance). The quantum results show oscillations with a period of about 0.75 ps with no sign of damping out to 1.5 ps. At this frequency and intensity (1.0 TW/cm^2) the solution is

well approximated by a two level system (i.e., the Rabi model[24]). In
contrast, the classical result oscillates with a frequency of about 0.4
ps and a smaller amplitude. Also, it appears as though the oscillations
may be damping.

Fig. III.4 shows the classical and quantum time dependent energy
adsorption for rotating HF with $\bar{\nu} = 4006$ cm^{-1} [one photon $(0,0) \rightarrow (1,1)$
resonance]. The results are similar to those in Fig. III.3 for
nonrotating HF. In this case, though, the classical result appears to
level off even faster. The behavior of the quantum solution is again
well approximation by the two level Rabi model. [24] The quantum solution
has been followed for up to 20 ps with no clear sign of damping.

The quantum result for the two photon resonance at 3937 cm^{-1} [$(0,0)$
$\rightarrow (2,2)$ resonance] is considerably different (Fig. III.5). The
complicated nature of the oscillations may be contrasted with the Rabi
oscillations of Fig III.4. From Fig. III.5, it can be seen that the two
photon absorption is a long time process. The corresponding classical
result (Fig. III.6) also seems to show some aspects of the slower growth
in absorption, although the solution is reasonably level by 0.9 ps.

In Figs. III.7, 8, and 9, plots are shown for some transition
probabilities as a function of time, again for $I=1.0$ TW/cm^2. Here, the
classical solution is actually broken up into rotational levels, so that
the discrepancy with quantum mechanics can be seen. The quantum
solutions for P_{01} and P_{10} are not shown since they are very small
($\leq 10^{-2}$). Qualitatively, the probabilities show the same behavior as
the energy absorption as a function of time, i.e., the classical
solutions tend to level off more and the quantum solutions appear

periodic. Note that in reality there are high frequency, small
amplitude oscillations that are superimposed on the quantum
probabilities. These oscilations have not been resolved on our graphs
and thus give rise to some roughness, particularly near peak maxima.

The classical probabilities for rotating HF at $\bar{\nu} = 3937$ cm^{-1} are
shown in Fig. III.8. It can be seen that the v = 2 states gets
significantly populated, but the v = 1 state is also significantly
populated. The quantum probabilities near the two photon resonance at $\bar{\nu}$
= 3937 cm^{-1} are shown in Fig III.9. The resonance probability $P_{22}(t)$
displays a long period which essentially matches the period of $\langle E(t)\rangle_{QM}$
in Fig. III.5. Another reasonably significant probability is P_{11}, which
is not shown. $P_{11}(t)$ displays a higher frequency oscillation and can
reach a maximum of ~ 0.13. The other two photon resonance at $\bar{\nu}$ = 3879
cm^{-1} is not plotted here. Qualitatively, the classical results for this
frequency show much less excitation than for 3937 cm^{-1}. There is a
small amount of v = 1 excitation and no v = 2 excitation. Essentially
no rotational excitation is seen in the classical results for this
frequency. The quantum results for 3879 cm^{-1} show somewhat less
excitation into the (1,1) state than foe 3937 cm^{-1}, and again the
resonant probability P_{20} displays a long period.

d. Laser phase effect

Based on the classical and quantum equations of motion [Eqs.
(III.3) and (III.8)] without additional approximations, one would expect
the solution to be dependent on the choice of laser phase δ. Without
allowing for the details of how the field is turned on, complete study
should involve averaging over the laser phase to obtain the most

meaningful results[118].

The laser phase dependence, however, disappears from the quantum equations in the rotating wave approximation[24,119], as shown in Appendix II.B for the two state model. However, for sufficiently large field strengths or de-tuning of ω from resonance, the rotating wave approximation will break down[119b]. Thus, for example, Moloney and Meath[118] have shown the laser phase dependence of probabilities as a function of time for a two state model. They found increasing phase effects for larger field strengths and at multiphoton resonances.

The situation is not quite as clear in the classical analysis. However, if only the relative difference between laser phases is important, then it would be sufficient to average only over the vibrational phase, without averaging over the laser phase, i.e., the laser phase would not matter. The conditions for this to be true probably include ω be close to resonance.

To assess the effects of laser phase δ on the present problem, consider first nonrotating HF. For an intensity of 1.0 TW/cm^2 and frequencies of 3966 and 3879 cm^{-1}, the classical solutions were obtained for fixed δ of 0 and $\pi/2$. 500 trajectories were run for each solution to insure no statistical error. Over the entire 1.5 ps range, $\langle E(t) \rangle_{CL}$ for the two phases agreed to between two and four significant figures. The quasiclassical probabilities also were in excellent agreement. Similarly, the nonrotating quantum results for the same conditions showed little phase dependence.

We also examined rotating HF at 1.0 TW/cm^2 for the possibility of phase effects. Within the Monte Carlo error ($\lesssim$ 15%), no clear phase

effect can be distinguished in the classical results. However, slight discrepancies in the time dependent quantum solutions may be seen, since no statistical error is present. Table III.4 lists some relevant probabilities and the energy absorption both as a function of time for δ = 0 and $\pi/2$, at $\bar{\nu}$ = 4006 cm^{-1}. Other phases phases between 0 and π were also examined, but the largest differences were found between δ = 0 and δ = $\pi/2$. Despite $\bar{\nu}$ being almost exactly on resonance, slight differences may be noted, particularly in the probabilities. These diferences become larger near peak maxima and can be as much as 4%. However, such differences are comparable in amplitude to the high frequency oscillations that are superimposed on the Rabi oscillations, and do not appreciably affect the overall behavior. Notice that $\langle E(t) \rangle_{QM}$ is not affected much by these differences, indicating that the differences of the other probabilities, which are smaller and not listed, tend to compensate. Table III.5 presents similar results for $\bar{\nu}$ = 3937 cm^{-1}. Although this is a two photon resonance, the discrepancies due to laser phases are comparable to the $\bar{\nu}$ = 4006 cm^{-1} results. Thus, for intensities ~ 1.0 TW/cm^2, and the present frequency range, the effects of laser phase is small and can be neglected for most practical purposes.

2. Multiphoton absorption

Here we examine the absorption of nonrotating HF when the laser frequency is fixed at $\bar{\nu}$ = 3922 cm^{-1} (44 cm^{-1} lower than the v=0 + v=1 resonance frequency), and the initial vibrational state is varied. This is an interesting problem from the point of view of a quantum and classical comparison since, as will be shown in a later section, the

region of classical phase space examined includes a 1:1 resonance, a 1:2 resonance, and a region of overlapping higher order resonances with chaotic trajectories.

Figure III.10 shows a quantum and classical comparison of pulse time averaged energy absorbed for initial states $0 - 10$. The agreement throughout this region is extremely good except for $v = 9$, 10 where the discrepancy may be partly due to the lack of continuum states in the wave function expansion. In light of our results in section C.1 at 1.0 TW/cm^2 laser intensity which showed moderate agreement for initial state $v = 0$ at this frequency, this agreement is a little surprising. The behavior of the time averaged energy absorbed (i.e., the sharp dip followed by the slow rise to zero then the sharp increase) can be explained qualitatively for both the quantum and classical results. The classical results are due to a classical 1:1 resonance at lower actions and a region of overlapping resonances at higher actions. This will be discussed in detail in section C.4 where the surface of section is shown. The dominating features of the quantum results are overlapping resonances which result in many states becoming populated. The loss of energy for initial vibrational states 2, 3, and 4 results from being more in resonance with stimulated emission than absorption. At intermediate initial states (5, 6, 7, 8), all states are further off resonance, so there are less transitions out of the initial state. At high initial states (9, 10) overtone transitions begin to become significant. This domination of overlapping resonances is in contrast with the two state resonances of sections C.1 and C.3. For comparison, interesting model calculations have been carried out by Eberly et.

al.[120] showing the time evolution of the populations of groups of states which are off resonance by varying amounts.

Table III.6 shows the time averaged transition probabilities which correspond to the averaged energies plotted in Fig. III.10. Again the agreement between the quantum and classical results is fairly good. For initial vibrational states $0 - 4$, the agreement is essentially exact. At intermediate initial states where absorption and desorption are approximately equal, there are fewer transitions from the initial state in the quantum results. For initial states 9, 10 there is greater discrepancy which may be due, as stated above, to the lack of continuum states in the wave function expansion.

3. Overtone spectra

a. Time averaged energy absorbed

For both rotating and nonrotating HF the classical and quantum time averaged energy absorbed are plotted vs laser frequency in Figs. III.11 and III.12. For nonrotating HF both a linear and quadratic dipole function are used. In all the cases, the distinguishing characteristics between the quantum and classical results are (1) a shift of the classical peak by $100-200$ cm^{-1} toward higher frequencies, and (2) the classical peaks are lower and broader than the corresponding quantum peaks. The quantum peaks, within the resolution of our graphs, are near where they are expected from the $v=0 \rightarrow v=2$ resonance frequency. There probably are small, unresolved power shifts[105c] in the peaks which are not significant for our considerations here. The classical spectra, with the linear dipole function, peak at nearly twice the $v=0 \rightarrow v=1$ absorption frequency. With the nonlinear dipole function the classical

spectrum peaks closer to the quantum result, but is still shifted by over 100 cm^{-1}. It should be noted that both the quantum and classical results show greater absorption with a nonlinear dipole function. The quantum peak becomes about twice as broad, and the classical peak becomes 50% higher and somewhat broader. The maximum of all the quantum peaks approximately equals the expected value from the two state Rabi model[24], as we found for the $v=0 \rightarrow v=1$ resonance and two photon absorption in Sec. III.A.

These results are interesting considering that we found better agreement between the quantum and classical results for $v=0 \rightarrow v=1$ absorption (section C.1) and the multiphoton results at $\bar{v} = 3922 \text{ cm}^{-1}$ (section C.2). One would expect best agreement between quantum and classical results for averaged quantities since quantum effects tend to be averaged over. Even so, it is clear that in at least some circumstances, it would be misleading to look exclusively at the classical results even for an averaged quantity as the time averaged energy absorbed without accounting for possible discrepancies with the quantum mechanical results. More discussion of this will follow in the summary.

b. Time averaged transition probabilities

Table III.7 shows the approximate time averaged vibrational transition probabilities with a linear dipole function (rotating and nonrotating HF) and a quadratic dipole function (nonrotating HF). For rotating HF, the transition probabilities in Table III.7 are summed over rotational states. One can see quite dramatically that the quasiclassical results do not describe the transition probabilities of

the v=0 → v=2 overtone absorption correctly. For both rotating and
nonrotating HF the classical calculations with the linear dipole
function show no excitation above the v = 1 level. But for all the
quantum results there is basically a coherent two state excitation (Rabi
oscillation)[24] between the v = 0 and v = 2 levels. Even with a
nonlinear dipole function for nonrotating HF, while there is some
quasiclassical absorption into the v = 2 state, most of the absorption
is still into the v = 1 state.

c. Energy absorbed as a function of time

It is important to consider molecular properties as a function of
pulse time since these should be important for comparison with
experiment. In Figs. III.13 and III.14 the time evolution of the
energy absorbed is shown for nonrotating HF with a linear dipole
function. Figures III.15 and III.16 show the time evolution of the
energy absorbed for rotating HF. The quantum results show the
characteristic sine squared shape of a Rabi oscillation. The classical
results have a much smaller oscillation with a larger frequency which
appears to be possibly damping out at longer times, more quickly for
rotating HF. These results are closely analogous to the results in
section C.1 obtained about the fundamental frequency. The results for
nonrotaitng HF with a quadratic dipole function are not shown since they
are qualitatively the same as those with a linear dipole. The only
significant differences are a shorter period of the oscillations of
slightly more than a factor of 2 for the quantum results and slightly
less than a factor of two for the classical results.

d. Transition probabilities as a function of time

The time evolution of the transition probabilities for rotating HF are displayed in Figs. III.17 and III.18. The equivalent graphs for nonrotating HF are not shown since they give essentially no new information. The interest for rotating HF comes from the rotational excitation of the $v=0$, $j=1$; $v=2$, $j=0$; and $v=2$, $j=2$ states in the quantum results. This is quite surprising considering that these states are far off resonance. The classical results which have a few small oscillations that appear to damp out are again quite reminiscent of the results near the fundamental frequency (section C.1). Classically, the $v=1$, $j=0$ state becomes most populated with some excitation into the $v=0$, $j=1$ and $v=1$, $j=1$ states.

A simple numerical experiment shows that the apparent quantum rotational excitation is just that. For example, if a numerical calculation is carried out with only the $v=0$, $j=0$ and $v=0$, $j=1$ states in the expansion, there is absorption with the correct frequency and magnitude that would be expected from the high frequency oscillations of Fig. III.17. The dynamics displayed in Fig. III.17 can be described as a high frequency oscillation between different rotational states within a vibrational manifold superimposed on a low frequency near resident oscillation between the $v = 0$ and $v = 2$ levels. These can be thought of independently because of the differences in time scales and the near equivalence of the matrix elements for vibrational transitions of the different rotational states. In Fig. III.19 the quantum tranition probabilities summed over all rotational levels for rotating HF are plotted as a function of pulse time. It shows an amazingly smooth oscillation.

The oscillation between the different vibrational levels, as shown in Fig. III.19, can be described quite well by a Rabi two state model[24]. Assuming the frequency is on resonance, the Rabi model would predict a period of 1.85 ps for the $v=0, j=0 \rightarrow v=2, j=1$ transition and $v=0, j=1 \rightarrow v=2, j=0$ transition, and 2.07 ps for the $v=0, j=1 \rightarrow v=2, j=2$ transition. The transition probability into the $v = 2$ level never reaches unity which can be due to a breakdown of the two state model, or a breakdown of the Rabi model which assumes the rotating wave approximation[24,119]. The same is not true of the rotational transitions. For the $v=0, j=0 \rightarrow v=0, j=1$ transition, the Rabi model predicts a maximum absorption of about half of the observed value and an oscillation frequency of about a factor of 7 too large. This is not surprising since one of the assumptions in the rotating wave approximation is that the transition is near the resonance. Since the rotational transitions are nowhere near resonance, the rotating wave approximation, and therefore the Rabi model, should not be valid.

4. Poincaré surfaces of section

In this section we use surfaces of section to understand the nature of the classical solution for nonrotating HF with a linear dipole function. First we examine the surfaces of section for the overtone absorption of section C.3, followed by the multiphoton results of section C.1. Many excellent reviews of nonlinear classical mechanics exist,[98a,121,122] so much of the background is omitted for brevity.

a. Overtone absorption

In Fig. III.20 we show two surfaces of section for overtone absorption, the first at the quantum resonance frequency $\bar{v} = 7757.8$ cm^{-1}

and the second at the frequency of maximum classical energy absorption $\bar{\nu}$ = 7980 cm^{-1}. At both frequencies the solutions are all regular in the region of phase space examined up to a time of 100 periods of the laser field, about 0.43 ps. It should be restated that the surface of section is generated by the mapping discussed in section B.4 and is not an actual trajectory. For illustration, there is one actual trajectory for two periods of the laser field, in Fig. III.20(a) shown as a dashed line. With more oscillations of the field the trajectory will touch all of the points on the ellipse. Both surfaces of section display a large, isolated 1:2 classical resonance. The fixed points of the mapping are clearly marked, and the separatrix connects the unstable fixed points. The stable fixed points result from a strictly periodic trajectory where the molecule oscillates one period per two oscillations of the field.

It is easy to infer the magnitude of the time averaged energy absorbed from these plots. Following the usual quasiclassical procedure, initial conditions are chosen using a fixed action and a range of angles between 0 and 2π. One can see from Fig. III.20(a) that if a trajectory is started with zero initial action and any angle, the trajectory averaged over time will gain or lose little energy since after every laser period, the action remains near zero. In Fig. III.21, the time averaged energy absorbed is plotted as a function of initial actions for $\bar{\nu}$ = 7757.8 cm^{-1}. This shows that starting near the bottom of the resonance stucture, energy is gained on the average; but staring near the top of the resonance structure, energy is lost. At $\bar{\nu}$ = 7980 cm^{-1} the resonance structure is pushed to lower actions than at $\bar{\nu}$ = 7757.8 cm^{-1}. This explains why there is classical absorption at $\bar{\nu}$ =

7980 cm^{-1}. The narrowness of the resonance explains why there is no quasiclassical absorption into the v = 2 states. (The top of the resonance has an action of less than 1.2.) The semiclassical nature of the classically forbidden overtone transition in this case may be interpreted in a fashion analogous to that which leads to certain local mode energy splittings[123] as discused by Gray[124].

b. Multiphoton absorption

The surface of section for $\bar{\nu} = 3922$ cm^{-1} in Fig. III.22 displays a more interesting behavior. At low actions there is a dominating, isolated 1:1 resonance. From the plot one can see that there is strong absorption from the $N_v = 0$ initial state, and that the absorption populates states as high as $N_v = 4$. The classical dynamics at other low of intermediate levels can be comparably understood. The more interesting region of the phase space occurs at actions greater than $N_v = 8$. The first interesting feature of this region is a 2:3 secondary resonance. Clearly visible about this resonance is a chain of tertiary islands. These islands can be understood from the viewpoint of classical secular perturbation theory as described in Ref. [122]. An even finer structure of higher order islands is on a scale too fine to see. The size of these higher order resonances depends on the magnitude of the perturbation (in this case the field strength). A manifestation of this complicated structure, even if the higher order resonances cannot be directly observed, is the growth of a stochastic layer around the separatrix of the secondary resonance which is separated from the regular regions by KAM structures[122]. The random points near the hyperbolic fixed points of the 2:3 resonance were generated by a

trajectory which began approximately on the separatrix. This is evidence for a stochastic layer around the separatrix.

At actions above the 2:3 resonance, the secondary resonance structures become large enough that they begin to overlap. Overlapping resonances can be related to the growth of global chaos[121]. Noid and Stine[102a] have speculated on the role of overlapping resonances in the dissociation of a diatomic molecule with two lasers. This growth of global chaos can be seen surrounding regions where there are parts of resonance structures corresponding to 5:7 and 3:5 secondary resonances. Immersed in this chaotic region, parts of the primary 1:2 resonance are clearly visible. In the chaotic region the points of the surface of section are generated by two dissociating trajectories and one nondissociating trajectory. The surface of section of the trajectories in the chaotic region seem to follow the vague tori of Shirts and Reinhardt[125]. The points generated by a chaotic trajectory appears to be constrained to a particular resonance structure for several intersections of the mapping. Then the mapping carries the trajectory near the intersection of two resonances where it can move to the other resonance. The dissociating trajectories became associated with the 1:2 primary resonance where they were carried to large actions. It appears that there could be another unresolved resonance structure which is affecting the motion of the nondissociating trajectory.

We also performed a few calculations with the exponential form of the dipole used by Davis and Wyatt[101], and obtained similar interesting behavior and dissociation at higher actions.

D. Summary and Conclusions

We have performed quantum and classical calculations for one and two photon absorption about the fundamental (v=0 → v=1) frequency on rotating and nonrotating HF, for overtone (v=0 → v=2) absorption on rotating and nonrotating HF , and for multiphoton absorption at a fixed frequency near the (v=0 → v=1) fundamental with different initial states on nonrotaing HF. For the one and two photon calculations, it is found that classical mechanics does not pridict the correct rotational state distributions. Also, the time behavior of the classical solution is qualitatively different from the quantum one. Classical mechanics does give the correct magnitude of pulse time averaged quantities, but does not give the detailed resonance peaks for two photon absorption. Classical mechanics does correctly indicate more two photon absorption as the frequency is red shifted from the one photon resonance, but it predicts far too little such absorption. The quantum results as a function of pulse time have oscillations characteristic of two state resonances. The classical results as a function of pulse time have small, high frequency oscillations which appear to possibly damp out. For these transitions the laser phase has been shown to be essentially unimportant for the intensities examined, although it could conceivably be important for much higher intensities.

At the overtone frequencies we have found a shift of about 200 cm^{-1} between quantum and classical absorption maxima for both rotating and nonrotating HF. Also, the maxima and widths of the peaks are qualitatively different. Inclusion of a quadratic term in the dipole

function increases both quantum and classical overtone absorption significantly indicating that a reasonable fit to the dipole will be needed to get quantitatively accurate results. All of the quantum overtone results can be analyzed in terms of two state resonances. The quasiclassical vibrational transition probabilities do not show significant absorption into the $v = 2$ level as the quantum results do. Classically, absorption is into the $v = 1$ state. As for the one and two photon absorption near the fundamental frequency, we found that the rotational state distribution for the classical results were qualitatively different from that for the quantum results. Interestingly, though, we find that pure rotational excitation was signifiacnt for the quantum results even though rotational absorptions are far from resonance. The time dependent behavior at overtone frequencies is quantitatively the same as that near the fundamental frequency.

In contrast to the generally poor quantum and classical agreement near the overtone frequency, there was very good agreement for the multiphoton absorption of nonrotating HF at a frequency $\bar{v} = 3922 \ cm^{-1}$ with different initial states for the time averaged transition probabilities. The quantum and classical agreement is best for low initial states and becomes somewhat worse for higher initial states. The quantum results in the case are characterized by overlapping resonances with the corresponding population of many states.

To better understand the classical results, we constructed surfaces of section corresponding to the overtone and multiphoton results. At the overtone frequency, the surfaces of section are dominated by an

isolated 1:2 resonances. We show how this resonance shifts at a different frequency, and how this explains the observed results. The surface of section at $\bar{\nu} = 3922$ cm^{-1} also explains that set of results. In this case the phase space is characterized by an isolated 1:1 resonance, a 2:3 secondary resonance with a chaotic layer around its separatrix, a region of chaos, and within this region of chaos, 5:7 and 3:5 secondary resonances and a 1:2 primary resonance which the secondary resonances surround. As expected, dissociating trajectories are found to be associated with the region of overlapping resonances.

From our results, one can see that erroneous conclusions can be reached if purely classical calculations are done. Our multiphoton results, though, show that there is still hope that classical calculations may be of some use in studying these problems. Not too surprisingly, the classical and quantum results differ most when there are essentially two state quantum resonances. It would be very useful if some relationship could be found between the nature of the classical phase space and the agreement with quantum mechanics. We have found one example where a chaotic region of classical phase space corresponds to overlapping quantum resonances, and reasonably good agreement between the classical and quantum mechanical results. Gray[124] has also performed some interesting ·miclassical calculations on nonrotating HF and additional semiclassical calculations would give more insight into this problem.

It is difficult to extend these conclusions to polyatomic systems[126] although hopefully a good framework has been established for working on these systems. It is possible that future work will clearify

the general nature of the agreement between classical mechanics and quantum mechanics not only for molecules in a laser field but for any excited molecular system.

Appendix III.A: Initial and final conditions for a diatomic molecule in the rotating Morse oscillator approximation

To classically determine probabilities, it is necessary to average over initial conditions. For an isolated diatomic molecule, one can change variables to action-angle variables[113] (N_v, Q_v), (J, Q_J), and (M, Q_M) such that $\dot{N}_v = \dot{J} = \dot{M} = 0$, with N_v being the vibrational action, J the rotational action or angular momentum, and M being the projection of the angular momentum onto the z axis. These variables allow a connection with quantum mechanics to be easily made. The probability P of some event may be obtained by averaging over the initial angle vabiables Q_v, Q_J, Q_M for fixed N_v, J, and M,

$$ P = (2\pi)^{-3} \int_0^{2\pi} dQ_v \int_0^{2\pi} dQ_J \int_0^{2\pi} dQ_M \chi_{N_v JM}(Q_v, Q_J, Q_M), \tag{A.1} $$

where $\chi = 1$ if the event occurs and 0 if it does not occur for the given initial conditions. Usually, the angular momentum is randomly oriented in space, so an average may be taken over M,

$$ \bar{P} = \int_{-J}^J dM \; P / \int_{-J}^J dM = \frac{1}{2J} \int_{-J}^J dM \; P. \tag{A.2} $$

To do the Monte Carlo integration[127], the variables of integration are changed to ξ, with $0 < \xi_i < 1$, such that

$$ 2\xi_1 - 1 = M/J = \lambda, $$
$$ 2\pi\xi_2 = Q_v, $$
$$ 2\pi\xi_3 = Q_J, $$
$$ 2\pi\xi_4 = Q_M. \tag{A.3} $$

Equation (A.2) then becomes

$$\bar{P} = \lim_{N \to \infty} \frac{1}{N} \sum_{1}^{N} \chi_{N_v JM}(\xi).$$
(A.4)

That is, one averages χ over N random evaluations of ξ (each component of ξ is taken to be a pseudorandom number for a given evaluation).

Approximate relations between the action-angle variables and ordinary molecular coordinates have been given by Porter, Raff, and Miller[113] for a rotating Morse oscillator. The orbits given by them for θ and ϕ are not strictly correct. The corrected orbits are

$$r(t) = r_e - \frac{1}{\alpha} \ln\{(-2a)[b + \sqrt{b^2 - 4ac} \sin(\omega_N t + Q_N)]\},$$
$$\theta(t) = \arccos[\sqrt{1 - \lambda^2} \cos(\omega_J t + Q_J + \text{sign}(p_r) J\Delta_J)],$$
$$\phi(t) = Q_M + \text{sign}(p_\theta) \arccos\left(\frac{\lambda \cot[\theta(t)]}{\sqrt{1 - \lambda^2}}\right),$$
(A.5)

where the formulas for a, b, c, ω_N, ω_J, and Δ_J may be found in Ref. 113 and are not repeated here. The errors in the angular orbits arose from omission of a $\text{sign}(p_r)$ and $\text{sign}(p_\theta)$ factor in the generators W_r and W_θ, respectively [Eqs. (8a) and (8b) of Ref. 113]. Another slight error is in Eqs. (30b) and (30c) of Ref. 113. Here, the factor r^2 should be replaced by the expansion for r^2 given in their Eq. III.3.

Thus, to generate the initial conditions for a diatomic we first pick λ, Q_v, Q_J, and Q_M randomly according to Eqs. (A.3). Then, since the calculations are to be made in spherical coordinates, r, θ, and ϕ are calculated from Eqs. (A.5). p_r, and p_θ may be obtained by either conservation of energy and angular momentum, or by differentiation of Eqs. (30) of Ref. 113. This procedure is completely equivalent to the more standard approach of randomly orienting the molecule and its

angular momentum vector, and picking only r and p_r from the action-angle variable formulas. Thus, the present approach offers no technical advantage over the ordinary approach for most applications, including the present one, except when the rotational variables play an important role, as in some semiclassical applications.

The vibrational action N_v is calculated at a time t from the approximate formula of Ref. 113,

$$N_v = -\frac{\hbar}{2} + \frac{\sqrt{2\mu}}{\alpha} \left(\frac{b}{2\sqrt{-c}} - \sqrt{-a} \right)$$

(A.6)

and only depends on the molecular energy and angular momentum state $J(J+\hbar) = (p_\theta^2 + p_\phi^2/\sin^2\theta)$. N_v was calculated numerically

$$\left(N_v = -\frac{\hbar}{2} + \frac{1}{2\pi} \oint p_r \, dr \right)$$

as a check on Eq. (A.6) and, for all N_v and J with $J \lesssim 10$, N_v from Eq. (A.6) is accurate to three significant figures. Thus, essentially no error is introduced by the use of Eq. (A.6) for N_v in the present study.

Appendix III.B: Effect of laser phase on the two state model

For a two state model with states labeled A and B Eqs. (III.8)
become ($\hbar = 1$)

$$i\dot{C}_A = C_A E_A^O + C_B D_{AB} E_o \sin(\omega t+\delta) + C_A D_{AA} E_o \sin(\omega t+\delta),$$

$$i\dot{C}_B = C_B E_B^O + C_A D_{AB} E_o \sin(\omega t+\delta) + C_B D_{BB} E_o \sin(\omega t+\delta).$$

$$(B.1)$$

If one now replaces C_A and C_B by S_A and S_B such that

$$C_A = S_A \exp(-iE_A^O t),$$

$$C_B = S_B \exp(-iE_B^O t),$$

$$(B.2)$$

one obtains ($E_{AB} \equiv E_A^O - E_B^O$)

$$\dot{S}_A = \frac{1}{2} \{ S_B D_{AB} E_o \{ \exp[-i(E_{AB}+\omega)t] \exp(-i\delta)$$

$$- \exp[-i(E_{AB}-\omega)t] \exp(i\delta) \}$$

$$(B.3)$$

$$+ S_A E_o D_{AA} \{ \exp[-i(\omega t+\delta)] - \exp[i(\omega t+\delta)] \} \},$$

$$\dot{S}_B = \frac{1}{2} \{ S_A D_{AB} E_o \{ \exp[i(E_{AB}-\omega)t] \exp(-i\delta)$$

$$- \exp[i(E_{AB} + \omega)t] \exp(i\delta) \}$$

$$+ S_B E_o D_{BB} \{ \exp[-i(\omega t+\delta)] - \exp[i(\omega t+\delta)] \} \}.$$

The rotating wave approximation   involves omitting the highly
oscillatory terms involving $\exp[\pm i(E_{AB} + \omega)t]$ and $\exp(\pm i\omega)$.   Thus,

$$\dot{S}_A = -\frac{1}{2} S_B D_{AB} E_o \exp[-i(E_{AB} - \omega)t] \exp(i\delta),$$

$$\dot{S}_B = \frac{1}{2} S_A D_{AB} E_o \exp[i(E_{AB} - \omega)t] \exp(-i\delta). \tag{B.4}$$

Within this approximation, it can easily be shown that the effect of the laser phase δ is not important. To see this, the substitution $S_B^{\prime} = S_B \exp(i\delta)$ is made, so that Eq. (B.4) becomes

$$\dot{S}_A = -\frac{1}{2} S_B^{\prime} D_{AB} E_o \exp[-i(E_{AB} - \omega)t],$$

$$\dot{S}_B^{\prime} = \frac{1}{2} S_A D_{AB} E_o \exp[i(E_{AB} - \omega)t], \tag{B.5}$$

i.e., S_A and $S_B^{\prime}$ may be obtained by solving Eq. (B.5) and the probabilities $P_A = |S_A|^2$ and $P_B = |S_B|^2 = |S_B^{\prime}|^2$ have no phase dependance. Alternatively, Eq. (B.4) can be expressed as a second order equation in which the radiation phase does not appear.

One should note carefully that the rotating wave approximation is valid only if[119b] (i) $\omega = E_{AB}$ and (ii) $\omega \gg D_{AB}E_o$, $D_{AA}E_o$, $D_{BB}E_o$. The second condition is often not stated, but is necessary if the oscillatory terms are to be unimportant. Consider, e.g., HF in a 1.0 TW/cm^2 laser near the one photon resonance at 4006 cm^{-1} with a state $A = (0,0)$ and $B = (1,1)$. Condition (i) is satisfied and, with $E_o = 0.00534$ a.u., $D_{AB} = 0.022$ a.u., $D_{AA} = D_{BB} = 0$, condition [ii] is $0.0182 \gg 0.0001$, which is reasonably satisfied.

References

1. See the papers in Atom–Molecule Collision Theory, edited by R. B. Bernstein (plenum, New York, 1979), and references therein.

2. W. L. Hase, in Dynamics of Molecular Colisions (Plenum, New York, 1976), Part B, pp. 121–169.

3. P. J. Robinson and K. A. Holbrook, Unimolecular Reaction (John Wiley and sons, New York, 1972).

4. E. E. Nikitin, Theory of Elementary Atomic and Molecular Processes in Gasses (Oxford University Press, New York, 1974).

5. H. S. Johnston, Gas Phase Reaction Rate Theory (The Ronald Press, New York, 1966).

6.(a) M. Born and J. R. Oppenheimer, Ann. der Phys. 84, 457 (1927); (b) A. Messiah, Quantum Mechanics (John Wiley and sons, New York, 1962), Vol II, Chap. 18.

7. H. F. Schaefer III, in Atom–Molecule Collision Theory ed. by R. B. Bernstein (P'enum, New York, 1979), pp. 45 – 78.

8. W. H. Miller, N. C. Handy, and J. E. Adams, J. Chem. Phys. 72, 99 (1980).

9. T. Carrington Jr. and W. H. Miller, J. Chem. Phys., to be published.

10. F. T. Smith, Phys. Rev. 179, 111 (1969).

11. J. C. Tully, in Dynamics of Molecular Collisions, ed. by W. H. Miller (Plenum, New York, 1976), Part B, pp. 217 – 267.

12. P. Avouris, W. M. Gelbart, and M. A. El-Sayed, Chem. Rev. 77, 794 (1977).

13. E. Bauer, E. R. Fisher, and F. R. Gilmore, J. Chem. Phys. 51, 4173

(1969).

14. J. C. Tully and R. K. Preston, J. Chem. Phys. 55, 562 (1971).

15. W. H. Miller and T. F. George, J. Chem. Phys. 56, 5637 (1972).

16. G. C. Schatz and A. Kuppermann, J. Chem. Phys. 65, 4668 (1976).

17. D. J. Bamford, M. F. Foltz, S. V. Filseth, C. B. Moore, and J. W. Hepburn, to be published.

18. M. Shapiro and R. Bersoln, Ann. Rev. Phys. Chem. 33, 409 (1982).

19. M. D. Pattengill, in Atomic-Molecular Collision Theory ed. by R. B. Berstein (Plenum, New York, 1979), pp 359 - 376.

20. Reference 6(b), Chap. 19.

21. G. C. Schatz, L. M. Hubbard, P. S. Dardi, and W. H. Miller, J. Chem. Phys. 81, 231 (1984).

22.(a) W. H. Miller, J. Chem. Phys. 50, 407 (1969); (b) B. C. Garrett and W. H. Miller, J. Chem. Phys. 68, 4051 (1978); (c) J. E. Adams and W. H. Miller, J. Phys. Chem. 83, 1505 (1979); (d) G. Wolken, Jr. and M. Karplus, J. Chem. Phys. 40, 1105 (1964).

23.(a) P. S. Dardi and S. K. Gray, J. Chem. Phys. 77, 1345 (1982); P. S. Dardi and S. K. Gray, J. Chem. Phys. 80, 4738 (1984).

24. M. Sargent III, M. O. Scully, and W. E. Lamb Jr., Laser Physics (Addison-Wesley, Reading, Massachusetts, 1974).

25. P. Pechukas, in Dynamics of Molecular Collisions, edited by W. H. Miller (Plenum, New York, 1976), Part B, p.269.

26. R. B. Walker and J. C. Light, Ann. Rev. Phys. Chem. 31, 401 (1980).

27. See papers in National Resource for Computation in Chemistry, University of California, Berkeley, NRCC, Proceedings No. 5 (1979).

28. J. C. Light, in Atom - Molecule Collision Theory, edited by R. B.

Berstein (Plenum, New York, 1979), p. 467.

29. R. E. Wyatt and J. F. McNutt, in Potential Energy Surfaces and Dynamics Calculations, edited by D. G. Truhlar (Plenum, New York, 1981), p. 495.

30. J. N. L. Connor, Comput. Phys. Commun. 17, 117 (1979).

31. M. Child, Molecular Collision Theory, (Academic Press, New York, 1974).

32. G. C. Schatz and A. Kuppermann, J. Chem. Phys. 65, 4642 (1976).

33. R. McWeeny and B. T. Sutcliffe, Methods of Molecular Quantum Mechanics, (Academic Press, New York, 1976).

34. L. M. Hubbard, S. H. Shi, and W. H. Miller, J. Chem. Phys. 78, 2381 (1983).

35. D. A. Micha, Ark. Fys. 30, 411, 425, 437 (1965).

36. K. T. Tang and M. Karplus, J. Chem. Phys. 49, 1676 (1968).

37. K. T. Tang and M. Karplus, Phys. Rev. A 4, 1844 (1971).

38. W. H. Miller, J. Chem. Phys. 49, 2373 (1968).

39. R. B. Walker and R. E. Wyatt, Chem. Phys. Lett. 16, 52 (1972).

40. R. B. Walker and R. E. Wyatt, J. Chem. Phys. 61, 4839 (1974).

41. R. G. Gilbert and T. F. George, Chem. Phys. Lett. 20, 187 (1973).

42. B. H. Choi and K. T. Tang, J. Chem. Phys. 61, 5147 (1974).

43. K. T. Tang and B. H. Choi, J. Chem. Phys. 62, 3642 (1975).

44. B. H. Choi and K. T. Tang, J. Chem. Phys. 63, 2854 (1975).

45. B. H. Choi and K. T. Tang, J. Chem. Phys. 65, 5161 (1976).

46. B. H. Choi, R. T. Poe, J. C. Sun, and K. T. Tang, J. Chem. Phys. 73, 4381 (1980).

47. J. C. Sun, B. H. Choi, R. T. Poe, and K. T. Tang, J. Chem. Phys.

$\underline{73}$, 6095 (1980).

48. Y. Y. Yung, B. H. Choi, and K. T. Tang, J. Chem. Phys. $\underline{72}$, 621 (1980)

49. J. C. Sun, B. H. Choi, R. T. Poe, and K. T. Tang, Phys. Rev. Lett. $\underline{44}$, 1211 (1980).

50. J. C. Sun, B. H. Choi, R. T. Poe, and K. T. Tang, J. Chem. Phys. $\underline{78}$, 4523 (1983); $\underline{79}$, 5376 (1983).

51. S. H. Suck, Phys. Rev. A $\underline{15}$, 1983 (1977).

52. S. H. Suck and R. W. Emmons, Phys. Rev. A $\underline{24}$, 129 (1981).

53. S. H. Suck, Int. J. Quantum Chem. $\underline{19}$, 441 (1981).

54. S. H. Suck, Chem. Phys. Lett. $\underline{77}$, 390 (1981).

55. R. W. Emmons and S. H. Suck, Phys. Rev. A $\underline{25}$, 178 (1982).

56. S. H. Suck, Phys. Rev. A $\underline{27}$, 187 (1982).

57. R. W. Emmons and S. H. Suck, Phys. Rev. A $\underline{25}$, 2385 (1982).

58. R. W. Emmons and S. H. Suck, Phys. Rev. A $\underline{27}$, 1803 (1983).

59. D. C. Clary and J. N. L. Connor, Chem. Phys. Lett. $\underline{66}$, 493 (1979).

60. D. C. Clary and J. N. L. Connor, Chem. Phys. Lett. $\underline{48}$, 175 (1980).

61. D. C. Clary and J. N. L. Connor, J. Chem. Phys. $\underline{74}$, 6991 (1981).

62. D. C. Clary and J. N. L. Connor, J. Chem. Phys. $\underline{75}$, 3329 (1981).

63. D. C. Clary and J. N. L. Connor, Mol. Phys. $\underline{41}$, 689 (1981).

64. D. C. Clary and J. N. L. Connor, Mol. Phys. $\underline{43}$, 621 (1981).

65. G. C. Schatz and J. Ross, J. Chem. Phys. $\underline{66}$, 1021, 1037, 2943 (1977); D. J. Zuijac and J. Ross, ibid. $\underline{68}$, 4468 (1978); C. L. Vila, J. L. Kinsey, J. Ross, and G. C. Schatz, ibid. $\underline{70}$, 2414 (1979).

66. B. C. Eu, Mol. Phys. $\underline{31}$, 1261 (1976).

67. S. Fischer and G. Venzl, J. Chem. Phys. $\underline{67}$, 1335 (1977).

68. Y. H. Band and K. F. Freed, J. Chem. Phys. $\underline{64}$, 2826 (1976).

69. D. J. Diestler, J. Chem. Phys. $\underline{54}$, 4547 (1971).

70. S. Wu and R. D. Levine, Mol. Phys. $\underline{22}$, 881 (1971).

71. B. R. Johnson, Chem. Phys. Lett. $\underline{13}$, 172 (1972).

72. S. Wu, B. R. Johnson, and R. D. Levine, Mol. Phys. $\underline{25}$, 609 (1973).

73. J. C. Light and R. B. Walker, J. Chem. Phys. $\underline{65}$, 4272 (1976).

74. J. T. Adams, R. L. Smith, and E. F. Hayes, J. Chem. Phys. $\underline{61}$, 2193 (1974).

75. D. J. Diestler, D. G. Truhlar, A. Kuppermann, Chem. Phys. Lett. $\underline{13}$, 1 (1972).

76. R. B. Walker, E. B. Stechel, and J. C. Light, J. Chem. Phys. $\underline{69}$, 2922 (1978).

77. A. Rosenthal and R. G. Gordon, J. Chem. Phys. $\underline{64}$, 1641 (1976).

78. D. K. Bondi and J. N. L. Connor, Chem. Phys. Lett. $\underline{92}$, 570 (1982).

79. J. W. Duff and D. G. Truhlar, Chem. Phys. Lett. $\underline{23}$,327 (1973)

80. R. N. Porter and M. Karplus, J. Chem. Phys. $\underline{40}$, 1105 (1964).

81. R. G. Newton, Scattering Theory of Waves and Particles, (Springer-Verlag, New York, 1982), 2nd edition, p. 492.

82. L. M. Delves, Nuc. Phys. $\underline{9}$, 391 (1959); $\underline{20}$, 275 (1960).

83. R. T. Pack, J. Chem. Phys. $\underline{60}$, 633 (1973).

84. R. Gordon, J. Chem. Phys. $\underline{51}$, 14 (1969).

85. A. Kuppermann, G. C. Schatz, and J. P. Dwyer, Chem. Phys. Lett. $\underline{45}$, 71 (1977).

86. A. B. Elkowitz and R. E. Wyatt, Mol. Phys. $\underline{31}$, 189 (1976).

87. G. C. Schatz, Chem. Phys. Lett. $\underline{94}$,183 (1983).

88. B. R. Johnson, National Resource for Computation in Chemistry,

University of California, Berkeley, NRCC Proceedings No. 5, 86 (1979).

89. B. R. Johnson, J. Chem. Phys. 69, 4678 (1978).

90. S. Shi, Ph.D. Thesis, University of California, Berkeley (1984).

91. See, for example, papers in Advances in Laser Chemistry ed. by A. H. Zewail (Springer, New York,1978) and Laser Induced Processes in Molecules, ed. by K. L. Kompa and S. D. Smith (Springer, New York, 1978).

92.(a) R. L. Swofford and A. C. Albrecht, Ann. Rev. Phys. Chem. 29, 421 (1978); (b) R. Beach, B. Brody, and S. R. Hartman, Laser Chem. 2, 3 (1983).

93. See the collection of papers in Adv. Chem. Phys. 47 (1981).

94. A. Kaldor, R. L. Woodin, and R. B. Hall, Laser Chem. 2, 335 (1983).

95. B. R. Henry, Accounts Chem. Res. 10, 207 (1977).

96. K. F. Freed, Top. Appl. Phys. 15, 1 (1976).

97. K. B. Eisenthal, Ann. Rev. Phys. Chem. 28, 207 (1977).

98.(a) S. A. Rice, Adv. Chem. Phys. 47, 117 (1981); (b) I. Orefand and B. S. Rabinovitch, Accounts of Chem. Res. 12, 166 (1979).

99. R. B. Walker and R. K. Preston, J. Chem. Phys. 67, 2017 (1977).

100. S. K. Gray, Chem. Phys. 75, 67 (1983).

101. M. J. Davis and R. E. Wyatt, Chem. Phys. Lett. 86, 235 (1982).

102.(a) D. W. Noid and J. R. Stine, Chem Phys. Lett. 65, 153 (1979); (b) J. R. Stine and D. W. Noid, ibid. 77, 287 (1981); (c) D. W. Noid, M. L. Koszykowski, R. A. Marcus, and J. D. MacDonald, ibid. 51, 540 (1977); (d) D. W. Noid, C. Bottcher, and M. L. Koszykowski, ibid. 72, 397 (1980); (e) J. R. Stine and D. W. Noid, J. Phys. Chem. 86, 3733 (1982).

103. D. Poppe, Chem. Phys. 45, 371 (1980).

104. K. M. Christoffel and J. M. Bowman, J. Phys. Chem. 85, 2159 (1981).

105.(a) S. C. Leasure and R. E. Wyatt, Opt. Eng. 19, 46 (1980); (b) Chem. Phys. Lett. 61, 625 (1979); (c) S. C. Leasure, K. F. Milfield, and R. E. Wyatt, J. Chem. Phys. 74, 6197 (1981); (d) R. E. Wyatt, G. Hose, and H. S. Taylor, Phys. Rev. A 28, 815 (1983).

106. D. C. Clary, Mol. Phys. 46, 1099 (1982).

107.(a) C. Leforestier and R. E. Wyatt, J. Chem. Phys. 78, 2334 (1983); (b) M. J. Davis, R. E. Wyatt, and C. Leforestier, in Intermolecular Dynamics (Reidel, Boston, 1982), pp. 403 - 427.

108. J. H. Shirley, Phys. Rev. B. 138, 979 (1965).

109. S.-I. Chu, J. Chem. Phys. 75, 2215 (1981).

110. See Ref. 25 pp.

111. W. H. Miller, J. Chem. Phys. 69, 2188 (1978).

112. A. D. Bandrauk and M. L. Sink, J. Chem. Phys. 74, 110 (1981).

113. R. N. Porter, L. M. Raff, and W. H. Miller, J. Chem. Phys. 63, 2214 (1975). Note Appendix A gives some corrections to this paper.

114. L. F. Shampine and M. K. Gordon, Computer Solution of Ordinary Differential Equations: The Initial Value Problem (Freeman, San Francisco, 1975). The actual program used was ODE from the Sandia Laboratory library.

115. C. W. Gear, SIAM Rev. 23, 10 (1981).

116.(a) M. L. Sage, Chem. Phys. 35, 375 (1978); (b) R. Wallace, Chem. Phys. Lett. 37, 115 (1976).

117. C. C. Rankin and W. H. Miller, J. Chem. Phys. 55, 3150 (1971).

118. J. V. Moloney and W. J. Mealth, Mol. Phys. 31, 1537 (1976).

119.(a) S. Flugge, Practicle Quantum Mechanics (Springer, New York, 1971), Vol. II, p.138; (b) M. Quack, J. Chem. Phys. 69, 1282 (1978).

120. J. H. Eberly, B. W. Shore, Z. Białynicka - Birula, and I. Białynicka - Birula, Phys. Rev. A 16, 2038 (1977).

121. P. Brumer, Adv. Chem. Phys. 47, 201 (1981).

122. A. J. Lichtenberg and M. A. Lieberman, Regular and Stochastic Motion (Springer, New York, 1983).

123. E. L. Sibert III, J. T. Hynes, and W. P. Reinhardt, J. Chem. Phys. 77, 3595 (1982).

124. S. K. Gray, Chem. Phys. 83, 125 (1984).

125.(a) W. P. Reinhardt, J. Phys. Chem. 86, 2158 (1982); (b) R. B. Shirts and W. P. Reinhardt, J. Chem. Phys. 77, 5204 (1982).

126. D. W. Noid, M. L. Koszykowski, and R. A. Marcus, J. Chem. Phys. 73, 391(1980).

127. R. N. Porter and L. M. Raff, in Modern Theoretical Chemistry, edited by W. H. Miller (Plenum, New York, 1976), Vol. 2, Part B, pp. 1-52.

Table II.1. Transition probabilities for J = 0.

Total energy (eV)[b]		Number of states (DWBA)[a]			EC[c]
		16	18	22	
0.30	$P^d_{00\to00}$		1.66(-14)[e]		1.50(-14)
	$P_{00\to01}$	3.07(-15)	3.07(-15)		2.76(-15)
	$P_{01\to01}$	5.53(-16)	5.53(-16)		5.12(-16)
0.35	$P_{00\to00}$		5.82(-10)		5.22(-10)
	$P_{00\to01}$	5.46(-10)	5.46(-10)		4.87(-10)
	$P_{01\to01}$	5.15(-10)	5.15(-10)		4.55(-10)
0.40	$P_{00\to00}$		2.74(- 7)		2.63(- 7)
	$P_{00\to01}$	3.39(- 7)	3.39(- 7)		3.31(- 7)
	$P_{01\to01}$	3.33(- 7)	3.24(- 7)		4.17(- 7)
0.45	$P_{00\to00}$		1.92(- 5)		1.81(- 5)
	$P_{00\to01}$	2.70(- 5)	2.70(- 5)		2.58(- 5)
	$P_{01\to01}$	3.83(- 5)	3.83(- 5)		3.68(- 5)
0.50	$P_{00\to00}$		4.41(- 4)		4.54(- 4)
	$P_{00\to01}$	6.82(- 4)	6.82(- 4)		7.14(- 4)
	$P_{01\to01}$	1.05(- 3)	1.05(- 3)		1.06(- 4)
0.55	$P_{00\to00}$		4.99(- 3)		4.83(- 3)
	$P_{00\to01}$	8.26(- 3)	8.24(- 3)		8.11(- 3)
	$P_{01\to01}$	1.36(- 2)	1.36(- 2)		1.30(- 2)
0.60	$P_{00\to00}$		2.96(- 2)	3.01(- 2)	2.49(- 2)
	$P_{00\to01}$	5.30(- 2)	5.26(- 2)		4.19(- 2)
	$P_{01\to01}$	9.29(- 2)	9.28(- 2)		7.13(- 2)
0.65	$P_{00\to00}$	7.50(- 2)	7.49(- 2)	5.52(- 2)	4.34(- 2)
	$P_{00\to01}$	1.45(- 1)	1.40(- 1)	1.02(- 1)	8.02(- 2)
	$P_{01\to01}$	2.62(- 1)	2.59(- 1)	1.83(- 1)	1.50(- 1)

[a]The particular basis sets used were 16 states: 4,4,4,4; 18 states;
5,5,4,4; 22 states: 5,5,4,4,4 where each number is the number of
rotational states within a paritcular vibrational level.   Each
successive number represents the next vibrational level.   For example,
5,5,4,4 means four vibrational levels; v = 0,1 have five rotational
states, v = 2,3 have four rotational states. The even — odd decoupling
of rotational states is used, so if four rotational levels are
specified, the states are all of either even or odd symmetry as
described in section B.2.d. This notation is used throughout the paper.
[b]The zero of energy is the bottom of the reactant diatom potential well.
[c]From Ref. 16.
[d]The probabilities given represent examples of each of the combinations
of even — odd symmetry decoupled results.
[e]The number in parenthesis is the power of ten that the preceding number
should be multiplied by.

Table II.2. Integral cross sections at several energies.[a]

| | E = 0.4 eV | | | E = 0.5 eV | | | E = 0.6 eV | |
	DWBA – CS	EQ[b]	DWBA – CC	DWBA – CS	EQ[b]	DWBA – CS	EQ[b]
$Q_{00\rightarrow01}$	0.878(-6)	0.667(-6)	0.139(-2)	0.137(-2)	0.124(-2)	0.958(-1)	0.780(-1)
$Q_{00\rightarrow02}$	0.160(-6)	0.114(-6)	0.644(-3)	0.532(-3)	0.473(-3)	0.496(-1)	0.437(-1)
$Q_{00\rightarrow03}$	0.108(-8)	0.137(-8)	0.899(-4)	0.484(-4)	0.553(-4)	0.962(-2)	0.983(-2)
Q_{00}	0.352(-5)	0.252(-5)	0.594(-2)	0.570(-2)	0.501(-2)	0.420	0.352
Q_{01}	0.162(-5)	0.120(-5)	0.350(-2)	0.312(-2)	0.306(-2)	0.255	0.228
Q_{02}	0.239(-6)	0.186(-6)	0.113(-2)	0.844(-3)	0.806(-3)	0.872(-1)	0.843(-1)
Q_{03}	0.246(-8)	0.333(-8)	0.149(-3)	0.717(-4)	0.908(-4)	0.140(-1)	0.166(-1)

[a] Cross sections are summed over final angular momentum projection quantum numbers and averaged over initial angular momentum projection quantum numbers. The number in parenthesis is the power of ten that the preceding number should be multiplied by.

[b] The exact quantum results are from Ref. 16.

Table III.3. Convergence of collinear exact H + H$_2$ reactive scattering
transition probabilities, v=0 → v'=0, with respect to basis size.[a]

Total Energy (eV)	Number of channels					
	1	2	3	4	5	6
0.3128	4.10(-9)	8.30(-9)	9.65(-9)	9.84(-9)	1.32(-8)	1.45(-8)
0.3628	1.46(-5)	3.31(-5)	3.86(-5)	4.01(-5)	4.81(-5)	4.67(-5)
0.4028	7.23(-4)	1.91(-3)	2.26(-3)	2.36(-3)	2.62(-3)	2.61(-3)
0.4334	6.55(-3)	2.02(-2)	2.43(-2)	2.52(-2)	2.73(-2)	2.69(-2)
0.4546	2.26(-2)	7.73(-2)	9.28(-2)	9.0 (-2)	1.02(-1)	1.01(-1)
0.4826	8.56(-2)	3.02(-1)	3.50(-1)	3.68(-1)	3.70(-1)	3.70(-1)
0.5000	1.64(-1)	5.22(-1)	5.78(-1)	5.97(-1)	6.01(-1)	6.01(-1)
0.6000	8.34(-1)	9.97(-1)	9.97(-1)	1.00	1.00	1.00
0.7000	9.91(-1)	9.93(-1)	9.92(-1)	9.91(-1)	9.91(-1)	9.90(-1)
0.8000[b]	9.96(-1)	9.68(-1)	9.47(-1)	9.50(-1)	9.51(-1)	9.49(-1)
0.8706	9.78(-1)	8.56(-1)	2.72(-1)	1.78(-1)	1.92(-1)	1.66(-1)
0.8976	9.72(-1)	4.95(-1)	6.28(-1)	6.78(-1)	6.56(-1)	6.70(-1)
1.2026	8.27(-1)	3.52(-1)	2.08(-1)	2.33(-1)	2.07(-1)	2.28(-1)
1.3966[c]	7.07(-1)	1.73(-1)	1.42(-1)	1.36(-1)	d	1.32(-1)
1.6466	5.44(-1)	3.37(-2)	8.08(-2)	7.86(-2)	d	7.39(-2)

[a]The number in parenthesis is the power of ten that the preceding number
should be multiplied by.
[b]The second channel has become open.
[c]The third channel has become open.
[d]There were some numerical problems with these calculations which are
still being investigated.

Table II.4. Convergence of collinear exact $H + H_2$ reactive scattering transition probabilities, $v=0 \rightarrow v'=0$, with respect to the number of grid points for the integration to obtain the S matrix.[a]

Total Energy (eV)	Number of Grid Points				
	41	45	51	56	61
0.4546	1.09(-1)	1.02(-1)	1.01(-1)	1.01(-1)	
0.6000	9.99(-1)	9.99(-1)	9.99(-1)	1.00	
0.8706	1.61(-1)	1.62(-1)	1.64(-1)	1.66(-1)	1.67(-1)
1.3966	1.34(-1)	1.33(-1)	1.32(-1)	1.32(-1)	

[a]All these calculations have 6 channels in the basis. The number in parenthesis is the power of ten that the preceding number should be multiplied by.

Table II.5. Comparison of our exact quantum scattering reaction
probabilities, v=0 → v'=0 with previous calculations.[a]

Total Energy (eV)	Our Calculation[b]	Previous Calculations		
0.3128	1.45(-8)	1.07(-8)[e]		
0.3628	4.67(-5)	4.37(-5)[e]		
0.4028	2.61(-3)	2.46(-3)[e]		
0.4334	2.69(-2)	2.65(-2)[f]	2.7 (-2)[g]	
0.4546	1.01(-1)	1.01(-1)[f]		
0.4826	3.70(-1)	3.6.(-1)[h]	3.72(-1)[i]	3.66(-1)[j]	3.71(-1)[f]
0.5000	6.01(-1)	6.01(-1)[k]		
0.6000	1.00	9.99(-1)[k]		
0.7000	9.90(-1)	9.91(-1)[k]		
0.8000[c]	9.49(-1)	9.50(-1)[k]		
0.8706	1.66(-1)	1.83(-1)[h]	1.60(-1)[i]	1.89(-1)[j]	
0.8976	6.70(-1)	6.62(-1)[h]	6.68(-1)[i]	6.69(-1)[j]	6.66(-1)[l]
1.2026	2.28(-1)	2.29(-1)[h]	2.34(-1)[i]	2.00(-1)[j]	2.28(-1)[l]
1.3966[d]	1.32(-1)	1.31(-1)[h]	1.49(-1)[i]		
1.6466	7.39(-2)	8.0 (-2)[h]	6.94(-2)[i]		

[a]The number in parenthesis is the power of ten that the preceding number
should be multiplied by.

[b]All calculations have 6 states in the basis and are converged to 1 - 2%
in the grid size.

[c]The second channel becomes open.

[d]The third channel becomes open.

[e]Hubbard, Shi, Miller[34] list these results (which agree within 1 - 2% of
their DWBA results) but do not reference them.

[f]Reference 79.   [g]Reference 72.   [h]Reference 73.

[i]Reference 77.   [j]Reference 69.   [k]Reference 71.

[l]Reference 74.

Table III.1. Relevant energy levels for HF, according to
the rotating Morse oscillator approximation.

v	j	E^o_{vj}	
		a.u.	cm^{-1}
0	0	0.0093309	2048
0	1	0.0095187	2089
0	2	0.0098941	2171
1	0	0.0274001	6014
1	1	0.0275819	6054.
1	2	0.0279454	6133
2	0	0.0446793	9806
2	1	0.0448551	9845
2	2	0.0452065	9922

Table III.2. Approximate time averaged probabilities for vibrational transitions of HF in a 1.0 TW/cm^2 laser.

$\bar{\nu}(cm^{-1})$	Nonrotating			Rotating		
	P_o	P_1	P_2	P_o	P_1	P_2
3850	0.88(QM)	0.08	0.04	0.99	0.01	0.00
	1.00(CL)	0.00	0.00			
3879	0.47	0.08	0.45	0.53	0.03	0.44
	0.88	0.12	0.00	0.99	0.01	0.00
3900	0.83	0.11	0.06	0.96	0.03	0.01
	0.73	0.19	0.08	0.94	0.04	0.02
3937	0.69	0.28	0.03	0.47	0.07	0.46
	0.69	0.24	0.06	0.67	0.27	0.06
3966	0.51	0.47	0.02	0.87	0.12	0.01
	0.63	0.36	0.01	0.58	0.40	0.02
4006	0.69	0.30	0.01	0.50	0.49	0.01
	0.68	0.32	0.00	0.66	0.34	0.00
4085	0.93	0.07	0.00	0.95	0.05	0.00
	0.90	0.10	0.00	0.88	0.12	0.00

Table III.3. Approximate time averaged vibrational
transition probabilities for rotating HF in a 2.5
TW/cm^2 laser.[a]

$\bar{\nu}(cm^{-1})$	P_o	P_1	P_2
3879	0.51(QM)	0.07	0.42
	0.88(CL)	0.07	0.05
3900	0.90	0.05	0.05
	0.67	0.17	0.16
3937	0.48	0.10	0.42
	0.50	0.31	0.19
3966	0.77	0.18	0.05
	0.52	0.39	0.09
4006	0.52	0.45	0.03
	0.61	0.37	0.02
4085	0.89	0.11	0.00
	0.78	0.20	0.00

[a]The classical results shown for $\bar{\nu}$ = 3879 and 3937
cm^{-1} were actually run at 3870 and 3927 cm^{-1},
respectively. The probabilities will not vary much
since the classical peak is broad. It was displayed
in the table this way to avoid confusion since the
overall trends are still clear.

Table III.4. Quantum mechanical transition probabilities and energy
absorbed as a function of pulse time for laser phases of 0 and $\pi/2$ at
$\bar{\nu}$ = 4006 cm^{-1} and I = 1.0 TW/cm^2.

t(ps)	P_{00}		P_{11}		$\langle E(t) \rangle_{QM}$(a.u.)	
	$\delta = 0$	$\delta = \pi/2$	$\delta = 0$	$\delta = \pi/2$	$\delta = 0$	$\delta = \pi/2$
0.0	1.00	1.00	0.00	0.00	0.0000	0.0000
0.4	0.30	0.32	0.63	0.66	0.0125	0.0126
0.8	0.13	0.14	0.81	0.83	0.0156	0.0158
1.2	0.94	0.95	0.05	0.05	0.0010	0.0009
1.6	0.51	0.53	0.44	0.45	0.0084	0.0086
2.0	0.03	0.03	0.92	0.92	0.0177	0.0179
2.4	0.81	0.81	0.17	0.17	0.0034	0.0033
2.8	0.73	0.73	0.24	0.24	0.0047	0.0048
3.2	0.01	0.01	0.95	0.94	0.0180	0.0182
3.6	0.62	0.62	0.36	0.36	0.0068	0.0069
4.0	0.88	0.90	0.09	0.09	0.0018	0.0017
4.4	0.08	0.09	0.87	0.88	0.0167	0.0169

Table III.5. Quantum mechanical transition probabilities and energy
absorbed as a function of pulse times for laser phases of 0 and $\pi/2$ at
$\bar{\nu} = 3937$ cm^{-1} and $\Sigma = 1.0$ TW/cm^2.

t(ps)	P_{00}		P_{22}		$\langle E(t)\rangle_{QM}$(a.u.)	
	$\delta = 0$	$\delta = \pi/2$	$\delta = 0$	$\delta = \pi/2$	$\delta = 0$	$\delta = \pi/2$
0.0	1.00	1.00	0.00	0.00	0.0000	0.0000
0.4	0.93	0.93	0.05	0.05	0.0021	0.0019
0.8	0.78	0.80	0.19	0.19	0.0072	0.0071
1.2	0.57	0.58	0.37	0.38	0.0142	0.0144
1.6	0.36	0.37	0.57	0.57	0.0218	0.0219
2.0	0.18	0.18	0.71	0.74	0.0282	0.0284
2.4	0.05	0.05	0.83	0.81	0.0320	0.0324
2.8	0.00	0.00	0.83	0.86	0.0333	0.0338
3.2	0.03	0.03	0.80	0.80	0.0322	0.0324
3.6	0.14	0.13	0.69	0.71	0.0283	0.0287
4.0	0.27	0.29	0.56	0.57	0.0231	0.0233
4.4	0.47	0.47	0.40	0.40	0.0169	0.0170

Table III.6. Classical and quantum time averaged vibrational probabilities at $\bar{\nu} = 3922$ cm^{-1} (in percent).

N_v	Initial	0	1	2	3	4	5	6	7	8	9	10
Final	0	42(CL)	21	16	16	5						
		39(QM)	22	19	16	3						
	1	22	36	24	12	8						
		21	39	21	14	4						
	2	16	25	31	16	11						
		18	21	31	19	10	2					
	3	17	12	16	28	17	13					
		17	14	17	24	22	7	1				
	4	4	6	12	17	31	21	9				
		3	4	11	21	34	22	4				
	5			2	11	21	37	22	6			
				2	7	22	44	20	3			
	6					8	23	40	24	5		
						4	22	52	18	3		
	7						6	24	39	23	6	
							3	19	55	16	3	2
	8							5	22	39	26	6
								2	18	60	14	3
	9								8	28	33	19
									3	16	59	7
	10									6	17	23
									1	2	11	30
	11										4	10
										1	5	8
	12										2	5
											2	10
	13										1	4
											1	6
	14											4
											2	21
	15											2
											1	3
	16											1
												2
	17											1
												7
	Dissociate(CL)										7	24

Table III.7. Classical and quantum time averaged
vibrational transition probabilities in the overtone
frequency range (in percent).

	$\overline{\nu}(cm^{-1})$	P_0	P_1	P_2
Nonrotating HF				
linear dipole				
(QM)	7200	81	0	19
	7757.8	50	0	50
	7800	82	0	18
(CL)	7900	90	10	0
	7990	76	24	0
	8080	91	9	0
nonlinear dipole				
(QM)	7680	82	0	18
	7757.8	51	0	49
	7840	80	0	20
(CL)	7750	90	8	2
	7900	66	25	9
	8100	78	22	0
Rotating HF				
linear dipole				
(QM)	7780	73	0	27
	7800	52	0	48
	7820	81	0	19
(CL)	7950	85	15	0
	7987.5	69	31	0
	8050	88	12	0
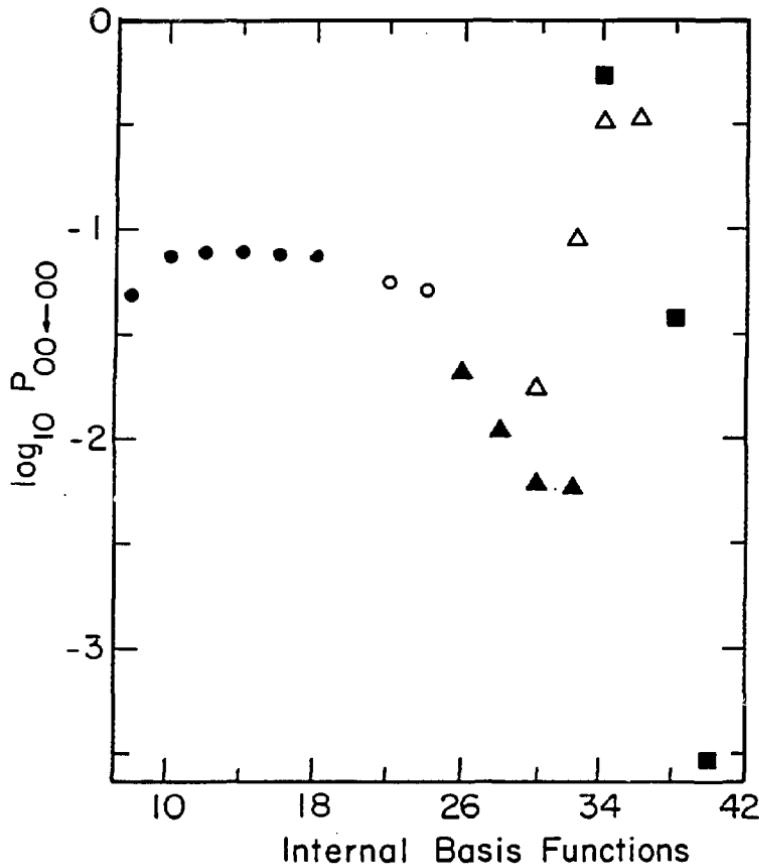
Fig. II.1. Transition probability from $v = 0$, $j = 0$ to $v' = 0$, $j' = 0$ as a function of vibration-rotation basis set at $E = 0.65$ eV, $J = 0$. The symbols on the plot indicate the number of vibrational states; (●) four vibrational states, (○) five, (▲) six, (△) seven, and (■) eight. This clearly shows the convergence problem at higher energies as the number of vibrational states is increased.
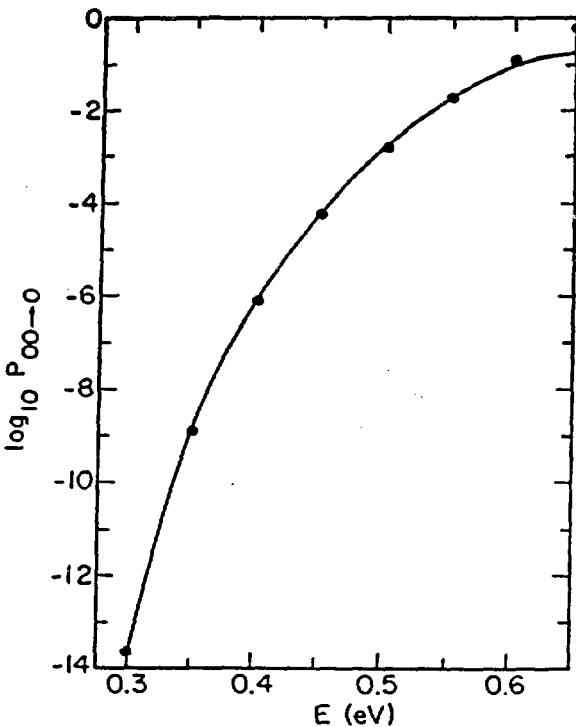
Fig. II.2. Transition probabilities $v = 0$, $j = 0 \rightarrow v' = 0$ summed over final rotational states with $J = 0$ as a function of total energy. The solid line indicates the exact quantum results, and the dots are the DWBA results. The DWBA results are calculated using 18 vibraional - rotational states, 5,5,4,4. See Table II.1 for more explanation of basis sets.
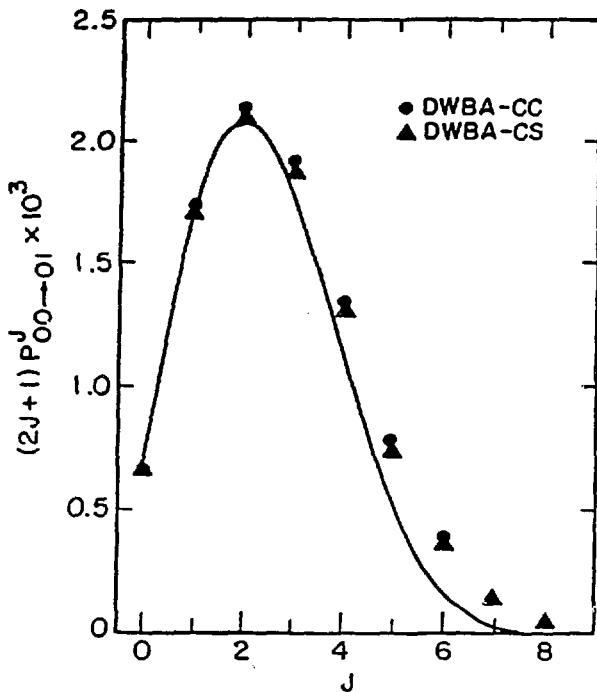
Fig. II.3. The transition probabilities multiplied by (2J+1) as a function of J for total energy E = 0.5 eV. The solid line indicates the exact quantum results. The DWBA-CC and DWBA-CS results are plotted using the indicated dots. For these results a basis of 4,4,3,3 (this notaiton is explained under Table II.1) is used with all of the allowed projection quantum number Ω states. Accounting for even and odd decoupling, a maximum of 114 states was used.
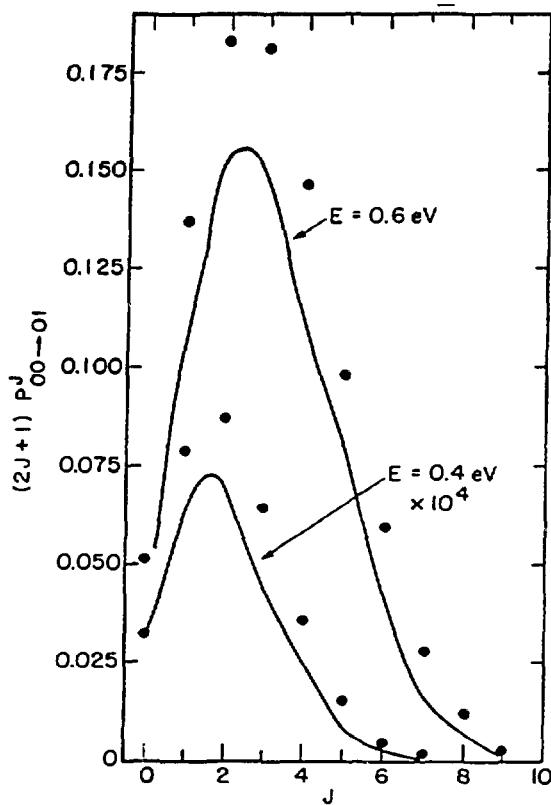
Fig. II.4. The transition probabilities multiplied by (2J+1) as a function of J for total energies E = 0.4 eV and E = 0.6 eV. The solid lines indicate the exact quantum results, and the DWBA-CS results are shown as dots. As indicated, the E = 0.4 eV results are multiplied by 10^4 before being plotted. For the DWBA results 14 basis functions, 4,4,3,3 are used. See Table II.1 for an explanation of basis sets.
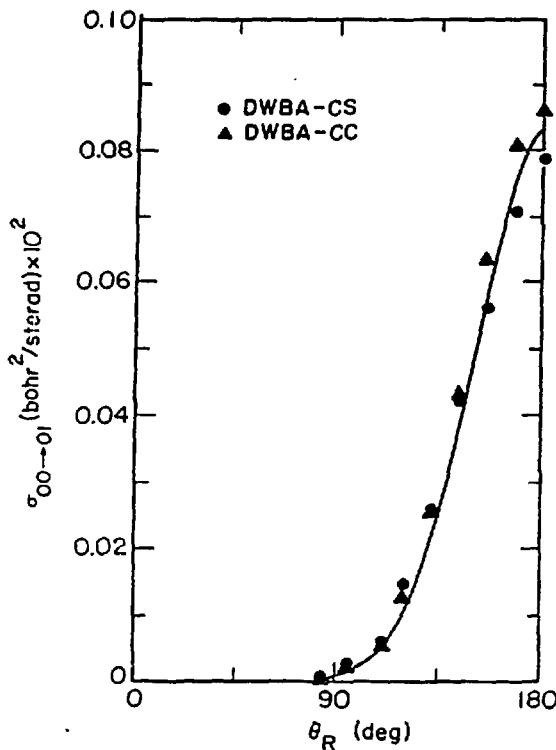
Fig. II.5. Differential cross sections as a function of scattering
angle $\theta_R = 180 - \theta$ at total energy $E = 0.5$ eV. The solid line is the
exact quantum results. The DWBA-CC and DWBA-CS results are plotted
using the indicated dots. See Fig. II.3 for a description of the basis.
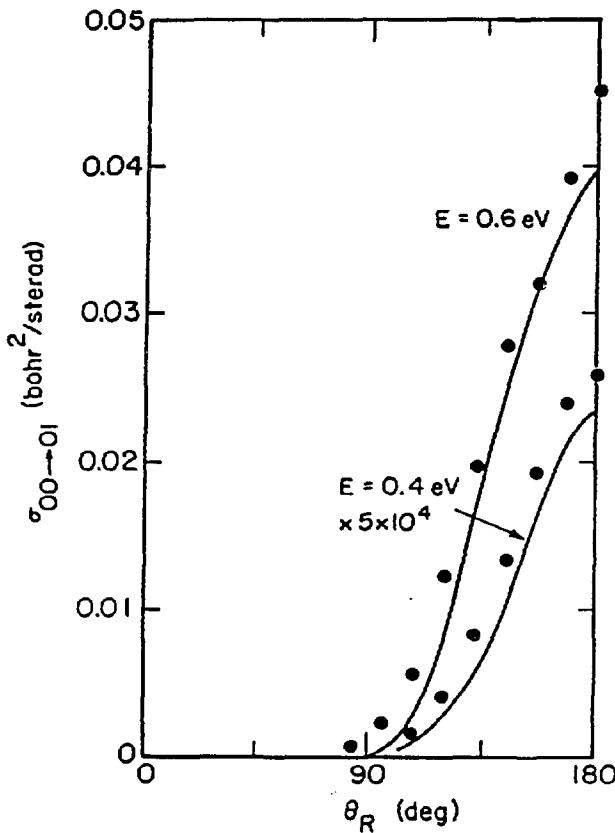
Fig. II.6. Differertial cross sections as a function of scattering angle $\theta_R = 180 - \theta$ for total energies 0.4 and 0.6 eV. The solid lines indicate the exact quantum results, and the dots are the DWBA-CS results. As indicated, the E = 0.4 results are multiplied by 5×10^4 before being plotted. See Fig. 4 for a description of the basis.
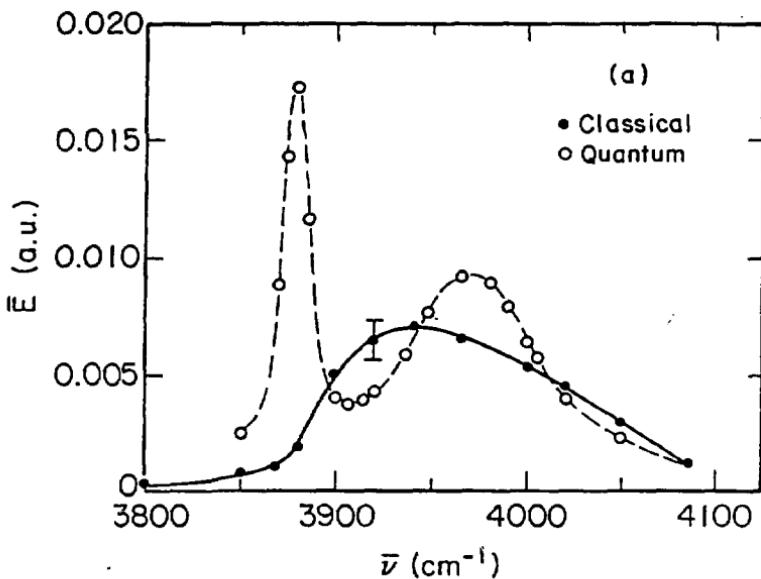
Fig. III.1(a). Classical and quantum mechanical time averaged energy absorption for nonrotating HF in a 1.0 TW/cm² laser.
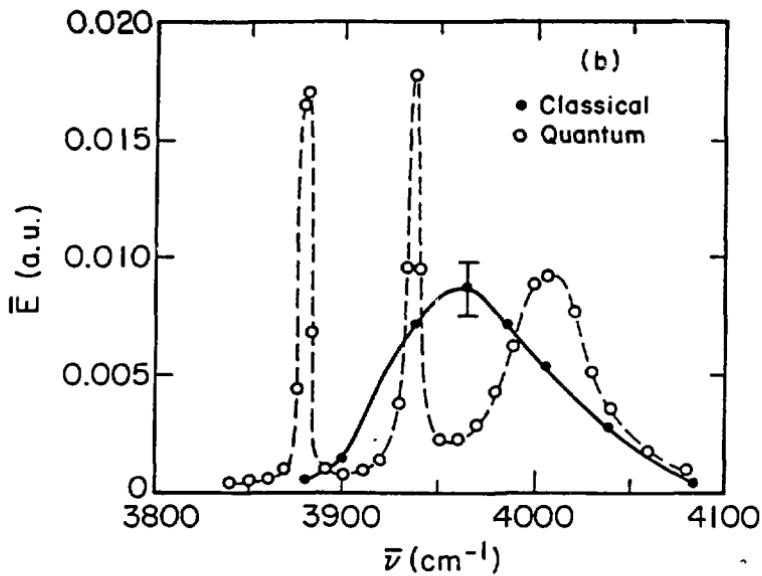
Fig. III.1(b). Classical and quantum mechanical time averaged energy
absorption for rotating HF in a 1.0 TW/cm^2 laser.
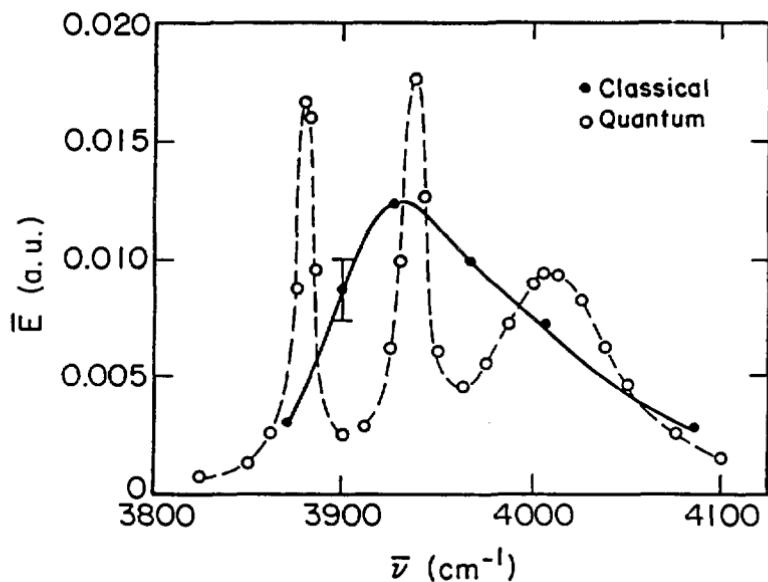
Fig. III.2. Classcial and quantum mechanical time averaged energy absorption for rotating HF in a 2.5 TW/cm^2 laser.
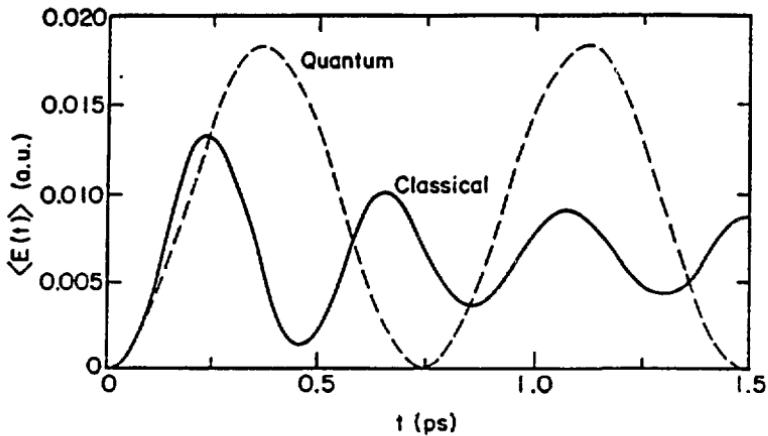
Fig. III.3. Time dependent energy absorption for nonrotating HF with $\bar{\nu} = 3966\text{cm}^{-1}$ and $I = 1.0$ TW/cm^2.
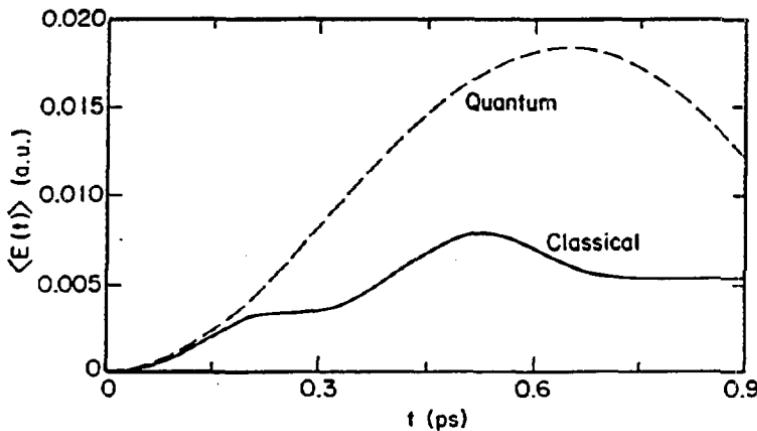
Fig. III.4. Time dependent energy absorption for rotating HF with $\bar{\nu} = 4006\,cm^{-1}$ and $I = 1.0$ TW/cm^2.
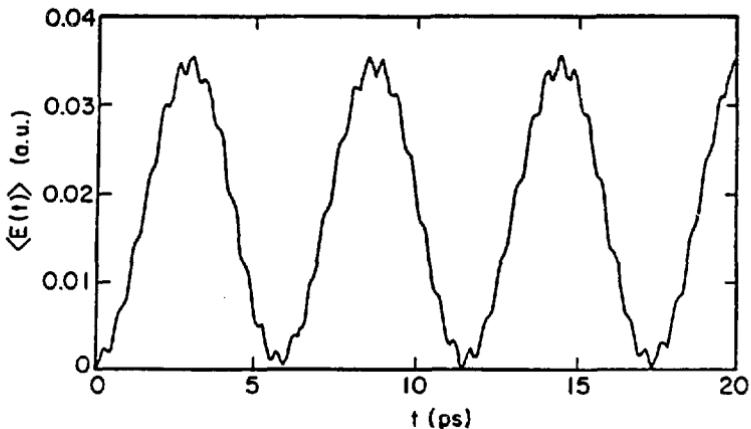
Fig. III.5. Quantum mechanical time dependent energy absorption for rotating HF with $\bar{\nu}$ = 3937 cm^{-1} and I = 1.0 TW/cm^2. Note that the jaggedness here and in Figs. III.7 and III.9 are due to poor resolution of the high frequency oscillations.

140
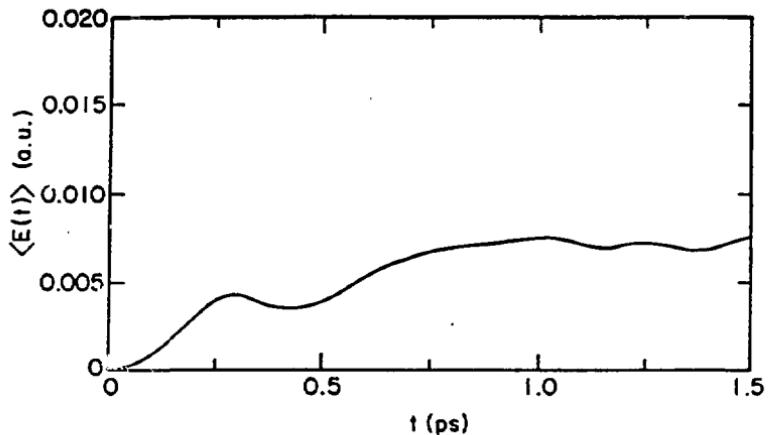
Fig. III.6. Classical time dependent energy absorption for rotating HF
with $\bar{\nu}$ = 3937 cm^{-1} and I = 1.0 TW/cm^2.
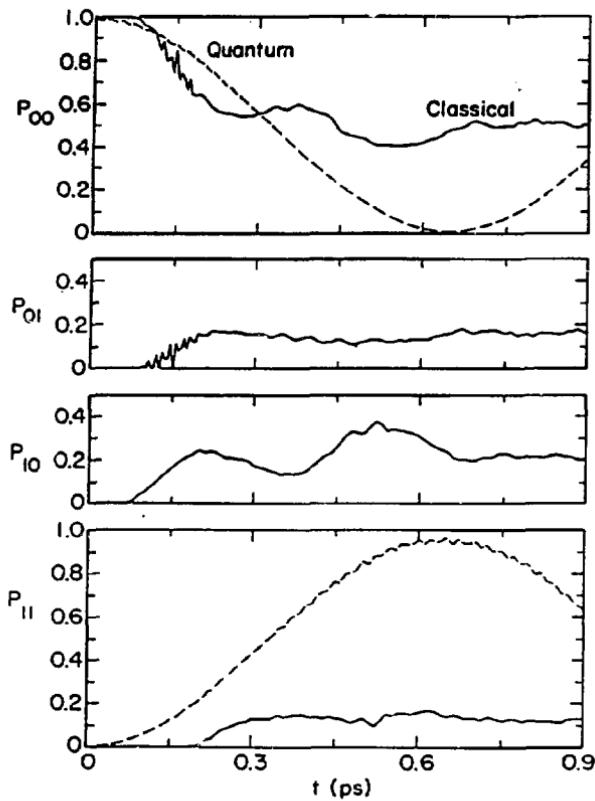
Fig. III.7. Classical and quantum mechanical probabilities P_{vj} for HF with $\bar{\nu} = 4006$ cm^{-1} and $I = 1.0$ TW/cm^2.
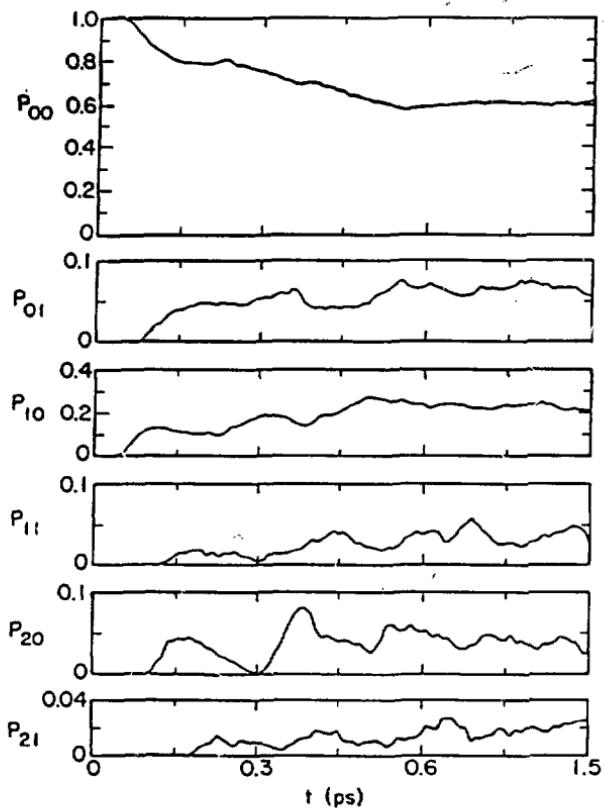
Fig. III.8 Classical probabilities P_{vj} for HF with $\bar{\nu} = 3937$ cm^{-1} and I = 1.0 TW/cm^2.
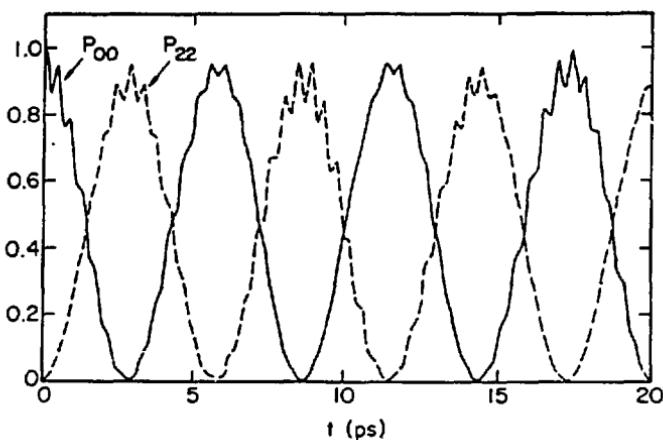
Fig. III.9. Quantum mechanical probabilities P_{00} and P_{22} for HF with $\bar{\nu} = 3937$ cm^{-1} and $I = 1.0$ TW/cm^2.
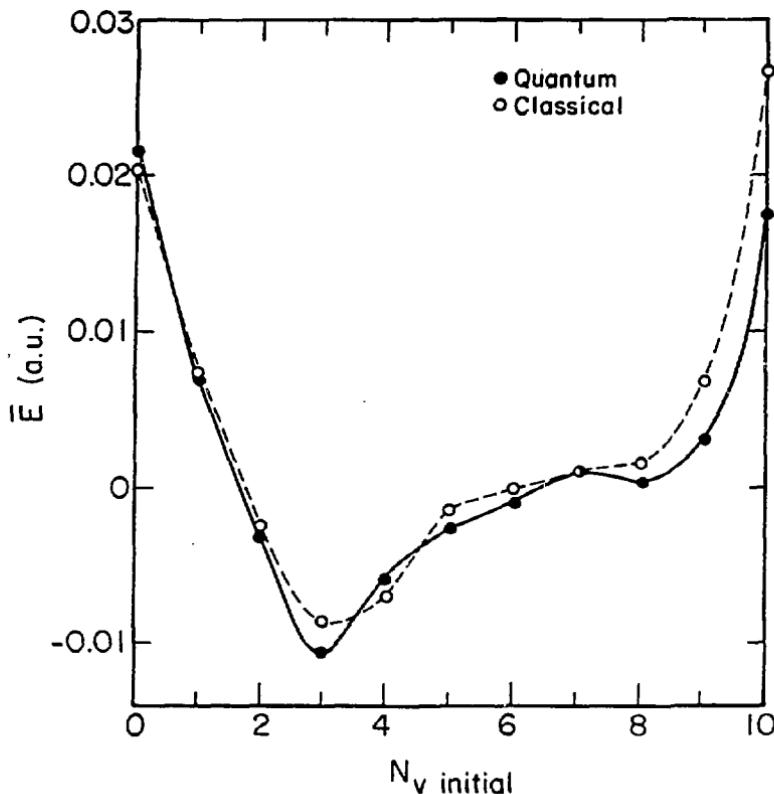
Fig. III.10. Quantum and classical time averaged energy absorbed as a function of initial vibrational state for nonrotating HF at $\bar{\nu} = 3922$ cm^{-1}.
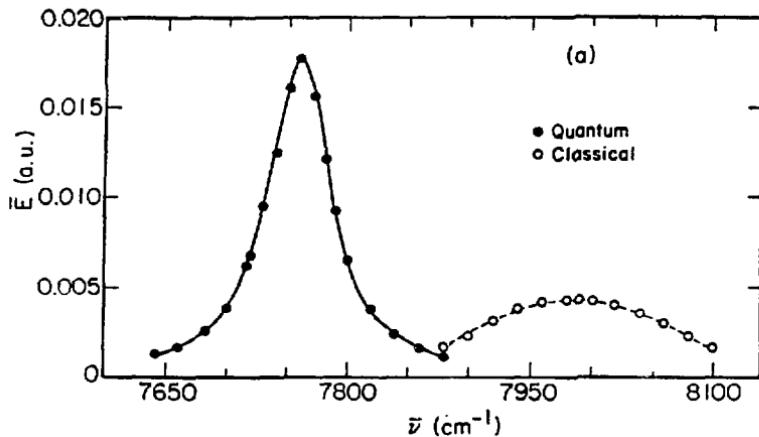
Fig. III.11(a). Quantum and classical time averaged energy absorbed as a function of frequency for nonrotating HF in the overtone frequency range with a linear dipole.
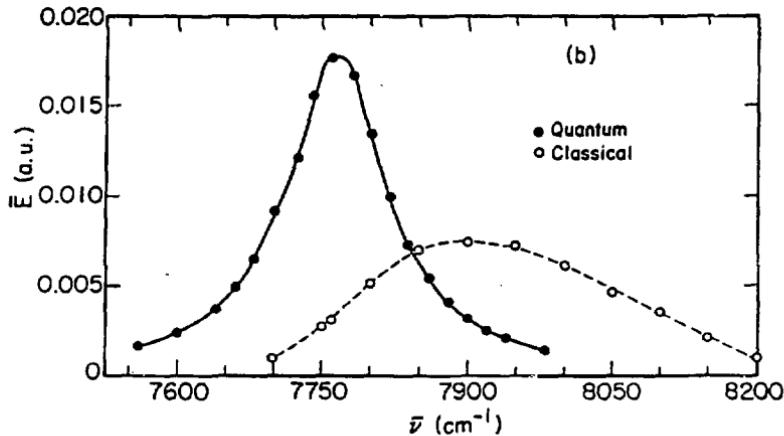
Fig. III.11(b). Quantum and classical time averaged energy absorbed as a function of frequency for nonrotating HF in the overtone frequency range with a quadratic dipole (note the different frequency scale from Fig. (a)).
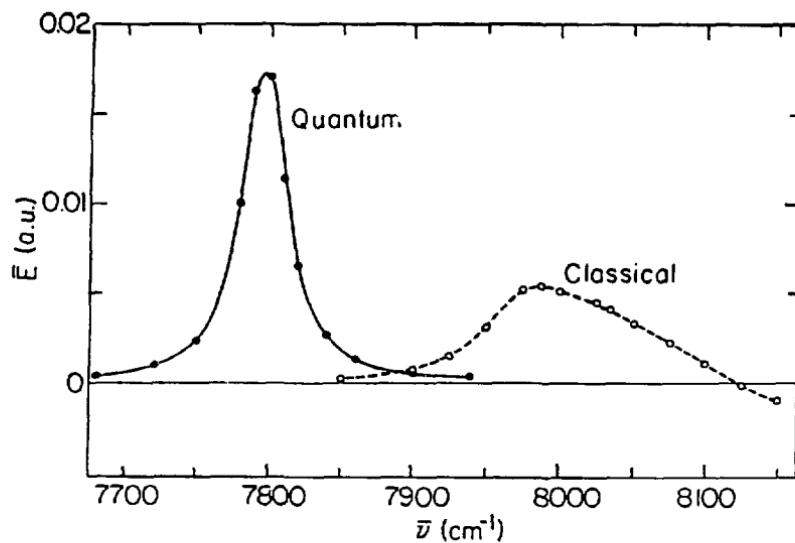
Fig. III.12. Quantum and classical time averaged energy absorbed as a function of frequency for rotating HF in the overtone frequency range.
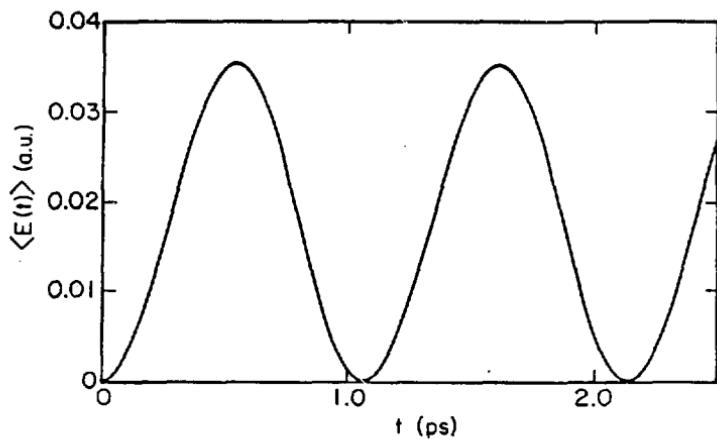
Fig. III.13. Quantum energy absorbed as a function of pulse time for nonrotating HF at $\bar{\nu} = 7757.8$ cm^{-1}.
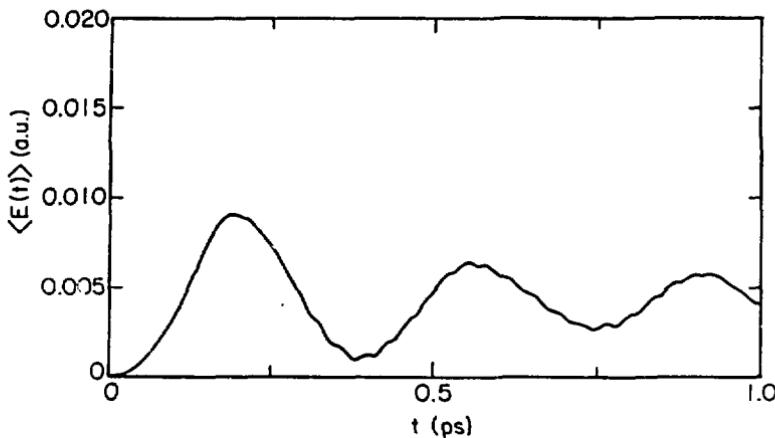
Fig. III.14. Classical energy absorbed as a function of pulse time for nonrotating HF at $\bar{\nu}$ = 7990 cm^{-1}.
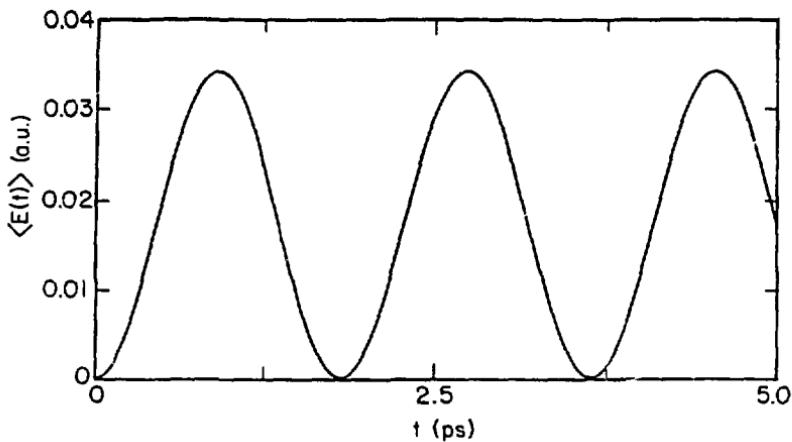
Fig. III.15. Quantum energy absorbed as a function of pulse time for rotating HF at $\bar{\nu} = 7800$ cm^{-1}.
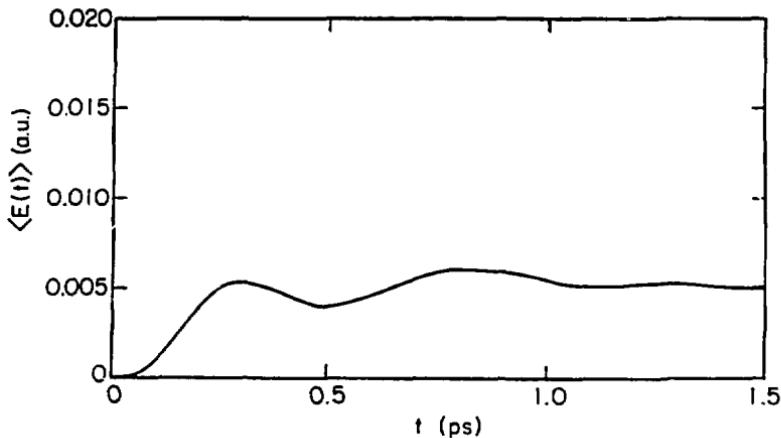
Fig. III.16. Classical energy absorbed as a function of pulse time for rotating HF at $\tilde{\nu}$ = 7987.5 cm^{-1}.
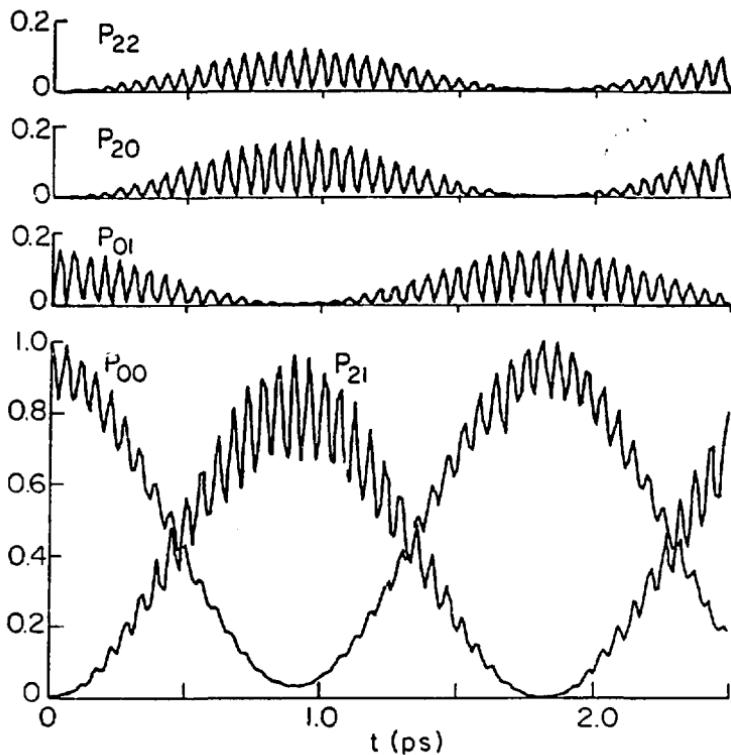
Fig. III.17. Quantum transition probabilities as a function of pulse time for rotating HF at $\bar{\nu} = 7800$ cm^{-1}.
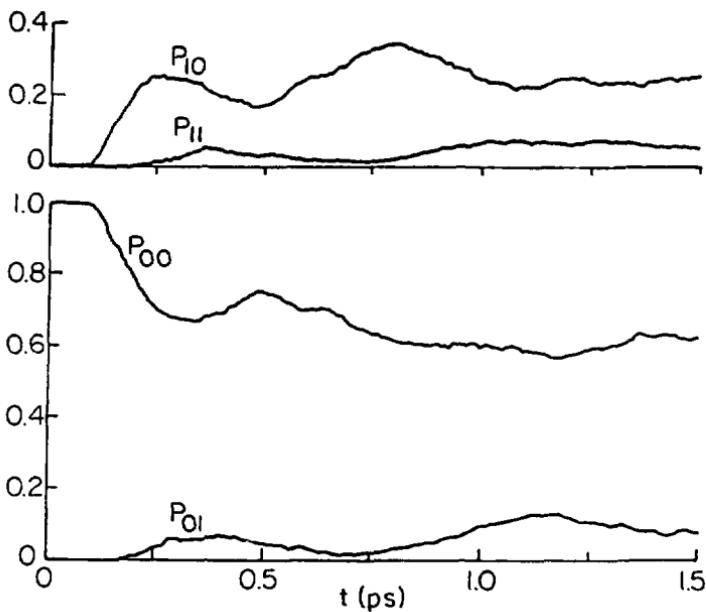
Fig. III.18. Classical transition probabilities as a function of pulse
time for rotating HF at $\bar{\nu} = 7987.5$ cm^{-1}.
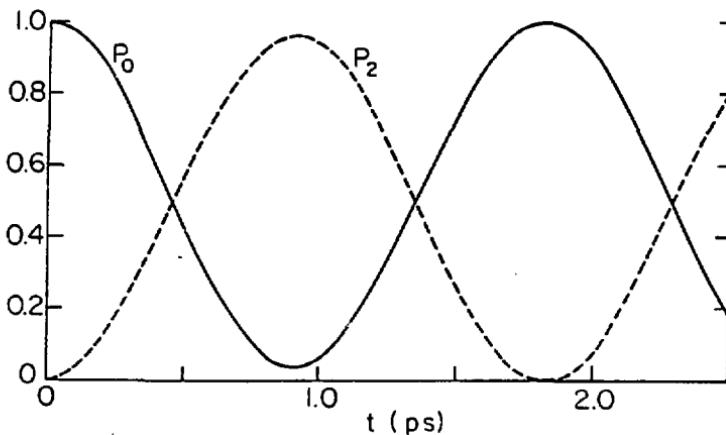
Fig. III.19. Quantum tansition probabilities summed over rotational states as a function of pulse time for rotating HF at $\bar{\nu} = 7800$ cm^{-1}.
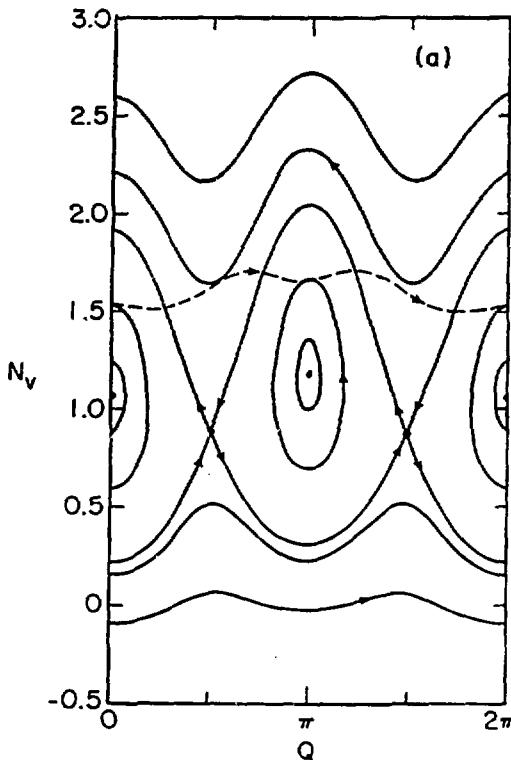
Fig. III.20(a). Poincaré surface of section at $\bar{\nu} = 7757.8$ cm^{-1} for nonrotating HF, (o) denote elliptic fixed points and (·) denote hyperbolic fixed points; the dashed line is an actual trajectory.
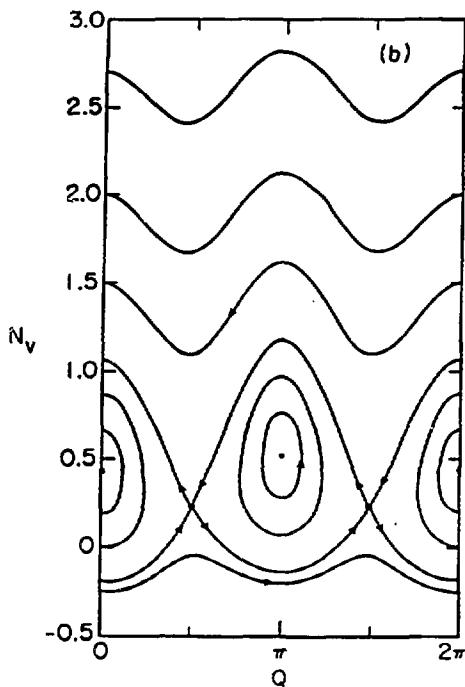
Fig. III.20(b). Poincaré surface of section at $\bar{\nu} = 7980$ cm^{-1} for nonrotating HF, (○) denote elliptic fixed points and (·) denote hyperbolic fixed points.
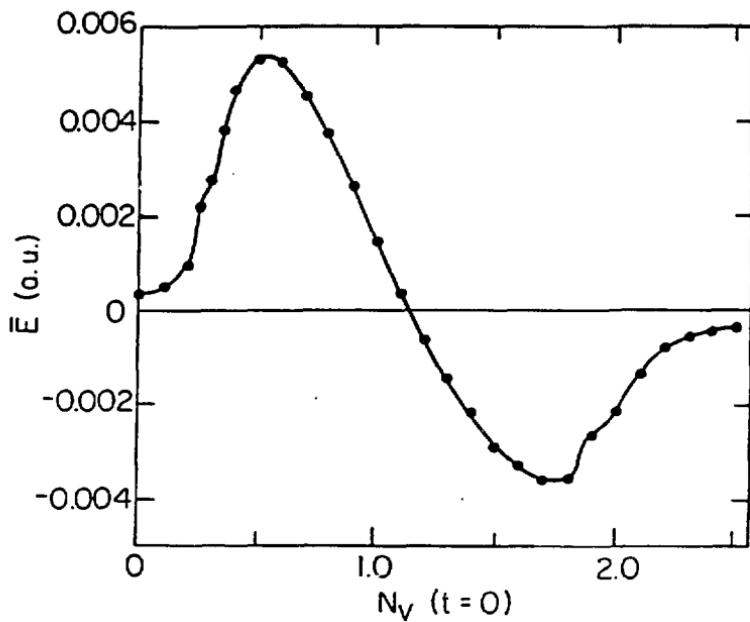
Fig. III.21. Classical time averaged energy absorbed as a function of the initial action for nonrotating HF at $\bar{\nu} = 7757.8$ cm^{-1}.
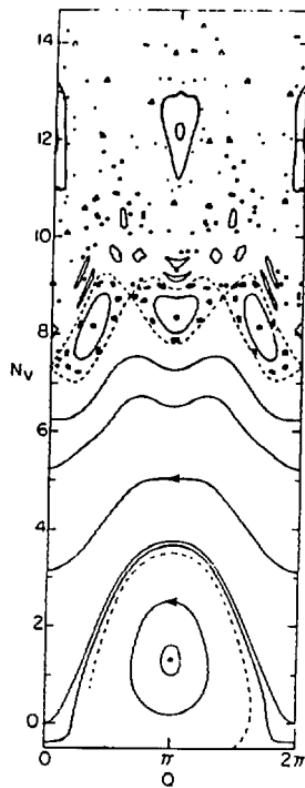
Fig. III.22. Poincaré surface of section for nonrotating HF at $\bar{\nu} = 3922$ cm^{-1}; (o) denote eliptic fixed points and (•) denote hyperbolic fixed points. The dashed lines indicate separatrices.